NASA CR-72765
MCR-70-350

COMPOSITE OVERWRAPPED METALLIC TANKS INTERIM REPORT

by

A. Feldman and A. Holston, Jr.

MARTIN MARIETTA CORPORATION
Denver Division

Prepared for

NATIONAL AERONAUTICS AND SPACE ADMINISTRATION

Lewis Research Center
Contract NAS3-12023
James R. Barber, Project Manager

NOTICE

This report was prepared as an account of Government-sponsored work. Neither the United States, nor the National Aeronautics and Space Administration (NASA), nor any person acting on behalf of NASA:

A.) Makes any warranty or representation, expressed or implied, with respect to the accuracy, completeness, or usefulness of the information contained in this report, or that the use of any information, apparatus, method, or process disclosed in this report may not infringe privately-owned rights; or

B.) Assumes any liabilities with respect to the use of, or for damages resulting from the use of any information, apparatus, method or process disclosed in this report.

As used above, "person acting on behalf of NASA" includes any employee or contractor of NASA, or employee of such contractor, ot the extent that such employee or contractor of NASA or employee of such contractor prepares, disseminates, or provides access to any information pursuant to this employment or contract with NASA, or his employment with such contractor.

Requests for copies of this report should be referred to

National Aeronautics and Space Administration
Scientific and Technical Information Facility
P.O. Box 33
College Park, Md. 20740

NASA CR-72765

INTERIM REPORT

COMPOSITE OVERWRAPPED METALLIC TANKS

By

A. Feldman and A. Holston, Jr.

MARTIN MARIETTA CORPORATION
Denver Division
P. O. Box 179
Denver, Colorado 80201

Prepared for

National Aeronautics and Space Administration

October 1971

Contract NAS3-12023

Lewis Research Center
Cleveland, Ohio
James R. Barber, Project Manager
Chemical Rocket Propulsion Branch

This report is submitted by Martin Marietta Corporation in partial fulfillment of Contract NAS3-12023 and covers Tasks I and II, Titanium Properties Determination and Pressure Vessel Design. These tasks were accomplished between July 1, 1968 and February 28, 1970.

The work was done through the direction of the Composites Fabrication Laboratory, Structures and Materials Research and Development, Denver Division, under the cognizance of J. A. Sterhardt and B. L. Bogema, department managers. Arthur Feldman was the Program Manager and was directly responsible for Task I. Alvin Holston, Jr. was responsible for the computer program revision and vessel design. J. B. Keough, of the Cold Flow Laboratory was responsible for the burst tests on Task I. Acknowledgment is also due for the efforts of D. A. Stang, R. R. Spangler, and T. Kiefer, who assisted in the design of the equipment and execution of the tests of Task I.

The NASA Project Manager for this program is James R. Barber of the Liquid Rocket Technology Branch, Lewis Research Center.

TABLE OF CONTENTS

Contents (Continued

Contents (Continued)

ABSTRACT

A two-part program involving tests of 5Al-2½Sn titanium (ELI) and a design computer program revision and use was undertaken to investigate the feasibility of a fiberglass/epoxy overwrapped titanium pressure vessel. The effects of cryogenic temperature and various manufacturing processes on the titanium were studied experimentally. An existing design computer program was revised to account for a variable thickness liner in the domes and thereby increase efficiency. A vessel was designed with the properties determined in the experimental phase. It is concluded that the operational concept of permitting a state of compressive stress in the liner with zero internal pressure will result in a lighter weight vessel.

SUMMARY

In order to better use the strength of fiberglass in a pressure vessel application, NASA originated the concept of forcing a metal liner to exist in a compressive stress state with zero internal pressure. This investigation is testing the concept first by examining the behavior of the candidate liner material, 5Aℓ-2½Sn titanium (ELI) under various loading conditions, temperatures, and subjecting it to several manufacturing processes. Second, an existing computer program for the design of vessels operating this way was revised to account for a liner of variable thickness in the domes, thus distributing the stresses in a more favorable fashion and increasing the possible weight savings over an all-metal vessel.

The liner material tests performed were uniaxial tensile tests at room temperature, liquid nitrogen temperature (-320°F), and liquid hydrogen temperature (-423°F); biaxial tensile tests at these temperatures on specimens that had been chem-milled, electron-beam welded, tungsten-inert gas welded, and explosively formed; compressive "creep" tests on specimens that had been electron-beam welded and overwrapped with fiberglass/epoxy; and uniaxial tensile tests on specimens that had been chem-milled and mechanically milled. The conclusion from these tests was that, though some of the processes reduced the ductility of the liner material, there was sufficient ductility remaining so as not to degrade pressure vessel performance.

Successful revision of the computer program to account for a variable liner thickness permitted studies to be made on the functional form the thickness variation should take. A piecewise linearly varying liner was chosen for its generality and seemed to produce an effective design and a good distribution of liner and overwrap stress. Studies, made of the effect of manufacturing tolerance on vessel weight and performance, indicated that a tradeoff has to be made between cost of increased care in manufacturing and cost of either lessened efficiency of the vessel or lessened reliability. It appeared that the end boss design would be dictated more by manufacturing considerations than the state-of-stress.

The general conclusion is drawn that the general concept of a compressively stressed liner, under an overwrap with tensile stress, may better use the overwrap material.

I. INTRODUCTION

The objective of this program is to develop a fiberglass overwrapped titanium pressure vessel for cryogenic service. Although filament winding of solid-fueled missile cases has become a reality, there has been a significant lag in the development of techniques for successfully applying filament winding to fabrication of glass-fiber/epoxy pressure vessels for gas or liquid containment. Considering the very attractive strength-to-density properties of filament-wound materials, it is essential that techniques necessary to make pressure vessels using this fabrication method be developed.

The principal difficulty that has prevented success in applying filament winding to pressure vessels is the lack of a reliable liner system for both room-temperature storable and cryogenic propellants. A liner is needed because the organic matrix materials used in filament winding are permeable. For room-temperature application, elastomeric liners would suffice except for problems of chemical compatibility; for cryogenic service the elastomeric liners are not suitable because of their brittle behavior. Therefore, metal liner systems are required.

The principal problem with the metal liner is one of mechanical compatibility, i.e., the strain imparted to the liner during pressurization and the attendant deformation of the glass-fiber vessel must be reabsorbed during depressurization of the vessel. Furthermore, it must be reabsorbed for each cycle without liner malfunction, in spite of the fact that full utilization of the overwrap may require the liner to experience some plastic straining.

Recent work (ref. 1) with overwrapping relatively thick inconel metal load-bearing liners has indicated that this overwrapping concept is a reliable means for providing a significant weight saving. The principle involved in overcoming the mechanical compatibility problem is to place the metal liner under compression during fabrication, and thus increase the strain range through which the liner may operate. At the same time the glass-fiber/epoxy overwrap is placed in tension. Matching the overwrap tension properly to the liner compression results in the operation of the overwrap at an efficient stress level while the liner remains elastic. The creep and biaxial strain properties of the liner material must be considered when the zero-pressure stress

levels are chosen, so that this prestressed state is not seriously diminished with time. Otherwise the inelastic strain to which the liner would be subjected on each cycle would degrade the fatigue resistance of the metal.

The performance factor (pressure x volume/weight) of a vessel thus designed is between that of an all-metal vessel and that of a glass-fiber/epoxy filament-wound vessel with a thin, non-load-bearing metal liner. Until such time as a non-load-bearing liner is developed, the overwrapped load-bearing liner can provide weight savings; these savings being strongly dependent on the elastic strain/weight ratio for the liner material. Titanium promises to provide even higher performance factors than inconel, especially if a liner of non-uniform thickness is used to approximate a uniform stress state.

The objective of this program is being pursued with an effort divided into four major tasks, as follows:

Task No.	Effort
I	Titanium Properties Determination
II	Design
	a. Computer Program Revision
	b. Pressure Vessel Design
III	Manufacture
	a. Explosive Forming Development
	b. Liner Fabrication
	c. Pressure Vessel Winding and Sizing
IV	Test
	a. Design and Fabrication of Test Fixtures
	b. Burst and Cyclic Tests
	c. Vibration and Life Tests

This interim report covers the effort on Tasks I and II. Vessel design criteria and specifications used in Task IIb are as follows:

1) Shape: cylinder with end closures;
2) Size: 25 in. maximum OD;

3) Volume: 7,365 $in.^3$ $\pm$ 1.5% after sizing;
4) Sizing conditions: 4,480 psi at 75°F (1.333 x operating pressure).

The performance requirements are:

1) Operating pressure: 3,360 psi;
2) Proof pressure: 4,050 psi at 160°F and -65°F (1.2 x operating pressure);
3) Burst pressure: 5,600 psi at 160°F and -65°F (1.666 x operating pressure).

II. TASK I - DETERMINATION OF TITANIUM PROPERTIES

A. INTRODUCTION

Before the pressure vessels to be made and tested on this program were designed, additional information, not available in the literature, about the particular alloy of interest (5Al-2½Sn ELI titanium) was required. In addition, we wished to base the design on the properties of the actual material to be used in the liners. Therefore, a program of testing was devised to: (1) characterize the liner material for the initial computer design program input; (2) investigate the effect on ductility of several of the anticipated manufacturing variables; (3) study the effect of high compression stress on creep rate; and (4) determine the properties of the actual liner material for final design. These four efforts are identified as preliminary tension tests, biaxial tests, creep tests, and liner material tension tests.

B. PRELIMINARY TENSION TESTS

1. Specimen Properties

To obtain some preliminary data for design, tension tests were made on seven specimens cut from a small sheet of 5Al-2½Sn alloy of 0.220 inch nominal thickness. Vendor data for this sheet are given in table I. The configuration of the test specimens is shown in figure 1, shape B. Two additional specimens were cut from the sheet, then milled, one mechanically and one chemically, to indicate the possible effect of chemical milling. The mechanically milled specimen was made according to shape C and the chemically milled one shape D, in figure 1. Grain direction in both instances was longitudinal. Measured dimensions of the test sections are given in table II. Measurements were made with a machinist's micrometer incorporating a 0.0001 inch vernier. Specimen designation nomenclature is given in table XXIV.

2. Test Set-Up

The preliminary tension tests were run at room temperature in a Wiedemann Mark G Universal Testing Machine at a strain rate of approximately 1500 μ in./in./min. Modulus and Poisson's ratio data were determined from the output of strain gages feeding the recorder on the testing machine. The gages were Budd Metalfilm Type C9-121-R2TC mounted with Bean BR610 cement. On the full

thickness specimens, two gages were mounted on each side of each specimen, one longitudinal and one transverse, and the outputs of the longitudinal gages were averaged to eliminate the effects of bending. Only longitudinal gages were used on the milled specimens. After initial runs in the elastic region to measure modulus and Poisson's ratio, a dual range microformer was mounted and used to record the entire stress-strain curve. Yield strengths at 0.2% offset and the slope in the inelastic region were deduced from these curves. Tensile strength was read from the load dial on the machine. Elongation at failure was determined by measuring the distance between scribe marks placed 2 in. apart before testing. Unfortunately, anomalous operation of the microformer resulted in some data being lost.

3. Results and Interpretation

The data from the tests described above are given in table III. These values were used to arrive at a set of numbers for initial vessel design runs on the computer. Stress-strain data input to the computer must be in the form of a bilinear relation, where the measure of yield strength is the artificial number representing the intersection of the elastic and inelastic slopes, rather than any value taken from the actual stress-strain diagram. Such a bilinear relation was developed which approximated a composite stress-strain curve based on the values in table III. The parameters describing this relation and which were used in preliminary design computations and liner thickness variation studies were as follows:

Elastic modulus (E_T) = 16.73×10^6 psi;

Inelastic modulus (E_2) = 97.3×10^3 psi;

Yield strength (intersection stress, σ_I) = 107.2×10^3 psi;

Poisson's ratio (ν) = 0.33 (elastic region).

The conclusions to be drawn from the data for the milled specimens are that there seems to be no effect on the measured properties due to machine milling and the only effect due to chemical milling is a reduction in ultimate elongation, though single tests do not support these conclusions in general.

C. BIAXIAL TESTS

The objective of these tests was to determine the effect of various manufacturing processes on the ductility of the alloy of interest under biaxial tension (1:1). Tests were to be made at

room temperature, liquid nitrogen temperature, and liquid hydrogen temperature. The manufacturing processes to be investigated were electron-beam welding (EBW), tungsten-inert gas (TIG) welding, and explosive forming.

1. Specimen Properties

a. Material - The biaxial test specimens were cut from a 3 x 10 ft piece of 5Al-2.5Sn Ti (ELI) with a nominal thickness of 0.062 in. Vendor data are given in table IV. To characterize the material before its use in making specimens for the biaxial tests, a series of tension tests were made on specimens cut from the same sheet. The configuration of the test specimens is shown in figure 1, shape B. Specimen designation nomenclature is given in table XXIV. Six specimens were made and tested, three cut parallel and three cut perpendicular to the grain direction. One specimen of each group had a longitudinal strain gage on each side of Type C9-121-R2TC (Budd Metalfilm) mounted with Bean BR610 adhesive. After initial runs in the elastic range to measure modulus, a dual range microformer was mounted and used to record the entire stress-strain curve for all six specimens. Strain rate was approximately 1500 μ in./in./min. Initial portions of these curves were used for modulus determination on those specimens without gages. The 0.2% offset stress was also read from these curves. Tensile strength was computed from the maximum load on the testing machine dial (Wiedemann Mark G) and elongation at failure was determined by measuring the distance between scribe marks placed 2 in. apart before testing. The results of these tests are given in table V.

b. Shape and Manufacture - The test specimens consisted of 9-3/4 in. diameter flat plate and hemispherical dome specimens, as shown in figures 2 and 3. Figures 4, 5, and 6 are the fabrication drawings for the domed specimens and for the blanks from which the flat specimens were cut. The flat specimens were cut from 0.062 in. thick sheet, with a 7-$\frac{1}{4}$ in. diameter test section chemically milled to approximately 0.040 in. thickness. When indicated by the test plan, welds were laid down with full penetration on the uncut blanks. The pattern was a 90° cross with each line 6-$\frac{1}{4}$ in. long. The dome specimens were explosively formed from 0.062 in. thick sheet, and chem-milled over a portion to 0.040 in. thickness. Because of the blank size limitation of the existing explosive forming die, a separate holding flange had to be made for the dome specimens and TIG-welded to the dome, as shown in figure 3. Both flange and dome were stress relieved

between forming shots and after forming. Specimen type, welding type, and test temperature are shown in table VI. Specimen designation nomenclature is given in table XXIV. A 2 x 2 in. photogrid, subdivided into 0.1 x 0.1 in. squares, was printed on the center of each specimen for use in determining permanent strains after fracture. Thickness of the specimens was measured before testing with a specially constructed deep-throat micrometer. Minimum and maximum thicknesses of the base material (exclusive of weld reinforcement) within the gridded area for the flat specimens are also given in table VI. Values for the dome specimens are for the entire chem-milled portion.

2. Test Fixturing

The test fixtures used for the biaxial tests are shown schematically in figures 7, 8, and 9. The holding fixture is shown in the sketch of figure 10 and in the photos in figures 11 and 12. The titanium gasket shown was used because a titanium/titanium interface gave the maximum static friction coefficient to prevent extrusion of the test specimen. The configuration proved satisfactory in clamping the specimens and providing a leak-free joint up to pressures of 4400 psig at -423°F. At 4400 psig, deflection of the 900 lb ASA rated flanges and 1-1/8 in. bolts caused leakage which outstripped the make-up capability of the pressurant supply system.

The cryostat used to immerse the holding fixture for the cryogenic tests consisted of a 30-gal. stainless steel drum (commercial item) insulated with 6 in. of foamed-in-place insulation. The cryostat lid was fitted with a dip-leg type fill tube, a vent tube and two thermocouple probes.

The pressurant supply system for the cryogenic tests included two cylindrical reservoirs having a combined volume of 64 cu in. The function of the reservoirs was to hold a quantity of liquefied gas approximately twice the volume required due to straining of the test specimen, so that there would be no intrusion of gas into the holding fixture. A restricter orifice (#60 drill hole) was placed in the liquid supply line between the reservoirs and the holding fixture to inhibit throughflow at specimen rupture. The orifice also provided a method of detecting leakage in the holding fixture, in that a noticeable pressure differential would exist between reservoir gas supply pressure and the pressure in the holding fixture whenever a flow condition existed. Liquid leakage was considered an unacceptable condition

due to possible depletion of the reservoir liquid supply and resultant intrusion of gas into the holding fixture. Existence of gas in the fixture at specimen rupture was known to produce explosive gas release.

The pressurant source for the room temperature tests was GN_2 over water. The pressurant source for the LN_2 tests was the regular laboratory 5500 psig regulated GN_2 system. The pressurant source for the LH_2 tests was a bank of two 2250 psig GH_2 cylinders (commercial ICC cylinders) supplying a GN_2-driven piston type boost pump.

3. Test Method

For all tests, the specimen was installed in the holding fixture as shown in figure 10. For room temperature tests, the holding fixture bolts were torqued to 460 ft-lbs. For the cryogenic tests (LN_2 and LH_2), the bolts were retroqued while cold after immersing the holding fixture in LN_2.

For the room temperature tests, the holding fixture was connected to the GN_2-over-water pressurization system and bled until a gas-free condition was obtained in the holding fixture. The supply system was then pressurized at a rate of approximately 1500 psi/minute until the specimen ruptured. Pressure in the holding fixture was recorded continuously on a Sanborn direct-writing recorder. Immediately after test, the pressure transducer and recording system were end-to-end calibrated against a 0.2% test gage. The specimen was then removed from the fixture and photographed.

For the LN_2-temperature tests, the holding fixture was installed in the empty cryostat, purged thoroughly with GN_2 and pressurized to 100-150 psig. After leak-checking the fixture, the cryostat was filled with LN_2 while the facility pressure regulator maintained the supply pressure. Liquefaction-filling of the fixture was considered to be complete when no pressure decay was observed after closing the supply valve. The system was then pressurized at an intended rate of approximately 1500 psi per minute until the specimen ruptured. Pressurization rates as low as 100 psi/min. occurred during some tests due to leakage.

The LH_2 tests were performed in much the same manner as that described for the LN_2 tests. The progress of GH_2 liquefaction was checked by monitoring the pressure decay in the supply cylinders. A final check was made by valving off the supply line as described for the LN_2 tests. The supply pressure from the GH_2 cylinders was then increased to the 750 psig pressure required at the boost pump inlet. Due to the characteristics of the boost pump, the delivery line pressure increased to the same pressure. The boost pump was then started, to increase pressure at approximately 1500 psi per minute. The cyclic rate of the pneumatically-driven pump was somewhat difficult to control, so that pressurization rates varied between about 160 psi/min. and 2000 psi per minute.

During all tests except the BNO test (LN_2 temperature test, unwelded flat plate specimen), the ruptrues were so quiescent that the occurrence could not be detected by observing the cryostat. In the BNO test, leakage from the holding fixture tubing fittings at pressures above approximately 3500 psig permitted some gas to intrude into the fixture, with the result that the rupture of the specimen was attended by a relatively energetic release of gas. The effect of this may be noted by comparison of posttest photos of BNO (fig. 14) and the other flat plate specimens.

4. Results and Conclusions

Figures 13 through 33 contain various views of the tested biaxial specimens. Duration of the tests and failing or maximum pressures are listed in table VI. The pressure values in table VI may be better understood if compared with computed values for the room temperature unwelded specimens. Storakers (ref. 2) gives the burst pressure for a circular flat plate of uniform thickness under transverse pressure as

$$p_b = \frac{0.9\ \sigma_o\ h_o}{r_o} \qquad (1)$$

where

p_b = burst pressure

$\sigma_o = \sigma_t / \epsilon_t^n$

σ_t = true stress

ϵ_t = true strain

n = slope of σ_t vs ϵ_t diagram in the plastic region

h_o = original thickness

r_o = original radius.

Using the stress-strain curve for 5Al-2.5Sn titanium (ELI) measured for specimen T63BL-3 (fig. 34 and 35), one obtains n = 0.100 and σ_o = 160,000 psi. Using h_o = 0.040 in. and r_o = 3.625 in., we obtain

$$p_b = \frac{0.9 \times 160{,}000 \times 0.040}{3.625} = 1{,}590 \text{ psi}$$

This value is to be compared with the burst pressure of 2,390 psi measured on specimen BRO.

The pressure at burst in a hemispherical dome neglecting the effect of biaxial stress on the material strength, is

$$p_b = \frac{2\, h_o\, \sigma_u}{r_h} \qquad (2)$$

where

p_b = burst pressure

h_o = original thickness of the material

σ_u = engineering tensile strength

r_h = radius of curvature of the hemisphere.

In our case, we have h_o = 0.040 in., r_h = 3.0 in., and σ_u = 122,800 psi (table V). Thus,

$$p_b = \frac{2 \times 0.040 \times 122{,}800}{3} = 3{,}275 \text{ psi}$$

This value is to be compared with the burst pressure of 3,120 psi measured on specimen BRD, where failure took place next to the dome flange weld in material approximately 0.063 in. thick.

Pieces of the failed flat specimens containing the grid were cut out and placed in a Nikon Profile Projector, which has a movable stage controlled by a micrometer graduated in 1/10,000 in. The coordinates of the intersection of the grid closest and next closest to the failure were determined and recorded on enlarged prints of the grid. Residual strain was computed by subtracting the coordinates and dividing the difference by the original grid spacing (0.1000 ± 0.0002 in.). The maximum values thus obtained, measured perpendicular to the rupture, are listed in table VI. No measurements were made on the dome specimens as none of the failures were attributable to the chem-milling or explosive forming processes used to make them.

Several conclusions can be drawn from the data. First, the unwelded material, though chem-milled, is considerably more ductile under biaxial loading than required for the present application. Second, explosive forming does not appear to have a major deleterious effect on ductility, provided the part is stress-relieved after the last forming operation. It is not known, from this work, what the effect would have been, had the specimens not been stress-relieved. Failure in the dome specimens did not initiate in the area most affected by the forming process, yet failure pressures were about as expected. Specimen BHD must be discounted as a poor specimen. Either there was a flaw in the dome or two flaws adjacent to the weld. Third, TIG welding appears to be better than EBW, though both seriously reduce the ductility primarily because of the effect on the adjacent material and the creation of geometric stress concentrations at the edge of the reinforcement. Though it seems to be supported strongly by the data, the last conclusion may not have an impact on the program. As will be explained below in section II.D.3.b, EB welded cylinders overwrapped with fiberglass in the creep test portion of the program withstood at least 2.4% strain with no evidence of distress. This strain level is adequate for the needs of the application being investigated.

D. CREEP TESTS

The objective of these tests was to determine the room temperature compressive creep characteristics of the alloy of interest as a function of compressive stress level. This information is needed to assess the feasibility of the design

concept of this program; that is, extending the elastic range of behavior of a titanium tank liner by forcing it to be in a compressive stress state when the tank is empty. The general scheme used was to overwrap titanium cylinders with fiberglass, pressurize them until the titanium yielded in tension, relieve the pressure which caused the titanium to be forced into compression by the stretched overwrap, and monitor the strains over a period of time.

1. Specimen Properties

a. Material - The cylindrical creep test specimens were cut from a 3 x 10 ft piece of 5Al-2.5Sn titanium (ELI) with a nominal thickness of 0.062 in. Vendor data are given in table VII. In order to characterize the material before its use, a series of tension tests were made on specimens cut from the same sheet. The configuration of the test specimens with axis parallel to the grain was as shown in figure 1, shape A, while the transverse specimens were shape B. Specimen designation nomenclature is given in table XXIV. Number of specimens, strain gages, equipment used and procedures, were the same as described for the bi-axial material coupon tests in section II.C.1.a. The results of these tests are given in table VIII. The roving used for overwrapping was U. S. Polymeric 20 end S-HTS/E-796 epoxy impregnated fiberglas with resin solids of 18-23% by weight.

b. Shape and Manufacture - Specimen blanks 14 x 36 in. were sheared from a 3 x 10 ft sheet of titanium, with the 14 inch dimension in the direction of the grain. The blanks were rolled into cylinders 10 in. in diameter at the Baltimore Facility and EB welded according to figure 36. Dimensions of the unwrapped cylinders are given in table IX. Random measurements of thickness with a vernier micrometer on all specimens about 1 in. in from the edge yielded values of 0.0620, + 0.0003, - 0.0000 in. Specimen designation nomenclature is given in table XXIV. Micromeasurements type EA06-500BH120 strain gages were mounted on the outside using Bean BR610 adhesive, three in the hoop direction at midlength 120° apart and two in the axial direction at midlength 180° apart, as far from the weld as possible. These gages were used with an X-Y plotter during pressurizing of the specimens. On all specimens except C-1, two additional gages were mounted for monitoring during the creep portion of the tests, one longitudinal and one transverse, at midheight. These latter

gages were read manually on a strain indicator. Figure 37 shows a bare cylinder with some gages attached. Next, the cylinder was wrapped in the hoop direction with preimpregnated glass roving. On all specimens except C-1, the gage leads were brought directly out from the gage tabs. Figure 38 shows specimen C-1 in the midst of overwrapping with the leads extending some distance under the wrap. This technique was found to be unsatisfactory, as explained later. Several specimens were strained within their elastic range before overwrapping to obtain the material modulus. The overwrap was uniform in thickness over the middle 9 in., then was increased in thickness toward the ends such that the outer 1 in. was thick enough to permit machining down to an overall diameter of approximately 10.86 in. After curing, the total thickness of each specimen was measured with a deep throat caliper at nine locations, that is, at midheight and at 2 in. above and below midheight on three equally spaced meridians. Net thickness of the overwrapped fiberglass/epoxy was determined by subtracting 0.062 in. from the overall thickness measurements. The number of layers of fiberglass/epoxy and threads/inch in each layer along with the resulting range and average of the values of overwrap thickness are given in table IX. The manufacturing plan is shown in figure 39.

2. Test Equipment and Procedure

The creep tests were conducted in a fixture designed and built especially for the purpose. It was intended that the fixture would apply hoop loading in the specimen with no axial restraint. This objective was substantially achieved. A schematic diagram of the arrangement is shown in figure 40. Figure 41 is a view of the assembled fixture and specimen. Originally, neoprene was used where the Adiprene L-100 is shown in figure 40, but it could not sustain the necessary pressures. The Adiprene gaskets were brushed in as the fixture and specimen were assembled, and discarded after one use. The mix was eight parts Adiprene L-100 to one part methyl-ortho-chloro-aniline (MOCA) by weight. The gaskets were cured in place for a minimum of 1 hour at 212°F.

Load was applied by pumping oil into the fixture with a hand hydraulic pump. Pumping was continued until a predetermined pressure level was achieved corresponding to a predetermined level of plastic strain in the titanium.

Unloading was accomplished by slowly bleeding the oil back into the pump. During the pumping operation strains and pressure were recorded on a Pace Double Arm 30 x 30 in. X-Y plotter. The pressure signal was taken from a strain-gage pressure transducer in the bleed line of the hydraulic system. The plotter had been previously calibrated by resistance bridges for strain and by a dead weight pressure calibrator for pressure. The strain signals drove the arms of the plotter and the one pressure signal drove both pens. The entire loading and unloading effort took 7 to 10 min.

In all tests except C-1, the gages that were intended primarily for monitoring creep were also read "on-the-run" during the pressurization phase of the test. A BLH Model 120 manual strain indicator was used together with a BLH Type 525 switch and balance unit. Bridge completion and temperature compensation were provided by a gage mounted on a bare creep specimen cylinder located next to the test specimen. It was covered by several layers of glass/epoxy cloth to simulate the overwrap. Pressurization runs made on the bare titanium cylinders to measure modulus were run in the same fashion as on the overwrapped cylinders except the range of loading was limited to about one-half the elastic range and the strains were monitored with a manual strain indicator.

After release of pressure on the overwrapped specimens, strain readings were taken immediately with the manual strain indicator. Readings were taken approximately every minute for the first few minutes, every 5 min. for a few increments thereafter, and then at longer intervals as the strain rate dropped. Time was recorded manually from an ordinary wrist watch. Readings were plotted manually as time permitted to provide an indication as to how long they should be taken. When the rate of strain dropped below 50 μ in./in. in 100 hours, the readings were stopped. When the time interval between readings would permit, the hydraulic hoses were disconnected and the oil was drained from the test fixture through a bottom hole. The specimen was allowed to remain in the pressurizing fixture while the strain readings were taken so that electrical leads would not have to be disconnected, though the fixture served no purpose during the "creep" test.

Specimens C-1 and C-2 were intended primarily to provide stress-strain relations as far into the compressive yield range as possible, within the limits of the pressurizing capability of the entire system. Based on these relations, it was intended that specimens C-70, C-80 and C-90 be designed and loaded in such a manner as to have compressive stress levels of 70, 80, and 90 ksi, respectively, at the end of the pressurization cycle. After the test of C-1, it was decided to record creep data from C-2 since it would be available with only a small extra effort. Also, because of the fact that the modulus of the overwrap and the actual stress-strain relation of a given specimen were unknown until after the test was over, the compressive stress at the beginning of the creep phase was difficult to predict. Actually, C-80 had a higher compressive stress after depressurization than C-90. Specimen C-70 had a lower stress than expected so CX-1 was tested to try to fill the gap between C-70 and C-90. However, CX-1 turned out to be practically a duplicate of C-70.

The time of initiation of creep and the creep phase of each test is somewhat arbitrary. There was evidence of nonlinear stress-strain behavior at low compressive stresses while pressure was still being bled off. We established the beginning of creep as being that time when the pressure had been bled back to zero. Actually, in every case, the titanium compressive stress level started to decrease before that. Note also that the tests were not true creep tests, but fell somewhere between creep and relaxation tests.

3. Results

a. Data Analysis - Before any sense could be made of the pressure-strain plots or strain-time data, it was necessary to know the modulus of the bare titanium. This value was available from the coupon data described in section D.1.a, but it was deemed advisable to obtain it directly for each bare cylinder using internal pressure and measuring the surface strain. The slope was taken from a plot of pressure versus hoop strain from which the modulus could be computed. This was done for all the specimens tested except C-1 and C-2. The formula is based on a simple pressure vessel hoop stress formula, and is as follows:

$$E_T = \frac{r_T}{t_T} \left(\frac{p}{\epsilon}\right)_h \qquad (3)$$

where

E_T = modulus of titanium

r_T = radius of mid-surface of bare cylinder

t_T = wall thickness of bare cylinder

$(p/\epsilon)_h$ = slope of pressure versus hoop strain plot.

The fixture was assumed to operate such that it took all the axial load and permitted the cylinder to contract axially unrestrained. The axial strain/hoop strain ratio was thus Poisson's ratio. How closely the ratio computed from the measured slopes of the plotter graphs agreed with accepted values of Poisson's ratio was then a measure of how well the fixture was operating; that is, how free from axial restraint the bare cylinder actually was. This question is discussed in detail later in this section. Poisson's ratio was computed thusly,

$$\nu = \frac{(p/\epsilon)_h}{(p/\epsilon)_a} \tag{4}$$

where

$(p/\epsilon)_h$ = slope of the pressure/hoop strain plot

$(p/\epsilon)_a$ = slope of the pressure/axial strain plot.

Having the titanium modulus it was possible to determine the hoop modulus of the fiberglass/epoxy on a complete specimen as follows. The pressure resisting capability of the specimen wall was taken as the sum of the capability of the overwrap plus the capability of the titanium. Thus

$$p = p_G + p_T \tag{5}$$

or

$$p = \frac{\sigma_G t_G}{r_G} + \frac{\sigma_T t_T}{r_T} \tag{5a}$$

where

σ_G = stress in the overwrap, = $E_G \epsilon_G$

σ_T = stress in the titanium, = $E_T \epsilon_T$

t_G = thickness of the overwrap

r_G = radius to midsurface of the overwrap

and the other terms are as before. Then

$$p = \frac{E_G \epsilon_G t_G}{r_G} + \frac{E_T \epsilon_T t_T}{r_T} \tag{6}$$

But perfect bonding between overwrap and titanium was assumed and the measured strain, ϵ, was taken as existing in both materials. So

$$\epsilon_G = \epsilon_T = \epsilon \tag{7}$$

or, from equation (6)

$$p/\epsilon = \left(\frac{Et}{r}\right)_G + \left(\frac{Et}{r}\right)_T \tag{8}$$

and

$$E_G = \left[(p/\epsilon)_h - \left(\frac{Et}{r}\right)_T\right] r_G/t_G \tag{9}$$

Once this value of E_G was obtained for each specimen, it was assumed to remain constant throughout the test, that is, it was assumed that there was no creep in the overwrap, no inelastic behavior and no hysteresis.

Having E_G, it was now possible to compute the entire stress-strain relation for the titanium exhibited during a test, elastic and inelastic, tension and compression, and to convert the creep strain measurements into stress loss. For selected values of hoop strain (ϵ) the corresponding pressure (p) was read from the plotter graph. Then the stress in the titanium was computed as

$$\sigma_T = \frac{p - \left(\frac{tE}{r}\right)_G \varepsilon}{(t/r)_T} \tag{10}$$

which comes from equation (10). Note that in equation (1), the overwrap is always assumed to be elastic ($E_G \epsilon$ substituted for σ_G) but not the titanium. The computed values of σ_T were plotted against the selected corresponding values of ϵ to yield the stress-strain relation. During the creep phase of the test, the pressure was zero and the stresses in the overwrap and titanium had to be in static equilibrium. From equation (10), we have

$$\sigma_T = \frac{-(tE/r)_G \epsilon}{(t/r)_T} \qquad (11)$$

Equation (11) was used after the pressure came to zero; that is, for all data taken manually with a strain indicator.

It is important to note the profound effect the computed modulus of the overwrap has on all subsequent determinations of the stress-strain and creep behavior of the titanium from the measured data. But, the overwrap modulus, in turn, is directly dependent on the initial value of elastic modulus of the titanium used in the data reduction process. The effect of changing the value for the titanium modulus is illustrated below, in the presentation of the results.

b. Test Data - To better understand the data presented, the reader is referred to figure 42, which is a schematic representation of the stress/strain characteristics of the titanium and overwrap and defines the symbols used in table X.

Column 2 in table X is the average of values of the coupon modulus transverse to the grain direction shown in table VIII. Column 3 is computed according to equation (3), and column 4 according to equation (4), using data from the bare cylinder tests. Column 5 is repeated from table IX for convenience. Columns 6 and 7 are computed from equation (9), using the initial slopes from the overwrapped specimen pressure/strain graphs where the values in column 6 are based on using E_T^c in place of E_T. Columns 9 and 10 are data recorded during the pressurizing phase of the tests. Columns 11 and 12 are computed from equation (10). (Note in column 10 that in three instances the maximum strain was 2.4%. Since there was no evidence of titanium fracture, the EB welds used to make the metal cylinders were obviously capable of

sustaining this strain level, in spite of the poor performance of specimen BRE in the biaxial tests.) The values in columns 13 and 14 are $\sigma_s = \epsilon_s E_G$.

Using equation (10) with each successive pressure/strain data point and E_G from column 6 or 7, it was possible to compute σ_T and plot σ_T vs ϵ. These plots for all specimens are given in figures 43 through 48. Four of the sheets have two stress-strain curves, one based on the coupon modulus and one based on the bare cylinder modulus. From these curves, one can pick off the values in columns 16 through 22. The unloading and reloading curve in figure 45 is explained below, in the discussion of specimen C-90.

For the creep phase of the tests, the strain/time data is shown in figures 49 through 53. A curve representing a constant strain rate of 50 x 10^{-6}/100 hours is also shown. This curve was arbitrarily located on each chart to illustrate the fact that the tests were continued until the creep rate was less than this amount, as required by the contract. Using equation (11), it was possible to compute the stress state at each time that a strain reading was taken, including, of course, that time when the creep test was considered to be over. These stress values are listed in columns 25 through 28. The differences between the end of the pressurization phase of the tests and the end of the creep tests are given in columns 31 through 35. Note that the terminations of the creep tests do not necessarily correspond exactly to a creep rate of 50 x 10^{-6}/100 hours, but rather are some arbitary points beyond the times when the creep rate fell below 50 x 10^{-6}/100 hours. Generally, the tests were terminated when the daily variation in strain readings due to temperature change, instrument drift, switch resistance, etc, was greater than any detectable strain change due to creep. This state was apparent when the readings started to reverse.

c. Data Interpretation - By using equation (11), the strain/time curves for the titanium were converted to stress/time curves. These are plotted for all tests in figure 54. Except for specimen C-2, a pair of curves is available for each specimen because of the two values of E_T used in the data analysis. However, only one is shown for each specimen in figure 54. A selection was made for E_T based on the "reasonableness" of the computed stress-strain diagrams and

consistency of approach. For example, the maximum stress computed for C-70 using E_T = 18.15 x 10^6 psi is 141 ksi, which is considerably higher than the strength of the material. Therefore, it was decided to use the coupon modulus, E_T^c for the computations for figure 54. As one would expect, the higher the stress at the start of the creep test, the more the loss in stress during the test.

In figure 55, the unloading portion of all the stress-strain diagrams was normalized along the strain axis so that they all passed through the same strain, thus providing a common starting point for the compression portion. Also shown is the state of stress at various times from the start of the creep test. This figure again illustrates the higher creep rate and greater total creep strain due to greater compressive stress at the start of creep and is notable for the departure from straight line behavior that is evident at low compressive stresses.

Several of the individual tests deserve special discussion. Creep readings were taken on specimen C-1 after the pressurization portion was finished. However, the data were very peculiar in that they seemed to have the wrong sign, that is, they seemed to indicate the titanium was growing. After thoroughly checking the polarity of the instrumentation system and finding nothing wrong, the readings were terminated. Inspection of the specimen after dismantling the fixture revealed slight bumps on the inside opposite the strain gage lead wire locations. Apparently during overwrapping the lead wires made an impression in the liner. During the creep test, these impressions yielded, relieving the strain in adjacent portions, where the strain gages were located. The strain gages recorded a decrease in compressive strain (an increase in size) while the gross change was to a smaller size. Based on this experience, it was decided in all subsequent tests to take the leads straight out through the overwrap.

After terminating the strain readings on the creep portion of the test of C-2 it was reloaded six times to the same level as during the initial pressurization. Each pressure/strain cycle exhibited hysteresis, but the strain at maximum pressure was always the same and the unloading curves, including the compression portion, were identical (fig. 44). The loading curve always had an inelastic portion the range of which depended only on how much time was permitted to elapse between

cycles. The longer the wait, the wider the hysteresis loop. On two of the six reloadings, the pressure was not allowed to drop to zero, though the titanium was in the inelastic compression range before repressurization.

During the pressurization of C-90, the Adiprene seal blew out. The titanium was already in the inelastic region. The liner was replaced and five days later another pressurization cycle was run. All electrical leads had to be disconnected to disassemble and reassemble the fixture. Still, the plot of the rerun fit the first run exactly at the point of first run maximum pressure, as can be seen in figure 45. The hysteresis in the reloading portion of the stress/strain diagram is a result of the inelastic behavior in the compression region and the small amount of creep that took place at the 40 ksi compressive stress level.

The abnormal values of modulus and Poisson's ratio determined on the unwrapped titanium cylinders bear discussing. The state of plane stress in a cylinder is defined by the equations

$$E\epsilon_h = \sigma_h - \nu\sigma_a$$

$$E\epsilon_a = \sigma_a - \nu\sigma_h \qquad (12)$$

where

E = modulus of the material

ϵ_a and σ_a = strain and stress in the axial direction

ϵ_h and σ_h = strain and stress in the hoop direction

ν = Poisson's ratio.

If there is no axial restraint, then $\sigma_a = 0$ and

$$E\epsilon_h = \sigma_h \quad (\text{or } E = \sigma_h/\epsilon_h), \qquad (13)$$

and

$$E\epsilon_a = -\nu\sigma_h \quad (\text{or } \nu = -\epsilon_a/\epsilon_h) \qquad (14)$$

Equation (13) is the classical way to determine E, that is, by measuring the major stress and strain in a uniaxial tension test. However, if there is axial restraint, then $\sigma_a \neq 0$ and we obtain

$$E = \sigma_h / \epsilon_h \left(1 - \nu \frac{\sigma_a}{\sigma_h}\right) \tag{15}$$

Taking the ratio σ_h / ϵ_h from a plot does not now give E, but rather something greater than E, since all values are positive. How much greater depends on the amount of axial restraint, that is, on the value of σ_a / σ_h. Equation (14) is the classical way of determining ν, that is, by measuring the principal strains in a uniaxial tension test. But, with $\sigma_a \neq 0$, the expression for Poisson's ratio becomes

$$\nu = - \frac{\epsilon_a}{\epsilon_h} \left\{ \frac{1 - \frac{\sigma_a}{\sigma_h} \frac{\epsilon_h}{\epsilon_a}}{1 - \frac{\sigma_a}{\sigma_h} \frac{\epsilon_a}{\epsilon_h}} \right\} \tag{16}$$

Since σ_a / σ_h is positive, and ϵ_a / ϵ_h is negative and less in absolute value than 1, the expression in brackets is always greater than 1. Thus $\nu > - (\epsilon_a / \epsilon_h)$ and taking ϵ_a / ϵ_h from a plot without multiplying by the quantity in brackets, gives a value of ν that is too low.

Referring to columns 3 and 4 in table X, both E_T and ν are higher than generally accepted values for C-90, C-70 and C-X1. Both departures from accepted values cannot be attributed simultaneously to axial restraint. If there were a consistent error in the hoop strain readings (say, a poor calibration) both E and ν would be too high but by the same percentage. Instead, the values of υ in question in table X are relatively much further from the accepted value (approx. 18%) than are the values of E_T different from the coupon value for these very sheets (approx. 3 - 8%). A combination of some axial restraint and a consistent error in the axial gage would account for the effects recorded. Assuming this to be the situation, it is instructive to estimate the amount of axial restraint present in the test of a bare cylinder, say C-70. Using equation (15) with E = 16.86 x 10^6 psi, σ_h / ϵ_h = 18.15 x 10^6

psi, and $\nu = 0.33$, we obtain $\sigma_a / \sigma_h = 0.215$. In other words, the axial stress was 21.5% of the hoop stress rather than the zero value assumed. Complete axial restraint, such as that in a pressure vessel, would yield a value of $\sigma_a / \sigma_h = 0.5$. Specimen C-70 is the worst case. The restraint computation for C-90 and C-X1, based on the same assumptions, yields $\sigma_a / \sigma_h = 0.121$ and 0.097, respectively. There is no way of knowing whether similar restraint existed when the overwrapped cylinders were tested.

4. Conclusions

In spite of some doubt which may exist about the absolute magnitude of the creep strains and stresses because of the question of axial restraint, some general conclusions may be drawn. Titanium departs from straight line behavior in compression, after having been loaded in tension, at compressive stresses whose absolute value is less than half the tensile yield strength. The determination of a compressive yield strength after tensile loading is thus quite arbitrary, and widely varying values can be obtained depending on the definition of yield strength one wishes to use. In a pressure vessel application such as the one under consideration, losses in compressive stress are quickly arrested and a state of equilibrium is reached because of the decreasing load level which accompanies the creep. Successive tensile loadings starting from a state of high compressive stress, after creep has been allowed to take place, exhibit hysteresis and some plastic deformation in both tension and compression, though the titanium always goes through essentially the same maximum tensile stress-strain point: it must, if the overwrap remains elastic.

E. LINER MATERIAL TENSION TESTS

The design of the pressure vessel of interest was sensitive to the properties of the titanium liner material. Therefore, it was decided to make the tests needed to obtain data for input to the computer program on samples of the actual material to be used in the liners. Tension tests were made at room temperature, liquid nitrogen temperature, and liquid hydrogen temperature.

1. Specimen Properties

The tension specimens were cut from three 4 x 10 ft pieces of 5Al -2.5Sn titanium (ELI) with a nominal thickness of 0.220 in. obtained from Reactive Metals, Inc. Vendor data are given in table XI; the configuration of the specimens is shown in figure 56. Corners 8.2 x 16.4 in. were cut from three plates to provide the specimen blanks. Measured dimensions of the coupons are given in table XII. Specimen designation nomenclature is given in table XXIV. Measurements were made with a machinist's micrometer, incorporating a 0.0001 in. vernier. The first letter in the designation indicates the plate from which the coupon was cut.

2. Test Plan and Set-Up

The quantities to be determined from these tests were the modulus of elasticity, yield strength, Poisson's ratio, stiffness in the inelastic region of behavior, elongation at fracture, and fracture strength, at 70°F, -320°F, and -423°F. Several measurement methods were used, including strain gages, an extensometer, and an ordinary machinist's rule. Strain gages were used to determine Poisson's ratio by straining the specimen six times within the elastic limit and recording the output of longitudinal gages three times and of transverse gages three times. The plots were also used to compute the modulus of elasticity. Strain gage output was also used to determine the yield strength and corresponding strain, and the slope of the initial portion of the inelastic region of behavior. An extensometer was mounted on the specimens tested at room temperature in order to obtain the entire stress-strain relation, including fracture strain. The resulting plots are shown in figure 57. Elongation at fracture was also measured with an ordinary machinist's scale. The disposition of each of the tensile specimens is given in table XIII.

All the tests were run in a 60,000 pound capacity BLH hydraulic testing machine fitted with an SRA-7 type recorder. The extensometer used is a custom built unit comprising strain gages mounted on flexure beams. It was calibrated by mounting it on a supermicrometer and recording the output from incremental changes. The strain gages on the test coupons were Micromeasurements Type WK-06-250BG-350 mounted with BR610 or GA-5 cement. For the cryogenic tests a specially built cryostat was fitted into the testing machine which permitted the chang-

ing of specimens without emptying. A coupon was completely immersed in the cryogen throughout its test.

3. Results

The data from the tensile tests of the liner material coupons are presented in tables XIV through XVIII. In table XIV, the unusual values of Poisson's ratio were disregarded and a room temperature value of 0.34 was determined by extrapolation from the cryogenic values. In table XV the extensometer data is presented for comparison to establish the reliability of the values measured from the strain gage outputs. The data in table XVI are self-explanatory. Except for some elongation values at -320°F, the data are consistent and agree with what was expected.

The quantities listed in table XVII were determined directly from the load/strain plots on the recorder. Since the computer program requires a bi-linear form of stress vs strain relation as input, it was necessary to linearize the recorded plots. The intersection stress, σ_I, is defined as the stress at the intersection of the elastic and inelastic slopes. It is a point that does not exist on the real curve. To get the value of the inelastic slope, a straight line was passed through the real room temperature stress versus strain curves at strains of 0.0150 and 0.0275 (fig. 58). These values were chosen because 0.0150 was the median strain in the domes at room temperature and sizing pressure (4480 psi) and 0.0275 was the maximum head strain at burst (5600 psi) as determined at the time by the effort on Task II. (See chapter I - Introduction, for vessel design pressure specifications). Thus, stress calculations would be "correct" at two critical points. The values of σ_I at the cryogenic temperatures were determined by taking the ratio of σ_I to the 0.2% offset stress at room temperature ($\sigma_{0.2}$) and multiplying by the 0.2% offset stress at the cryogenic temperature, thus:

$$(\sigma_I)_{-320} = (\sigma_{0.2})_{-320} \left(\frac{\sigma_I}{\sigma_{0.2}}\right)_{RT}$$

and (17)

$$(\sigma_I)_{-423} = (\sigma_{0.2})_{-423} \left(\frac{\sigma_I}{\sigma_{0.2}}\right)_{RT}$$

To obtain the inelastic slope values at cryogenic temperatures, a straight line was passed between σ_I and the 0.015 strain point on the real curve. These inelastic slope values were not used, however, because they were quite erratic. The values of all the properties available from the data are summarized in table XVIII, with an explanation of the means for determining the derivatives with temperature, and are the values provided for input to the design computer program. Since the computer program did not distinguish between longitudinal and transverse values, they were averaged.

F. NOL RING TESTS OF FIBERGLASS/EPOXY COMPOSITE

In order to check the quality of the preimpregnated roving obtained for overwrapping the creep specimens, some tests were made of standard NOL rings. The material was 20 end S-HTS/E796 supplied by U. S. Polymeric Corp. A cylinder 4.80 in. long, consisting of six layers was wound at 18 threads/in. on an aluminum mandrel. It was cured at 150°F for 2 hours and 300°F overnight. The surface was machined, and five rings were cut from the cylinder, then tested at room temperature. The tests were run on a 50,000 lb capacity BLH hydraulic testing machine at a head movement rate of 0.1 in./min. Data from these tests are listed in table XIV. Assuming the "rule-of-mixtures" and a fiber content of 65% by volume yields a fiber strength of approximately 435 ksi.

III. TASK II - PRESSURE VESSEL DESIGN

A. INTRODUCTION

A procedure for designing filament overwrapped pressure vessels with load bearing liners has been given by Morris, et al (ref 3) along with a companion computer program (ref 4). The procedure was extended in this study, to allow the liner thickness to vary in the heads, and the computer program was modified accordingly. This extension provides lighter weight vessel designs by varying liner thickness in the heads to approach a fully stressed design. Extensions of the analysis and computer program are given in section III.B; the vessel design is given in section III.C.

Appendix A contains additional nomenclature, the flow chart for a new subroutine "VARLINR" is shown in appendix B, and the final vessel design computer run is shown, in part, in appendix C as a sample run.

Two changes in the computer program beyond those required for variable thickness liners were made. The subroutine "TESTO" has been deleted so that the entire program is written in FORTRAN IV and the duplicate printing of the second head, when both heads are identical, has been eliminated.

B. ANALYSIS AND COMPUTER PROGRAM

Since this task consisted of extending the work of reference 4 to variable thickness liners, the discussion is limited to those parts that were changed and frequent reference to that study is made. Reference 4 lists 13 assumptions on pages D-1 and D-2. The only one of these which was relaxed is the one regarding liner thickness. In this study the liner thickness in the head can vary with radial position and this variation need not be the same for both heads. The analysis of reference 4 is divided into five sections. Two of these, Analysis of Parameters, and Cylinder Design, did not require modification since they consider conditions at the equator of the head and in the cylinder respectively.

The head design is given in section II.B of reference 4 and it required extensive modification. It is based upon linear membrane theory for the combined liner and overwrap, netting analysis (ref. 5 and 6) for the overwrap, and an assumed stress state of the liner. The membrane theory equilibrium equations (eqs. 28 and 29 of ref. 4) remain valid for a variable thickness shell and the equations for the liner stress resultant (eqs. 31 and 31a of ref. 4) are modified by using the liner thickness at a generic point,

$$t_L = t_L(X) \tag{18}$$

This causes the constant "K", as defined by equation 32a of ref 4, to become a variable

$$K = K(X) \tag{19}$$

When these changes are carried through the final equation for head shape may be written in the form given in ref 4, equation 47, by multiplying "K" of ref 4 by $t_L(X)/t_L(a)$.

The section entitled Structural Analysis, in ref 4, calculates stresses and strains. Many of the equations in this section are used for the cylinder and heads. The only change required is to replace t_L with $t_L(X)$ when an equation is applied to the head.

Vessel characteristics, such as weight, volume and performance factor, are determined in the last section. The only formula in this section which required modification is the one used to calculate liner volume in the head (eq. 80). It was modified to

$$V_{LH} = 2\pi \sum^{N} t_{LN}(\bar{X})\ \bar{X}_N \sqrt{\Delta x^2 + \Delta y^2}\ \left\{ \frac{a - \frac{t_o}{2} + t_L(a)}{a} \right\}^2 \qquad (20)$$

The bracketed quantity in this expression is the "correction factor" of reference 4.

The computer program given in reference 4 has 8 subroutines. One of these, "TESTO", was eliminated as mentioned earlier and a new subroutine,"VARLINR" was added. Two of the remaining subroutines, "RUNKUT" and "SERCYC", and the main program had to be modified. The new subroutine calculates liner thickness at each point of each head. It is called whenever liner thickness is needed and has been written so that different functional forms for liner thickness variation may be inserted by changing the equation in this subroutine. Logarithmic, parabolic, exponential, and piecewise linear variations have been run. A sketch of the piecewise linear variation is shown in figure 59. The equation for liner thickness in the "jth" interval of the "ith" (i = 1,2) head is

$$LT(i,j) = CLT(i,2j) + \frac{CLT(i,2j+2) - CLT(i,2j)}{CLT(i,2j-1) - CLT(i,2j+1)} \left[CLT(i,2j-1) - Z \right] \qquad (21)$$

This form of variation was used in the sample problem given in appendix C and the final vessel design. It affords the greatest flexibility in prescribing liner thickness.

Modifications were required in the main program for input, output, liner thickness, "K", and calling the new subroutine. Subroutine "RUNKUT" numerically integrates the differential equation of head shape; equation 47 of reference 4. Since "K" is no longer constant, "RUNKUT" was modified to calculate "K" at each point of integration. It calls "VARLINR" for liner thickness at each point. Subroutine "SERCYC" calculates stresses and strains for the vessel. It uses liner thickness in these calculations; hence it was modified to use the proper liner thickness at each point of the heads.

Seven additional input cards are required in the modified program. The first six of these cards define liner thickness variation and the seventh card takes the place of subroutine "TESTO". Table XX shows the format and symbols for these cards. The CLT(i,j) are coefficients of liner thickness variation for the "ith" head as shown in figure 59. The symbols ISOLH, IEBLH, etc, are input zero if the quantity was input; otherwise they are input one. For example, if SOLH is input (including input zero) then ISOLH is input zero and if SOLH is blank, then ISOLH is input one. Similarly, if "C" was input, then "JJ" is input zero, otherwise "JJ" is input one. These seven cards go after the design conditions cards, of ref 4, and before the service cycle cards.

Additional output consists of the above input and liner thickness at each point of the heads. The CLT(i,j)are labeled and printed on the first page of output below the output of reference 4. This is followed by ISOLH, IEBLH, ..., IEBL; JJ is printed on the next line. Liner thickness, "LT", at each point of the head is printed after overwrap thickness "T" and before radial coordinate "X".

C. VESSEL DESIGN

1. Design Criteria and Specifications

The vessel was designed for minimum weight in accordance with ref. 4, and to have the following characteristics:

1) Shape: cylinder with end closures;
2) Size: 25 in. maximum OD;
3) Volume: 7,365 $in.^3$ $\pm$ 1.5% after sizing;

4) Sizing conditions: 4,480 psi at 75°F (1.333 x operating pressure).

The performance requirements were:

1) Operating pressure: 3,360 psi;

2) Proof pressure: 4,050 psi at 160°F and -65°F (1.2 x operating pressure);

3) Burst pressure: 5,600 psi at 160°F and -65°F (1.666 x operating pressure).

Material properties used for the design were obtained from Task I, ref 3, and the Project Manager. They are shown in table XXI along with their symbols and definitions. These values were used in the sample problem shown in appendix C. In addition to the aforementioned criteria, the maximum filament stress was limited to 375,000 psi at burst; liner stress after sizing to 90,000 psi compression; and the vessel must be elastic at the operating conditions.

2. Final Design and Stress Variations

In using the modified program one must iterate on the input to achieve a final design; this is reflected in the input value of 2.763×10^5 psi for filament stress. One inputs a liner thickness variation and filament stress, observes the resulting liner and filament stresses up the heads, and adjusts the input values to achieve the desired stress levels. The liner compressive stress after sizing must be checked for buckling. Reference 3 gives the following empirical equation for buckling allowable, σ_c.

$$\sigma_c = 150{,}000\ E \left(\frac{t_t}{D}\right)^3 \qquad (22)$$

where

E = modulus of elasticity

t_t = cylinder thickness

D = cylinder diameter.

Equation (22) is based on cylinder test data though it is used in reference 3 for the heads.

Final design computer input and part of the output is shown in appendix C and plotted in figures 60 through 64. The head shape is shown in figure 60 along with three others which will

be discussed later. Numbers along the curves (10, 20, 30, ...) refer to computer integration station numbers. Figure 61 shows the liner thickness (LT) and overwrap thickness (T) vs station number and meridional arc length. Liner thickness at the juncture is 0.156 in. which is maintained in the cylinder and produces -90,000 psi stress in the liner there after sizing. Liner thickness up the head varies and produces meridional stress after sizing as shown in figure 62. Filament stress at the design condition is shown in figure 63 and its peak value is 375,000 psi. These curves show why one must iterate on input values of filament stress and liner thickness to arrive at a design with peak filament stress at design, and liner stress after sizing, of specified values (375,000 psi and 90,000 psi respectively for this program). Liner stress at sizing and design condition are shown in the upper part of figure 62. Stresses at operating conditions are shown in figure 64. These curves show that the vessel will remain elastic in operation after sizing. Substitution into the buckling allowable equation for the design shown and solving for thickness gives 0.079 in., hence the design is not buckling critical according to ref 3. The contained volume of this vessel is 7,223 $in.^3$ and its weight, excluding end bosses, is shown in table XXII. Fabrication drawings for the final design are shown in figures 65 through 71.

3. Effect of Tolerance on Liner Thickness

Additional computer runs were made to evaluate the effect of liner thickness tolerance on this design. These runs were made by changing the liner thickness in the cylinder and each input point of the head by a constant amount. The overwrap thickness was maintained at the design value, hence the design pressure is different for each run. Head shapes for these runs are shown in figure 60, stresses in figures 72 through 80, and weights in table XXIII.

4. End Boss Analysis

The design of the end boss was dictated primarily by the considerations of joining with interfacing tubing, location of the flange/dome junction and its effect on making the domes, overwrap thickness build-up control and the desire to build in some radial flexibility. The final design is shown in figure 71. Though it was felt that a boss failure was highly unlikely, a

simplified analysis for stress was performed. A schematic of the end boss is shown in figure 81 with the appropriate dimensions needed for the analysis.

1) Shear stress at A -

Resisting area = $1.25 \times 2\pi \times 0.36 = 2.827$ sq. in.

Force = $5{,}600$ psi $\times \pi \times (1.25)^2 = 27{,}490$ lb.

Stress = $\sigma_q^A = 27{,}490/2.827 = 9{,}725$ psi

2) Membrane hoop stress at B and C -

$$\sigma_h^B = p\, r_e/t_e = \frac{5600 \times 1.12}{.26} = 24{,}125 \text{ psi}$$

3) Membrane longitudinal stress at B and C -

$$\sigma_\ell^B = p\, r_e/2t_e = 24{,}125/2 = 12{,}050 \text{ psi.}$$

4) Effect of bending at C.

In order to compute the stresses due to bending of the cylindrical portion of the end boss between sections B and C, this section is considered to be fixed at C. The boundary conditions at B are taken to be such that the cylinder is free to translate radially but not to rotate; that is, that the shear is zero but there is moment. This problem is treated by Timoshenko (ref. 7). Based on his development, it can be shown that

$$M_o = \frac{p}{2\beta^2} \chi_2 (2\alpha) \qquad (23)$$

and

$$Q_o = -\frac{p}{\beta} \chi_3 (2\alpha) \qquad (24)$$

where

M_o = bending moment at C

Q_o = shear at C

$\chi_2(2\alpha)$ and $\chi_3(2\alpha)$ = trigonometric functions of 2α

$2\alpha = \beta\ell$

ℓ = twice the cylinder length

$$\beta = \sqrt[4]{3(1-\nu^2)/r_e^2\, t_e^2}$$

ν = Poisson's ratio

r_e = radius to the mid-surface

t_e = cylinder thickness

p = internal pressure.

For our case:

$r_e = 1.12$, $t_e = 0.26$, $\nu = 0.33$, so $\beta^2 = 5.615$ and $\beta = 2.370$.

For $\ell/2 = 0.40$, $\ell = 0.80$ and $\beta\ell = 2\alpha = 1.896$. From table 46 of the reference, $\chi_2(2\alpha) = 0.55$ and $\chi_3(2\alpha) = 0.89$. So,

$$M_o = \frac{0.55p}{2\beta^2} = \frac{0.55 \times 5600}{2 \times 5.615} = 202.5 \text{ in. lb./in.}$$

and

$$Q_o = -\frac{0.89p}{\beta} = -\frac{0.89 \times 5600}{2.37} = -1{,}390 \text{ lb./in.}$$

Now the flexural stress, σ_m, at C is

$$\sigma_m^C = 6M_o/h^2 \qquad (25)$$

and the shear stress, $\sigma_q^C = Q_o/h.$ (26)

Thus

$$\sigma_m^C = \frac{6 \times 202.5}{(0.26)^2} = 17{,}970 \text{ psi}$$

and

$$\sigma_q^C = -1{,}390/0.26 = -5{,}350 \text{ psi.}$$

It is inconceivable that any combination of the above stresses could cause failure in a titanium end boss, and thus it is judged that the design is adequate with respect to stress state at the design burst pressure.

IV. CONCLUDING STATEMENT

The work reported in the preceding sections permits several conclusions to be inferred regarding the expected behavior of the pressure vessel design concept considered herein.

Titanium departs from straight-line behavior in compression, after sustaining inelastic tensile stress at compressive stresses whose absolute value is less than half the tensile yield strength. The determination of a compressive yield strength, to use as a guide in selecting a liner stress after sizing, is thus quite arbitrary. After sizing, the stress in the liner will decrease with time. The rate of change of this stress will also decrease due to the elastic character of the overwrap which loads the liner. If the overwrap remains elastic, it would appear that considerable compressive stress loss can occur between successive loadings without changing the stress state in the liner at any subsequent loading to the sizing pressure level. Thus, it would appear that perhaps the use of a compressive yield stress for design criteria should be abandoned and only the liner buckling allowable considered in determining liner thickness. Should this approach be adopted, it would reinforce the need for additional study to determine a liner buckling criteria for the heads.

None of the manufacturing processes considered appear to degrade the performance of the titanium to the extent that the vessel efficiency would suffer. The processes of chemical milling, electron beam welding, and tungsten-inert gas welding all reduced the ductility of the material but sufficient inelastic capability was still available to meet the demands of the operation concept. Explosive forming did not appear to have any deleterious effect.

The design modification used in this effort (varying the liner thickness in the domes) promises to provide savings in weight over a uniformly thick liner. However, the design process is not automatic and the computer input must be iterated to achieve a final design. Manufacturing tolerances on liner thickness affect vessel weight, and maximum stress values and a tradeoff must be made between the cost of more careful processing and the cost of lower vessel efficiency.

APPENDIX A

NEW NOMENCLATURE FOR COMPUTER PROGRAM

Symbol	Units	Definition
$t_L(X)$, LT, LTS	Length	Liner thickness at a generic point of head
K(X), YAK	Dimensionless	"K", as defined by eq. 32a of ref. 4, multiplied by $t_L(X)/t_L(a)$
CLT(i,j)	Dimensionless when "j" is odd; length when "j" is even	Coefficient of liner thickness variation; see figure 59.
V_{LH}	Length cubed	Volume of liner in head

APPENDIX B

FLOW CHART FOR SUBROUTINE "VARLINR"

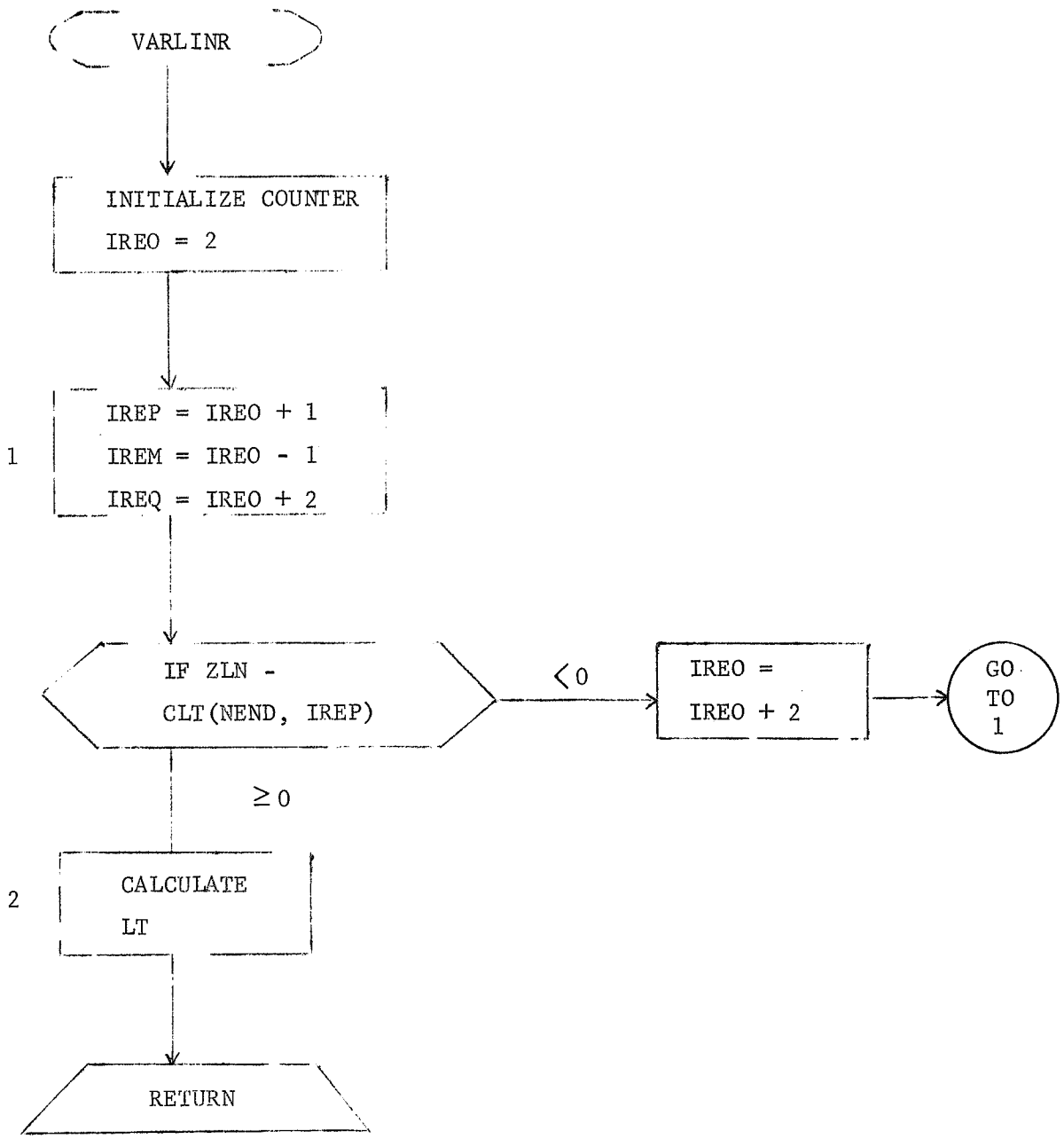

APPENDIX C

SAMPLE PROBLEM

Sample output from the modified program is shown on the following pages. Only two pages of output are shown to indicate changes that have been made. Each page of computer output has been divided into two pages in this report. Information contained in blocks is not part of the output.

PIECEWISE LINEAR LINER VARIATION
INPUT

VLEN	A	XO1	XO2	C
21.480	12.0400	1.250	1.250	.06000

RHOL	ALFL	SYL	DSYLDT	SYLC	DSYCDT
.162	.00000390	119600.0	-178.5	90000.0	-180.5

EL	DELDT	E1	DEIDT	VL	DNULDT
17.2000000E+06	-2920.0	31.0000000E+04	600.0	.34000	-.0000870

ROHG	ALFF	EF	DEFDT	B1K
.07200	20.1000000E-07	12.4000000E+06	-2410.0	.67300

PD	SOF	SOL	TR	TDF	TDL
5600.0	47.0000000E+03	0.	75.00	160.00	160.00

First part of input data page

TO	SFO	EBLH	TL	SOLH	CYLN
-0.	2.7630000E+05	-0.	.1560	0.	

EBL
-0.

CLT(1, 1)	CLT(1, 2)	CLT(1, 3)	CLT(1, 4)	CLT(1, 5)	CLT(1, 6)
1.0000000E+00	1.5600000E-01	9.9500000E-01	1.0500000E-01	6.4500000E-01	1.1600000E-01
CLT(1, 7)	CLT(1, 8)	CLT(1, 9)	CLT(1,10)	CLT(1,11)	CLT(1,12)
5.2500000E-01	1.3100000E-01	4.0000000E-01	1.5100000E-01	2.7500000E-01	1.8500000E-01
CLT(1,13)	CLT(1,14)	CLT(1,15)	CLT(1,16)	CLT(1,17)	CLT(1,18)
1.8000000E-01	2.4400000E-01	5.0000000E-02	3.1000000E-01	-0.	-0.
CLT(2, 1)	CLT(2, 2)	CLT(2, 3)	CLT(2, 4)	CLT(2, 5)	CLT(2, 6)
1.0000000E+00	1.5600000E-01	9.9500000E-01	1.0500000E-01	6.4500000E-01	1.1600000E-01
CLT(2, 7)	CLT(2, 8)	CLT(2, 9)	CLT(2,10)	CLT(2,11)	CLT(2,12)
5.2500000E-01	1.3100000E-01	4.0000000E-01	1.5100000E-01	2.7500000E-01	1.8500000E-01
CLT(2,13)	CLT(2,14)	CLT(2,15)	CLT(2,16)	CLT(2,17)	CLT(2,18)
1.8000000E-01	2.4400000E-01	5.0000000E-02	3.1000000E-01	-0.	-0.

0 1 0 0 1 0 1
0

Second part of input data page

PIECEWISE LINEAR LINER VARIATION

DESIGN DATA FOR BALANCED IN PLANE WRAP CONTOUR

CONTOUR INPUT DATA ABIG = .116387 C = .022185 V LEN = 21.480000

	1	2	3	4	5	6
Z	1.00000000E+00	9.99926893E-01	9.99707279E-01	9.99340274E-01	9.98824398E-01	9.98157557E-01
U	0.	1.00000000E-02	2.00000000E-02	3.00000000E-02	4.00000000E-02	5.00000000E-02
PHI	9.00002426E+01	8.91620663E+01	8.83211020E+01	8.74741073E+01	8.66180221E+01	8.57497444E+01
ALPHA	6.64025706E+00	6.65903692E+00	6.67841045E+00	6.69844038E+00	6.71918444E+00	6.74069512E+00
THETA	8.87288386E+01	8.86620384E+01	8.85950208E+01	8.85277545E+01	8.84602073E+01	8.83923450E+01
R ONE	8.23717283E+00	8.22344424E+00	8.18210227E+00	8.11387091E+00	8.01992316E+00	7.90183689E+00
R TWO	1.20400000E+01	1.20404075E+01	1.20416451E+01	1.20437588E+01	1.20468265E+01	1.20509594E+01
T	8.59982096E-02	8.60077836E-02	8.60300787E-02	8.60652012E-02	8.61133197E-02	8.61746673E-02
LT	1.56000000E-01	1.55254306E-01	1.53014242E-01	1.49270800E-01	1.44008863E-01	1.37207077E-01
X	1.20400000E+01	1.20391198E+01	1.20364756E+01	1.20320569E+01	1.20258458E+01	1.20178170E+01
Y	0.	1.20400000E-01	2.40800000E-01	3.61200000E-01	4.81600000E-01	6.02000000E-01
XFO	1.20415882E+01	1.20821191E+01	1.20794722E+01	1.20750477E+01	1.20688274E+01	1.20607858E+01
YFO	4.29697626E-02	1.21028921E-01	2.42060283E-01	3.63096507E-01	4.84140038E-01	6.05193352E-01
XFI	1.20384118E+01	1.19961205E+01	1.19934791E+01	1.19890661E+01	1.19828641E+01	1.19748481E+01
YFI	-4.29697626E-02	1.19771079E-01	2.39539717E-01	3.59303493E-01	4.79059962E-01	5.98806648E-01
XM	1.20326496E+01	1.18408828E+01	1.18405305E+01	1.18399403E+01	1.18391060E+01	1.18380184E+01
YM	-1.98863310E-01	1.17500526E-01	2.35056606E-01	3.52724918E-01	4.70564459E-01	5.88637755E-01
SOL	0.	0.	0.	0.	0.	0.
SOLH	0.	0.	0.	0.	0.	0.
SOF	4.70000000E+04	4.70000000E+04	4.70000000E+04	4.70000000E+04	4.70000000E+04	4.70000000E+04
EOL	0.	0.	0.	0.	0.	0.
EOLH	0.	0.	0.	0.	0.	0.
EOF	3.79032258E-03	3.79032258E-03	3.79032258E-03	3.79032258E-03	3.79032258E-03	3.79032258E-03

First part of design data page

SOLP	-1.36250937E+04	-1.36773232E+04	-1.38373037E+04	-1.41132630E+04	-1.45201223E+04	-1.50816234E+04
SOLHP	-1.84650455E+02	-1.86417732E+02	-1.89707230E+02	-1.94663625E+02	-2.01529247E+02	-2.10677349E+02
SOFP	3.72225188E+04	3.71852982E+04	3.70707698E+04	3.68730372E+04	3.65814030E+04	3.61788422E+04
EOLP	-7.88506546E-04	-7.91508209E-04	-8.00744373E-04	-8.16690545E-04	-8.40209437E-04	-8.72674017E-04
EOLHP	2.58597757E-04	2.59527452E-04	2.62498606E-04	2.67665453E-04	2.75308856E-04	2.85876431E-04
EOFP	3.00181604E-03	2.99881437E-03	2.98957821E-03	2.97363204E-03	2.95011314E-03	2.91764856E-03
SOLT	-1.39738265E+04	-1.40274136E+04	-1.41915570E+04	-1.44747024E+04	-1.48921657E+04	-1.54683190E+04
SOLHT	-1.89376563E+02	-1.91189356E+02	-1.94563987E+02	-1.99648942E+02	-2.06692952E+02	-2.16079155E+02
SOFT	3.81752252E+04	3.81371083E+04	3.80198307E+04	3.78173523E+04	3.75187140E+04	3.71064744E+04
EOLT	-4.89111318E-04	-4.92236892E-04	-5.01853631E-04	-5.18456826E-04	-5.42945108E-04	-5.76748681E-04
EOLHT	5.94503811E-04	5.95448285E-04	5.98469811E-04	6.03725335E-04	6.11500697E-04	6.22251489E-04
EOFT	3.30121126E-03	3.29808569E-03	3.28846895E-03	3.27186575E-03	3.24737747E-03	3.21357390E-03
SBL	1.14964565E+05	1.15006241E+05	1.15131039E+05	1.15339975E+05	1.15634754E+05	1.16017800E+05
SBLH	1.14964593E+05	1.14965162E+05	1.14966878E+05	1.14969776E+05	1.14973904E+05	1.14979321E+05
SFO	2.76299829E+05	2.77698103E+05	2.81884978E+05	2.88894210E+05	2.98782589E+05	3.11631007E+05
EDL	1.90370613E-02	1.91517195E-02	1.94950425E-02	2.00697982E-02	2.08806434E-02	2.19342112E-02
EDLH	1.90371771E-02	1.89810296E-02	1.88129333E-02	1.85315773E-02	1.81347306E-02	1.76192004E-02
EFO	2.28273839E-02	2.29420421E-02	2.32853651E-02	2.38601208E-02	2.46709660E-02	2.57245338E-02

Second part of design data page

SYMBOLS

The reader is referred also to appendix A and table XXI.

D = cylinder diameter

E = Young's modulus

E_G = modulus of the overwrap in the fiber direction

E_T = modulus of titanium

E_T^c = modulus of titanium measured from coupon tests

E_2 = slope of tensile inelastic portion of titanium stress vs strain diagram

GN_2 = gaseous nitrogen

h_o = original biaxial plate thickness

ℓ = length of fixed-fixed cylinder

LH_2 = liquid hydrogen

LN_2 = liquid nitrogen

M_o = unit bending moment

n = slope of σ_t vs ϵ_t diagram in the inelastic region

p = pressure

p_b = burst pressure

p_G = proportion of pressure loading carried by cylinder overwrap

p_T = proportion of pressure loading carried by titanium cylinder

Q_o = unit shear

r_e = radius of end boss cylinder section at mid-surface

r_G = radius to mid-surface of cylinder overwrap

r_h = radius of curvature of hemispherical domes

r_o = original biaxial circular plate radius

r_T = radius to mid-surface of bare titanium cylinder

t_e = thickness of end boss cylinder section

t_G = thickness of cylinder overwrap

t_t = wall thickness of bare cylinder

$\alpha = \beta\ell/2$

$\beta = \sqrt[4]{3(1 - \nu^2)/r_e^2\, t_e^2}$

ϵ = strain

ϵ_a = axial strain

ϵ_e = strain at termination of creep test

ϵ_G = strain in the overwrap

ϵ_h = hoop strain

ϵ_o = strain at zero cylinder stress

ϵ_I = strain corresponding to σ_I

ϵ_r = strain at maximum cylinder compressive stress

ϵ_s = maximum strain in cylinder overwrap

ϵ_t = true strain

ϵ_T = strain in the titanium

ν = Poisson's Ratio

σ_a = axial stress

σ_c = critical buckling stress

σ_{eG} = stress in overwrap at termination of creep test

σ_{eT} = stress in titanium at termination of creep test

σ_G = stress in the fiberglass/epoxy overwrap

σ_h = hoop stress

σ_I = intersection stress, defined as the intersection of the elastic and linearized inelastic portions of the titanium stress vs strain diagram

σ_ℓ = longitudinal stress

σ_m = flexural stress

σ_{mc} = maximum cylinder compressive stress

σ_{mt} = maximum cylinder tensile stress

$\sigma_o = \sigma_t/(\epsilon_t)^n$

σ_q = shear stress

σ_r = stress in overwrap at zero pressure

σ_s = maximum stress in cylinder overwrap

σ_t = true stress

σ_T = stress in the titanium

σ_u = engineering tensile strength

$\sigma_{0.2}$ = 0.2% offset stress

$\chi_2(2\alpha)$ and $\chi_3(2\alpha)$ = trigonometric functions of (2α) in bending theory of shells

REFERENCES

1. Morris, E. E.: Glass-Fiber Reinforced Metallic Tanks for Cryogenic Service. NASA CR-72224, July, 1967.

2. Storåkers, B.: "Finite Plastic Deformation of a Circular Membrane under Hydrostatic Pressure". International Journal of Mechanical Sciences, October, 1966.

3. Morris, E. E., Darms, F. J., Landes, R. E., and Campbell, J. W.: "Parametric Study of Glass-Filament-Reinforced Metal Pressure Vessels." NASA CR-54-855, April, 1966.

4. "Computer Program for the Analysis of Filament-Reinforced Metal-Shell Pressure Vessels." Contract NAS3-6292, Aerojet-General Corp., May, 1966. NASA CR-72124.

5. Schultz, J. C.: "Netting Analysis of Filament-Wound Pressure Vessels." ASME 63WA-223.

6. Rosato, D. V., and Grove, C. S., Jr.: Filament Winding, Interscience Publishers, New York, 1964.

7. Timoshenko, S. P.: Theory of Plates and Shells. McGraw-Hill, New York, First Edition, 1940, p. 402.

TABLE I. - PROPERTIES OF 5AL-2.5SN TI (ELI)
USED FOR TASK I - PRELIMINARY TESTS
(Vendor data)

Supplier - Titanium Metals Corporation of America

Heat Number G-7622 Test Number J-5379

Nominal Thickness - 0.220 in. (0.5588 cm)

Element	Percent
Carbon	0.022
Iron	0.15
Nitrogen	0.008
Aluminum	5.0
Hydrogen	0.005
Tin	2.6
Manganese	0.003
Oxygen	0.06

Grain Direction	Yield Strength psix10^3	Yield Strength $N/cm^2 x 10^3$	Tensile Strength psix10^3	Tensile Strength $N/cm^2 x 10^3$	Elongation %
Longitudinal	109.9	75.77	116.0	79.98	18.5
Transverse	113.3	78.12	117.3	80.88	19.5

TABLE II. - CROSS-SECTION DIMENSIONS OF PRELIMINARY TENSILE SPECIMENS

Specimen No.	Grain Direc.*	Surface Treatment	Width		Thickness		Area	
			in.	cm.	in.	cm.	sq. in.	sq. cm.
PL250-1	L	As received	0.4772	1.212	0.2140	0.5436	0.1021	0.6587
PL250-2	L	As received	0.4935	1.253	0.2143	0.5443	0.1058	0.6826
PL250-3	L	As received	0.4542	1.154	0.2154	0.5471	0.0978	0.6310
PL250-4	L	As received	0.4981	1.265	0.2183	0.5545	0.1087	0.7013
PT250-1	T	As received	0.4940	1.254	0.2162	0.5491	0.1068	0.6890
PT250-2	T	As received	0.4993	1.268	0.2152	0.5466	0.1074	0.6929
PT250-3	T	As received	0.4893	1.243	0.2145	0.5448	0.1050	0.6774
T63M-1	L	Machined	0.4993	1.268	0.0625	0.1588	0.0312	0.2013
T63C-1	L	Chem-milled	0.3390	0.861	0.0640	0.1626	0.0217	0.1400

*L - Longitudinal, T - Transverse

TABLE III. - RESULTS OF PRELIMINARY TENSION TESTS

Specimen No.	Elastic Tensile Modulus		Poisson's Ratio	Yield Strength (0.2% offset)		Inelastic Slope		Tensile Strength		Elongation %
	psix10^6	$N/cm^2 x10^6$		psix10^3	$N/cm^2 x10^3$	psix10^3	$N/cm^2 x10^3$	psix10^3	$N/cm^2 x10^3$	
PL250-1	17.00	11.72	0.33	105.6	72.8	-	-	111.6	76.9	17.5
PL250-2*	17.08	11.78	0.31	-	-	-	-	-	-	-
PL250-3	16.67	11.49	0.33	108.4	74.7	-	-	112.5	77.6	15.5
PL250-4	16.07	11.08	0.33	107.6	74.2	99.0	68.2	113.1	78.0	18
PT250-1	17.00	11.72	0.32	109.5	75.5	80.5	55.5	113.9	78.5	19
PT250-2	16.79	11.58	0.34	108.4	74.7	83.8	57.8	113.6	78.3	18
PT250-3	17.31	11.93	0.34	104.6	72.1	126.0	86.9	111.5	76.9	17
T63M-1	16.09	11.09	0.32	110.0	75.8	-	-	116.8	80.5	18
T63C-1	16.60	11.44	0.31	107.2	73.9	-	-	113.3	78.1	12

*This specimen was not tested beyond the elastic range

TABLE IV. - PROPERTIES OF 5AL -2.5SN TI (ELI)
USED FOR TASK I - BIAXIAL TESTS
(Vendor data)

Supplier - Titanium Metals Corporation of America

Heat Number D-9453 Test Number F-3776

Nominal Thickness - 0.062 in. (0.157 cm)

Element	Percent
Carbon	0.026
Iron	0.150
Nitrogen	0.012
Aluminum	5.0
Hydrogen	0.009
Tin	2.3
Manganese	0.007
Oxygen	0.09

Grain Direction	Yield Strength		Tensile Strength		Elongation
	$psix10^3$	N/cm^2x10^3	$psix10^3$	N/cm^2x10^3	%
Longitudinal	109.7	75.6	120.8	83.3	16.5
Transverse	109.9	75.8	119.2	82.2	17

TABLE Va. - RESULTS OF CHARACTERIZATION TESTS ON BIAXIAL SPECIMEN
MATERIAL (5Al-2.5Sn Titanium, ELI)
(U. S. Customary Units)

Specimen No.	Width in.	Thickness in.	Area sq. in.	Elastic Modulus psi x 10^6	0.2% Offset Stress psi x 10^3	Tensile Strength psi x 10^3	Elongation %	Grain Direction**
T63BL-1	0.4953	0.0627	0.0311	15.90*	112.5	123.4	12	L
T63BL-2	0.4983	0.0626	0.0312	14.95	110.9	123.0	15½	L
T63BL-3	0.5021	0.0622	0.0312	15.40	112.5	122.8	16	L
T63BT-1	0.4838	0.0625	0.0302	16.63*	116.5	121.5	18	T
T63BT-2	0.4889	0.0610	0.0298	16.30	116.0	120.9	14	T
T63BT-3	0.4966	0.0603	0.0299	16.10	116.8	123.7	13	T

*Strain gages (others used microformer) **L - Longitudinal, T - Transverse

TABLE Vb. - RESULTS OF CHARACTERIZATION TESTS ON BIAXIAL SPECIMEN
MATERIAL (5Aℓ-2.5Sn Titanium, ELI)
(International System of Units)

Specimen No.	Width cm.	Thickness cm.	Area sq. cm.	Elastic Modulus $N/cm^2 \times 10^6$	0.2% Offset Stress $N/cm^2 \times 10^3$	Tensile Strength $N/cm^2 \times 10^3$	Elongation %	Grain Direction**
T63BL-1	1.258	0.1593	0.2006	10.96*	77.57	85.08	12	L
T63BL-2	1.266	0.1590	0.2013	10.31	76.46	84.81	15½	L
T63BL-3	1.275	0.1580	0.2013	10.62	77.57	84.67	16	L
T63BT-1	1.229	0.1588	0.1948	11.47*	80.32	83.77	18	T
T63BT-2	1.242	0.1549	0.1923	11.24	79.98	83.36	14	T
T63BT-3	1.261	0.1532	0.1929	11.10	80.53	85.29	13	T

*Strain gages (other used microformer) **L - Longitudinal, T - Transverse

TABLE VI. - BIAXIAL TEST SPECIMENS

Designation	Specimen Type	Type of Weldment	Test Temperature °F	Test Temperature °K	Thickness Minimum in.	Thickness Minimum cm.	Thickness Maximum in.	Thickness Maximum cm.	Burst Pressure psi	Burst Pressure N/cm^2	Maximum Residual Strain %	Time to Maximum Pressure seconds
BRO	Flat plate	None	70	294	0.040	0.102	0.041	0.104	2390	1650	10.0	52
BNO	Flat plate	None	-320	77	0.040	0.102	0.041	0.104	3700	2550	10.0	338
BHO	Flat plate	None	-423	20	0.041	0.104	0.042	0.107	2580	1780	8.5	87
BRE	Flat plate	Electron Beam	70	294	0.035	0.089	0.040	0.102	900	620	1.6	110
BNE	Flat plate	Electron Beam	-320	77	0.036	0.091	0.039	0.099	2140	1475	3.0	398
BHE	Flat plate	Electron Beam	-423	20	0.037	0.094	0.039	0.099	2070	1425	2.4	68
BRT	Flat plate	Tung. Inert Gas	70	294	0.035	0.089	0.038	0.096	1240	855	4.1	108
BNT	Flat plate	Tung. Inert Gas	-320	77	0.039	0.099	0.040	0.102	1670	1150	4.6	115
BHT	Flat plate	Tung. Inert Gas	-423	20	0.039	0.099	0.042	0.107	1700	1170	6.6	35
BRD	Dome	None	70	294	0.040	0.102	0.042	0.107	3120	2150	-	118
BND	Dome	None	-320	77	0.040	0.102	0.043	0.109	4390	3025	-	79
BHD	Dome	None	-423	20	0.040	0.102	0.042	0.107	1980	1365	-	6

Designation	Remarks
BRO	Figure 13
BNO	Figure 14 — Maximum strain not measured perpendicular to failure. The perpendicular strain is at least this much.
BHO	Figures 15, 16 — Maximum strain not measured perpendicular to failure. The perpendicular strain is at least this much.
BRE	Figures 17, 18, 19 — Ruptured along undercut side of weld.
BNE	Figures 20, 21, 22 — Ruptured along weld margin.
BHE	Figures 23, 24 — Rupture same as BRE.
BRT	Figures 25, 26 — Ruptured along heat-affected zone of weld.
BNT	Figures 27, 28 — Maximum strain value within grid. Failure was entirely outside grid.
BHT	Figures 29, 30 — Ruptured in weld heat-affected zone.
BRD	Figure 31 — Failed at flange weld, no residual strain measurements.
BND	Figure 32 — No rupture - fixture capability limit, no residual strain measurements.
BHD	Figure 33 — Failed at flange weld, no residual strain measurements.

TABLE VII. - PROPERTIES OF 5AL -2.5SN TI (ELI) USED FOR TASK I - CREEP TESTS (Vendor data)

Supplier - Titanium Metals Corporation of America

Heat Number D-9453 Test Number F-3776

Nominal Thickness - 0.062 in. (0.157 cm.)

Element	Percent
Carbon	0.026
Iron	0.150
Nitrogen	0.012
Aluminum	5.0
Hydrogen	0.008
Tin	2.3
Manganese	0.007
Oxygen	0.09

Grain Direction	Yield Strength		Tensile Strength		Elongation %
	psix10^3	N/cm^{2}x10^3	psix10^3	N/cm^{2}x10^3	
Longitudinal	110.4	76.12	125.5	86.53	16.0
Transverse	115.8	79.84	123.7	85.29	17.0

TABLE VIIIa. - RESULTS OF CHARACTERIZATION TESTS ON CREEP SPECIMEN MATERIAL (5Al -2.5 Sn Titanium, ELI) (U. S. Customary Units)

Specimen No.	Width in.	Thickness in.	Area sq. in.	Elastic Modulus psi x 10^6	0.2% Offset Stress psi x 10^3	Tensile Strength psi x 10^3	Elongation %	Grain Direction**
T63AL-1	0.5016	0.0617	0.0309	16.27*	112.6	123.1	14	L
T63AL-2	0.5023	0.0621	0.0312	15.82	110.9	122.0	13	L
T63AL-3	0.5000	0.0619	0.0310	16.11	110.2	122.0	14	L
T63AT-1	0.4895	0.0620	0.0303	17.18	116.2	120.9	13	T
T63AT-2	0.4877	0.0622	0.0303	16.78	116.5	121.5	15½	T
T63AT-3	0.5005	0.0625	0.0313	16.61	115.8	120.9	15	T
			Average	16.86				

*Strain gages (others used microformer) **L - Longitudinal, T - Transverse

TABLE VIIIb. - RESULTS OF CHARACTERIZATION TESTS ON CREEP SPECIMEN MATERIAL
(5Al-2.5Sn Titanium, ELI)
(International System of Units)

Specimen No.	Width cm.	Thickness cm.	Area sq. cm.	Elastic Modulus $N/cm^2 \times 10^6$	0.2% Offset Stress $N/cm^2 \times 10^3$	Tensile Strength $N/cm^2 \times 10^3$	Elongation %	Grain Direction**
T63AL-1	1.274	0.1567	0.1994	11.22	77.6	84.9	14	L
T63AL-2	1.276	0.1577	0.2013	10.91	76.5	84.1	3	L
T63AL-3	1.270	0.1572	0.2000	11.11	76.0	84.1	14	L
T63AT-1	1.243	0.1575	0.1955	11.84	80.1	83.4	13	T
T63AT-2	1.239	0.1580	0.1955	11.57	80.3	83.8	15½	T
T63AT-3	1.271	0.1588	0.2019	11.45	79.8	83.4	15	T
			Average	11.62				

*Strain gages (others used microformer) **L - Longitudinal, T - Transverse

TABLE IX. - DIMENSIONS OF CREEP SPECIMENS

U.S. CUSTOMARY UNITS

Specimen No.	Length: At Weld, in.	Length: 180° From Weld, in.	Inside Diameter: At Weld, in.	Inside Diameter: 90° From Weld, in.	Tool	Overwrap: Thickness: Range, in.	Overwrap: Thickness: Average, in.	Number of Layers and Threads/Inch
C-1	13.92	14.00	9.882	9.868	Inside Micrometer	0.108-0.114	0.111	8@16 and 2@14
C-2	13.96	13.98	9.882	9.869		0.121-0.127	0.124	*7@18 and 3@14
C-3	13.89	13.92	9.887	9.887		-	-	Not used
C-70	13.94	13.94	9.890	9.895	Vernier Calipers	0.057-0.061	0.059	*5@18
C-80	13.94	13.96	9.908	9.894		0.083-0.086	0.084	6@18 and 1@16
C-90	13.92	13.94	9.882	9.898		0.075-0.079	0.077	5@18 and 2@13
C-X1	13.94	13.94	9.856	9.861		0.048-0.053	0.051	3@18,1@10,1@9
C-X2	13.94	13.95	9.904	9.888		-	-	Not used

INTERNATIONAL SYSTEM OF UNITS

Specimen No.	Length: At Weld, cm.	Length: 180° From Weld, cm.	Inside Diameter: At Weld, cm.	Inside Diameter: 90° From Weld, cm.	Tool	Overwrap Thickness: Range, cm.	Overwrap Thickness: Average, cm.	Remarks
C-1	3.536	3.556	25.10	25.06		0.274-0.290	0.282	
C-2	3.546	3.551	25.10	25.07		0.307-0.323	0.315	
C-3	3.528	3.536	25.11	25.11		-	-	
C-70	3.541	3.541	25.12	25.13		0.145-0.155	0.150	
C-80	3.541	3.546	25.17	25.13		0.211-0.218	0.214	
C-90	3.536	3.541	25.10	25.14		0.190-0.201	0.196	
C-X1	3.541	3.541	25.03	25.05		0.122-0.135	0.129	
C-X2	3.541	3.543	25.16	25.12		-	-	

* Probable arrangement. Data not available

TABLE Xa. - CREEP TEST PARAMETERS AND RESULTS
(U. S. Customary Units)

Specimen Designation (1)	Coupon Tensile Modulus psix10^6 E_T^c (2)	Bare Cylinder Data: Tensile Modulus psi x 10^6 E_T (3)	Bare Cylinder Data: Poisson's Ratio ν (4)	Overwrap Thickness in. (5)	Overwrap Modulus, E_G, psi x 10^6: Using E_T^c (6)	Overwrap Modulus, E_G, psi x 10^6: Using E_T (7)
C-1	16.86	-	-	0.111	8.36	-
C-2	16.86	-	-	0.124	8.29	-
C-90	16.86	17.55	0.395	0.077	9.34	8.78
C-80	16.86	15.65	0.339	0.084	8.38	9.30
C-70	16.86	18.15	0.396	0.059	9.40	8.03
C-X1	16.86	17.40	0.383	0.051	8.98	8.32

Specimen Designation (8)	Maximum Pressure psi (9)	Maximum Tensile Strain ϵ_s, x 10^{-6} (10)	Maximum Tensile Stress in Metal, σ_{mt}, ksi: Using E_T^c (11)	Maximum Tensile Stress in Metal, σ_{mt}, ksi: Using E_T (12)	Maximum Tensile Stress in Overwrap, σ_s, ksi: Using E_T^c (13)	Maximum Tensile Stress in Overwrap, σ_s, ksi: Using E_T (14)
C-1	5890	23950	119.4	-	200.2	-
C-2	6400	23970	122.6	-	198.7	-
C-90	4515	22000	109.7	124.8	205.5	193.2
C-80	4990	24020	131.1	106.8*	201.4	223.5
C-70	3840	22080	113.6**	141.0	207.6	177.3
C-X1	3430	22100	113.8	125.7	198.6	183.8

*At $\epsilon = 9450 \times 10^{-6}$; **At $\epsilon = 15000 \times 10^{-6}$

TABLE Xa (cont)

Specimen Designation (15)	Strain at Zero Metal Stress ϵ_o, x 10^{-6}		Beginning of Creep Test				
			Strain at Maximum Compressive Stress ϵ_r, x 10^{-6}	Maximum Compressive Stress, σ_{mc}, ksi		Stress in Overwrap at Zero Pressure, σ_r, ksi	
	Using E_T^c (16)	Using E_T (17)	(18)	Using E_T^c (19)	Using E_T (20)	Using E_T^c (21)	Using E_T (22)
C-1	16850	-	7100	102.9	-	59.4	-
C-2	16150	-	6230	98.0	-	51.6	-
C-90	15130	14500	7600	86.1	80.9	71.0	66.7
C-80	16090	17450	7820	85.8	95.4	65.6	72.8
C-70	15150	13950	8600	75.9	64.8	80.9	69.0
C-X1	15560	15030	9850	71.9	66.6	88.5	81.9

Specimen Designation (23)	Strain ϵ_e x 10^{-6} (24)	End of Creep Test			
		Stress in Overwrap, σ_{eG}, ksi		Stress in Metal, σ_{eT}, ksi	
		Using E_T^c (25)	Using E_T (26)	Using E_T^c (27)	Using E_T (28)
C-1	-	-	-	-	-
C-2	5315	44.1	-	86.3	-
C-90	6830	63.8	60.0	78.1	73.4
C-80	6720	56.4	62.5	75.1	83.4
C-70	8020	75.4	64.4	70.8	60.4
C-X1	9215	82.8	76.6	67.3	62.2

TABLE Xa (concl)

Specimen Designation (29)	Elapsed Time min. (30)	Strain Change $\Delta\epsilon$, x 10^{-6} (31)	Stress Change in Metal, $\Delta\sigma_T$, ksi		Stress Change in Overwrap, $\Delta\sigma_G$, ksi	
			Using E_T^c (32)	Using E_T (33)	Using E_T^c (34)	Using E_T (35)
C-1	-	-	-	-	-	-
C-2	7045	915	11.7	-	7.5	-
C-90	4623	770	8.0	7.5	7.2	6.7
C-80	8469	1100	10.7	12.0	9.2	10.3
C-70	6149	580	5.1	4.4	5.5	4.6
C-X1	7239	635	4.6	4.4	5.7	5.3

TABLE Xb. - CREEP TEST PARAMETERS AND RESULTS
(International System of Units)

Specimen Designation (1)	Coupon Tensile Modulus, $N/cm^2 \times 10^6$ E_T^c (2)	Bare Cylinder Data: Tensile Modulus, $N/cm^2 \times 10^6$ E_T (3)	Bare Cylinder Data: Poisson's Ratio ν (4)	Overwrap Thickness cm. (5)	Overwrap Modulus, E_G: Using E_T^c $N/cm^2 \times 10^6$ (6)	Overwrap Modulus, E_G: Using E_T $N/cm^2 \times 10^6$ (7)
C-1	11.62	-	-	0.282	5.76	-
C-2	11.62	-	-	0.315	5.72	-
C-90	11.62	12.10	0.395	0.196	6.44	6.05
C-80	11.62	10.79	0.339	0.214	5.78	6.41
C-70	11.62	12.51	0.396	0.150	6.48	5.54
C-X1	11.62	12.00	0.383	0.129	6.19	5.74

Specimen Designation (8)	Maximum Pressure N/cm^2 (9)	Maximum Tensile Strain, $\epsilon_s \times 10^{-6}$ (10)	Maximum Tensile Stress in Metal, σ_{mt}, $N/cm^2 \times 10^3$: Using E_T^c (11)	Maximum Tensile Stress in Metal, σ_{mt}, $N/cm^2 \times 10^3$: Using E_T (12)	Maximum Tensile Stress in Overwrap, σ_s, $N/cm^2 \times 10^3$: Using E_T^c (13)	Maximum Tensile Stress in Overwrap, σ_s, $N/cm^2 \times 10^3$: Using E_T (14)
C-1	4060	23950	82.3	-	138.0	-
C-2	4410	23970	84.5	-	137.0	-
C-90	3115	22000	75.6	86.0	141.7	133.2
C-80	3440	24020	90.4	73.6*	138.9	154.1
C-70	2650	22080	78.3**	97.2	143.1	122.2
C-X1	2365	22100	78.5	86.7	136.9	126.7

*At $\epsilon = 9450 \times 10^{-6}$; **At $\epsilon = 15000 \times 10^{-6}$

TABLE Xb (cont)

Specimen Designation (15)	Beginning of Creep Test: Strain at Zero Metal Stress, ϵ_o, x 10^{-6}		Strain at Max. Compressive Stress, ϵ_r, x 10^{-6}	Maximum Compressive Stress, σ_{mc}, $N/cm^2 x 10^3$		Stress in Overwrap at Zero Pressure σ_r, $N/cm^2 x 10^3$	
	Using E_T^c (16)	Using E_T (17)	(18)	Using E_T^c (19)	Using E_T (20)	Using E_T^c (21)	Using E_T (22)
C-1	16850	-	7100	70.9	-	41.0	-
C-2	16150	-	6230	67.6	-	35.6	-
C-90	15130	14500	7600	59.4	55.8	49.0	46.0
C-80	16090	17450	7820	59.2	65.8	45.2	50.2
C-70	15150	13950	8600	52.3	44.7	55.8	47.6
C-X1	15560	15030	9850	49.6	45.9	61.0	56.5

Specimen Designation (23)	End of Creep Test: Strain ϵ_e x 10^{-6} (24)	Stress in Overwrap σ_{eG}, $N/cm^2 x 10^3$		Stress in Metal σ_{eT}, $N/cm^2 \times 10^3$	
		Using E_T^c (25)	Using E_T (26)	Using E_T^c (27)	Using E_T (28)
C-1	-	-	-	-	-
C-2	5315	30.4	-	59.5	-
C-90	6830	44.0	41.4	53.8	50.6
C-80	6720	38.9	43.1	51.8	57.5
C-70	8020	52.0	44.4	48.8	41.6
C-X1	9215	57.1	52.8	46.4	42.9

TABLE Xb (concl)

Specimen Designation (29)	Elapsed Time Min. (30)	Strain Change $\Delta\epsilon$, x 10^{-6} (31)	Stress Change in Metal, $\Delta\sigma_T$, $N/cm^2 x 10^3$		Stress Change in Overwrap, $\Delta\sigma_G$, $N/cm^2 x 10^3$	
			Using E_T^c (32)	Using E_T (33)	Using E_T^c (34)	Using E_T (35)
C-1	-	-	-	-	-	-
C-2	7045	915	8.1	-	5.2	-
C-90	4623	770	5.5	5.2	5.0	4.6
C-80	8469	1100	7.4	8.3	6.3	7.1
C-70	6149	580	3.5	3.0	3.8	3.2
C-X1	7239	635	3.2	3.0	3.9	3.6

TABLE XI. - PROPERTIES OF 5AL-2.5SN TI (ELI)
USED FOR LINER COUPON TESTS
(Vendor data)

Supplier - Reactive Metals, Incorporated

Specification - MIL-T-9046F Type II Comp. B

Ingot No. 294455, Lot 01

Nominal Thickness - 0.220 in. (0.5588 cm.)

Element	Percent
Carbon	0.02
Nitrogen	0.012
Iron	0.05
Aluminum	5.2
Tin	2.6
Manganese	< 0.01
Oxygen	0.109
Hydrogen	81 parts/million

Grain Direction	Yield Strength (0.2% Offset) psi x 10^3	Tensile Strength psi x 10^3	Elongation %
Longitudinal	109.6-113.5	120.8-124.8	14
Transverse	118.5-123.3	120.9-131.2	12-13
	N/cm^2 x 10^3	N/cm^2 x 10^3	
Longitudinal	75.6-78.2	83.3-86.0	
Transverse	81.7-85.0	83.4-90.5	

Annealed at 1500°F for 30 minutes and air cooled

TABLE XII. - LINER MATERIAL COUPON DIMENSIONS

Specimen Designation	Width		Thickness		Area		Grain Direction
	in.	cm.	in.	cm.	sq. in.	sq. cm.	
A011	0.4945	1.256	0.2410	0.6121	0.1191	0.7684	Longitudinal
A012	0.4980	1.265	0.2410	0.6121	0.1200	0.7742	Transverse
A013	0.4940	1.254	0.2390	0.6071	0.1180	0.7613	Longitudinal
A014	0.4900	1.245	0.2390	0.6071	0.1171	0.7555	Transverse
A015	0.4960	1.260	0.2395	0.6083	0.1187	0.7658	Longitudinal
A016	0.4930	1.252	0.2420	0.6147	0.1193	0.7697	Transverse
ASPL	0.4940	1.254	0.2415	0.6134	0.1193	0.7697	Longitudinal
ASPT	0.4960	1.260	0.2430	0.6172	0.1205	0.7774	Transverse
B011	0.4920	1.250	0.2300	0.5842	0.1131	0.7297	Longitudinal
B012	0.4930	1.252	0.2295	0.5829	0.1129	0.7284	Transverse
B013	0.4975	1.264	0.2290	0.5817	0.1137	0.7335	Longitudinal
B014	0.4970	1.262	0.2300	0.5842	0.1142	0.7368	Transverse
B015	0.4920	1.250	0.2295	0.5829	0.1128	0.7277	Longitudinal
B016	0.4920	1.250	0.2300	0.5842	0.1131	0.7297	Transverse
BSPL	0.4980	1.265	0.2290	0.5817	0.1140	0.7355	Longitudinal
BSPT	0.4900	1.245	0.2300	0.5842	0.1125	0.7258	Transverse
C011	0.4960	1.260	0.2290	0.5817	0.1135	0.7323	Longitudinal
C012	0.4960	1.260	0.2270	0.5766	0.1125	0.7258	Transverse
C013	0.4970	1.262	0.2280	0.5791	0.1133	0.7310	Longitudinal
C014	0.4960	1.260	0.2290	0.5817	0.1135	0.7323	Transverse
C015	0.4910	1.247	0.2280	0.5791	0.1119	0.7219	Longitudinal
C016	0.4920	1.250	0.2280	0.5791	0.1121	0.7232	Transverse
CSPL	0.4910	1.247	0.2290	0.5817	0.1124	0.7252	Longitudinal
CSPT	0.4950	1.257	0.2295	0.5829	0.1136	0.7329	Transverse

TABLE XIII. - DISPOSITION OF LINER COUPON SPECIMENS

Specimen Designation	Grain Direction	Test Temperature °F	Test Temperature K	Strain Gaged* A	Strain Gaged* T	Extensometer	Tested to Fracture
A011	L	70	294	X	X	X	X
A012	T	70	294	X	X	X	X
A013	L	-423	20	X			X
A014	T	Not tested					
A015	L	-320	77	X			X
A016	T	Not tested					
ASPL	L	Used for Compensating Gages - Not tested					
ASPT	T	-320	77	X			X
B011	L	-320	77	X	X		X
B012	T	-320	77	X	X		
		-423	20				
B013	L	-423	20	X			X
B014	T	-423	20	X			X
B015	L	70	294	X		X	X
B016	T	70	294	X		X	X
BSPL	L	-423	20	X			X
BSPT	T	-423	20	X			X
C011	L	-320	77	X	X		
		-423	20				
C012	T	Not tested					
C013	L	70	294	X		X	X
C014	T	70	294	X		X	X
C015	L	-320	77	X			X
C016	T	-320	77	X			X
CSPL	L	-423	20	X			X
CSPT	T	-320	77	X			X

*A - Axial, T - Transverse

TABLE XIV. - LINER COUPON DATA - POISSON'S RATIO

Specimen Designation	Grain Direction	Test Temperature °F	Test Temperature °K	Poisson's Ratio
A011	Longitudinal	70	294	0.382*
A012	Transverse -	70	294	0.418*
B011	Longitudinal	-320	77	0.249*
B012	Transverse	-320	77	0.392
C011	Longitudinal	-320	77	0.366 - Average=0.379
B012	Transverse	-423	20	0.409
C011	Longitudinal	-423	20	0.366 - Average=0.388

*Disregard

TABLE XV. - LINER COUPON DATA - MODULUS OF ELASTICITY

Specimen	Grain Direction	Test Temperature		SOURCE					
				Poisson's Ratio Tests		Strain Gages		Extensometer	
		°F	°K	psix10^6	N/cm^{2}x10^6	psix10^6	N/cm^{2}x10^6	psix10^6	N/cm^{2}x10^6
A011	L	70	294	16.2	11.2	16.3	11.2	16.3	11.2
B015	L			-	-	16.3	11.2	16.1	11.1
C013	L			-	-	16.3	11.2	15.7	10.8
A012	T			17.6	12.1	17.8	12.3	-	-
B016	T			-	-	18.2	12.5	18.3	12.6
C014	T	70	294	-	-	18.1	12.5	18.1	12.5
					Average	= 17.2	11.9		
A015	L	-320	77	-	-	17.3	11.9	-	-
B011	L			17.5	12.1	17.5	12.1	-	-
C011	L			17.9	12.3	-	-	-	-
C015	L			-	-	17.6	12.1	-	-
ASPT	T			-	-	18.3	12.6	-	-
B012	T			19.0	13.1	-	-	-	-
C016	T			-	-	19.6	13.5	-	-
CSPT	T	-320	77	-	-	18.4	12.7	-	-
				Average = 18.2 psix10^6 (12.5 N/cm^{2}x10^6)					
A013	L	-423	20	-	-	17.8	12.3	-	-
B013	L			-	-	18.0	12.4	-	-
BSPL	L			-	-	17.9	12.3	-	-
C011	L			18.4	12.7	-	-	-	-
CSPL	L			-	-	17.2	11.9	-	-
B012	T			20.0	13.8	-	-	-	-
B014	T			-	-	19.7	13.6	-	-
BSPT	T	-423	20	-	-	19.6	13.5	-	-
				Average = 18.8 psix10^6 (13.0 N/cm^{2}x10^6) (weighted)					

TABLE XVIa. - LINER COUPON DATA - STRENGTHS AND ELONGATION
(U. S. Customary Units)

Specimen	Grain Direction	Test Temp. ^{o}F	0.02% Offset Strength psi x 10^3	0.2% Offset Strength, psi x 10^3		Tensile Strength psi x 10^3	Elongation %
				Strain Gages	Extensometer		
A011	L	70	105.0	109.2	110.0	123.8	18.0
B015	L	70	109.0	-	112.6	125.4	16.5
C013	L	70	111.2	115.6	115.6	129.7	16.25
A012	T	70	111.7	116.7	117.5	122.5	15.0
B016	T	70	117.6	123.8	122.9	129.1	15.5
C014	T	70	118.1	124.2	122.5	128.6	15.5
A015	L	-320	-	-	-	193.8	17.5
B011	L	-320	172.9	182.6	-	197.6	18.5
C015	L	-320	-	-	-	200.2	17.5
ASPT	T	-320	163.9	180.1	-	190.0	17.25
C016	T	-320	-	-	-	195.4	9.0
CSPT	T	-320	169.9	184.0	-	195.0	13.0
A013	L	-423	205.1	211.9	-	219.1	10.75
B013	L	-423	-	-	-	233.9	6.5
BSPL	L	-423	-	-	-	224.6	9.0
CSPL	L	-423	196.6	-	-	235.8	*
B014	T	-423	-	-	-	218.9	11.5
BSPT	T	-423	183.1	204.4	-	216.0	14.0

*Lost gage marks

TABLE XVIb. - LINER COUPON DATA - STRENGTHS AND ELONGATION
(International System of Units)

Specimen	Grain Direction	Test Temp. ^{o}K	0.02% Offset Strength $N/cm^2 x10^3$	0.2% Offset Strength, $N/cm^2 x10^3$		Tensile Strength $N/cm^2 x10^3$	Elongation %
				Strain Gages	Extensometer		
A011	L	294	72.4	75.3	75.8	85.4	18.0
B015	L	294	75.2	-	77.6	86.5	16.5
C013	L	294	76.7	79.7	79.7	89.4	16.25
A014	T	294	77.0	80.5	81.0	84.5	15.0
B016	T	294	81.1	85.4	84.7	89.0	15.5
C014	T	294	81.4	85.6	84.5	88.7	15.5
A015	L	77	-	-	-	133.6	17.5
B011	L	77	119.2	125.9	-	136.2	18.5
C015	L	77	-	-	-	138.0	17.5
ASPT	T	77	113.0	124.2	-	131.0	17.25
C016	T	77	-	-	-	134.7	9.0
CSPT	T	77	117.1	126.9	-	134.4	13.0
A014	L	20	141.4	146.1	-	151.1	10.75
B013	L	20	-	-	-	161.3	6.5
BSPL	L	20	-	-	-	154.9	9.0
CSPL	L	20	135.6	-	-	162.6	*
B014	T	20	-	-	-	150.9	11.5
BSPT	T	20	126.2	140.9	-	148.9	14.0

*Lost gage marks

TABLE XVIIa. - LINER COUPON DATA - DERIVED PROPERTIES
(U. S. Customary Units)

Specimen	Grain Direction	Test Temp. °F	Intersection Stress, σ_I, psix10^3		Intersection Strain, ϵ_I		Inelastic Slope, E_2, psix10^6	
			Strain Gages	Extensometer	Strain Gages	Extensometer	Strain Gages	Extensometer
A011	L	70	-	112.5	-	0.0069	-	0.32*
B015	L	70	-	114.4	-	0.0071	-	0.26*
C013	L	70	117.6	116.5	0.0072	0.0074	0.22	0.36*
A012	T	70	118.7	-	0.0067	-	0.17	-
B016	T	70	-	124.7	-	0.0068	-	0.14
C014	T	70	126.2	125.1	0.0070	0.0069	0.02	0.10
			Average =	119.6 (weighted)			Average* =	0.31
B011	L	-320	185.7	-	0.0106	-	-	-
ASPT	T	-320	183.2	-	0.0100	-	-	-
CSPT	T	-320	187.1	-	0.0102	-	0.11	-
		Average =	185.4 (weighted)					
A013	L	-423	215.5	-	0.0121	-	-	-
BSPT	T	-423	207.9	-	0.0107	-	0.62	-
		Average =	211.7					

TABLE XVIIb. - LINER COUPON DATA - DERIVED PROPERTIES
(International System of Units)

Specimen	Grain Direction	Test Temp. ^oK	Intersection Stress, σ_I, $N/cm^2 x10^3$		Intersection Strain, ϵ_I		Inelastic Slope, E_2, $N/cm^2 x10^6$	
			Strain Gages	Extensometer	Strain Gages	Extensometer	Strain Gages	Extensometer
A011	L	294	-	77.6	-	0.0069	-	0.22*
B015	L	294	-	78.9	-	0.0071	-	0.18*
C013	L	294	81.1	80.3	0.0072	0.0074	0.15	0.25*
A012	T	294	81.8	-	0.0067	-	0.12	-
B016	T	294	-	86.0	-	0.0068	-	0.10
C014	T	294	87.0	86.3	0.0070	0.0069	0.01	0.07
			Average = 82.5 (weighted)				Average* = 0.21	
B011	L	77	128.0	-	0.0106	-	-	-
ASPT	T	77	126.3	-	0.0100	-	-	-
CSPT	T	77	129.0	-	0.0102	-	0.08	-
		Average = 127.8 (weighted)						
A013	L	20	148.6	-	0.0121	-	-	-
BSPT	T	20	143.3	-	0.0107	-	0.43	-
		Average = 146.0						

TABLE XVIII. - LINER COUPON DATA -
DERIVATIVES OF PROPERTIES WITH RESPECT TO TEMPERATURE

Room Temperature Properties

Modulus of Elasticity, E_T = 17.2 x 10^6 psi (See Table XV)
Inelastic Slope, E_2 = 310,000 psi (See Table XVIIa)
Poisson's Ratio, ν, = 0.34 (See below)
Intersection Stress, σ_I, = 119.6 x 10^3 psi (See Table XVIIa)

Temperature Derivatives	Remarks
$\partial E / \partial T$ = -2920 psi/^oF	Straight line through R.T. value
$\partial E_2 / \partial T$ = +600 psi/^oF	Longitudinal R.T. value with slope selected to make value zero at -423^oF
$\partial \nu / \partial T$ = -87 x 10^6/^oF	Straight line through values at -423^oF and -320^oF, which gives R.T. value of 0.345.
$\partial \sigma_I / \partial T$ = -178.5 psi/^oF	Straight line through R.T. value

NOTE: This table is not presented in the International System of Units since the computer program requires the use of U. S. Customary Units.

TABLE XIX. - STRENGTH TESTS OF FIBERGLASS/EPOXY ROVING

Material: S-HTS/E-796 20-end roving

Supplier: U. S. Polymeric Corporation

Resin Content: 18-23% by weight

Ring Specimen Number	Tensile Strength psi x 10^3	Tensile Strength N/cm^2 x 10^3
1RT	275	190
2RT	291	201
3RT	277	191
4RT	292	201
5RT	285	196
Average =	284	196

TABLE XX. - ADDITIONAL INPUT CARDS

Card	Format	Symbols
1	6E12.8	CLT(1,1) ..... CLT(1,6)
2		CLT(1,7) ..... CLT(1,12)
3		CLT(1,13) ..... CLT(1,18)
4		CLT(2,1) ..... CLT(2,6)
5		CLT(2,7) ..... CLT(2,12)
6	6E12.8	CLT(2,13) ..... CLT(2,18)
7	8I5	ISOLH,IEBLH,ISFD,ITL,ITO,IPD,IEBL,JJ

NOTES:
1) These cards go after the last design condition card, of Reference 4, and before the service cycle cards.

2) The CLT(i,j) are shown in Figure 59.

3) If SOLH, etc., is input (including input zero) then ISOLH, etc. is input zero; otherwise ISOLH, etc. is input one.

4) If "C", of Reference 4, is input, then JJ is input zero; otherwise, JJ is input one.

TABLE XXI. - MATERIAL PROPERTIES USED IN COMPUTER ASSISTED DESIGN

SYMBOL	VALUE	DEFINITION	UNITS
RHØL (P_L)	.162	Density of liner	$lb./in^3$
ALFL (α_L)	.0000039	Coefficient of thermal expansion of liner	$^oF^{-1}$
SYL (σ_{YL})	119,600.	Tension yield strength of liner	psi
DSYLDT $\left(\frac{d\sigma_{YL}}{dt}\right)$	-178.5	Derivative of σ_{YL} with respect to temperature	$psi/^oF$
SYLC(σ_{YLC})	90,000.	Compressive yield strength of liner or buckling limit	psi
DSYLCDT $\left(\frac{d\sigma_{YLC}}{dt}\right)$	-180.5	Derivative of σ_{YLC} with respect to temperature	$psi/^oF$
EL (E_L)	17.2×10^6	Young's Modulus of liner at reference temperature	psi
DELDT $\left(\frac{dE_L}{dt}\right)$	-2,920.	Derivative of E_L with respect to temperature	$psi/^oF$
EI (E_1)	310,000.	Plastic modulus of liner at reference temperature	psi
DEIDT $\left(\frac{dE_1}{dt}\right)$	600.	Derivative of E_1 with respect to temperature	$psi/^oF$
VL (ν_L)	.34	Poisson's ratio of liner at reference temperature	-
DNULPT $\left(\frac{d\nu_L}{dt}\right)$	-.000087	Derivative of ν_L with respect to temperature	$^oF^{-1}$
RØHG (ρ_g)	.072	Density of filament composite	$lb/in.^3$
ALFF (α_F)	20.1×10^{-7}	Coefficient of thermal expansion of composite	$^oF^{-1}$
EF (E_f)	12.4×10^6	Elastic modulus of filament at reference temperature	psi

TABLE XXI (concl)

SYMBOL	VALUE	DEFINITION	UNITS
DEFDT $\left(\frac{dE_f}{dt}\right)$	-2,410.	Derivative of E_f with respect to temperature	psi/^{o}F
BIK(K)	.673	Filament fraction in composite	-
SOF (σ_{OF})	47,000.	Meridian filament stress due to winding pressure	psi
SFD (σ_{fd})	2.763×10^5	Design stress in meridian filaments	psi

NOTE: This table is not presented in the International System of Units since the computer program requires the use of U. S. Customary Units

TABLE XXII. - VESSEL WEIGHT

	Overwrap		Liner	
	Pounds	Kilograms	Pounds	Kilograms
One head	7.74	3.51	14.70	6.67
Cylinder	8.87	4.02	8.69	3.94
Vessel	24.35	11.0	38.09	17.3

TOTAL 62.44 pounds

277.8 kilograms

TABLE XXIII. - EFFECTS OF TOLERANCE ON LINER THICKNESS

Liner Thickness in Cylinder, in.	0.156	0.151 (-.005)	0.161 (+.005)	0.166 (+.010)
Design Pressure, psi	5,600	5,505	5,695	5,791
Vessel Contained Volume, $in.^3$	7,223	7,244	7,202	7,181
Vessel Weight, lbs	62.43	61.11	63.75	65.06
Maximum Filament Stress, psi Station No.	375,500 10	383,700 10	367,500 10	359,600 10
Maximum Liner Stress in Head after Sizing, psi Station No.	-89,240 81	-95,880 79	-85,850 81	-80,930 82
Liner Stress in Cylinder after Sizing, psi	-89,000	-94,030	-84,220	-79,680

NOTE: This table is not presented in the International System of Units because the computer output is in U. S. Customary Units, as were the design requirements.

TABLE XXIV. - SPECIMEN DESIGNATION NOMENCLATURE

1. Preliminary Tensile Specimens - P series
   First letter (P) - Preliminary tensile test
   Second letter (T or L) - Grain direction: T-transverse, L-longitudinal
   First three numbers (250) - Nominal thickness in mils
   - Replicate specimen number
2. Preliminary Tensile Specimens - T series
   First letter (T) - Tensile test
   First two numbers (63) - Nominal thickness in mils
   Second letter (C or M) - Surface treatment: C-chem milled, M-machined
   Last number - Replicate specimen number
3. Biaxial and Creep Specimen Material Tensile Specimens
   First letter (T) - Tensile test
   First two numbers (63) - Nominal thickness in mils
   Second letter (A or B) - Source sheet: A-Creep test specimen material
   B-Biaxial test specimen material
   Third letter (T or L) - Grain direction: T-transverse, L-longitudinal
   Last number - Replicate specimen number
4. Biaxial Test Specimens
   First letter (B) - Biaxial test
   Second letter (R,N, or H) Test temperature: R-room
   N-liquid nitrogen
   H-liquid hydrogen
   Third letter (O,E,T, or D) - Specimen treatment and shape:
   O - flat
   E - electron beam welded, flat
   T - tungsten inert gas welded, flat
   D - explosively formed into a dome
5. Creep Test Specimens
   First letter (C) - Creep test
   Single digit number - Replicate specimen number of specimens used primarily for compression stress-strain property determination.
   Double digit number - Approximate level of compressive stress in ksi at start of creep test.
   X1 and X2 - Spare specimens.

6. Liner Material Coupon Tensile Specimens

First letter - Serial designation of source plate

Next three symbols:

Numbers - Replicate specimen number: Odd-longitudinal grain, Even-transverse grain.

Letters - Spare coupons: L-longitudinal grain, T - transverse grain.

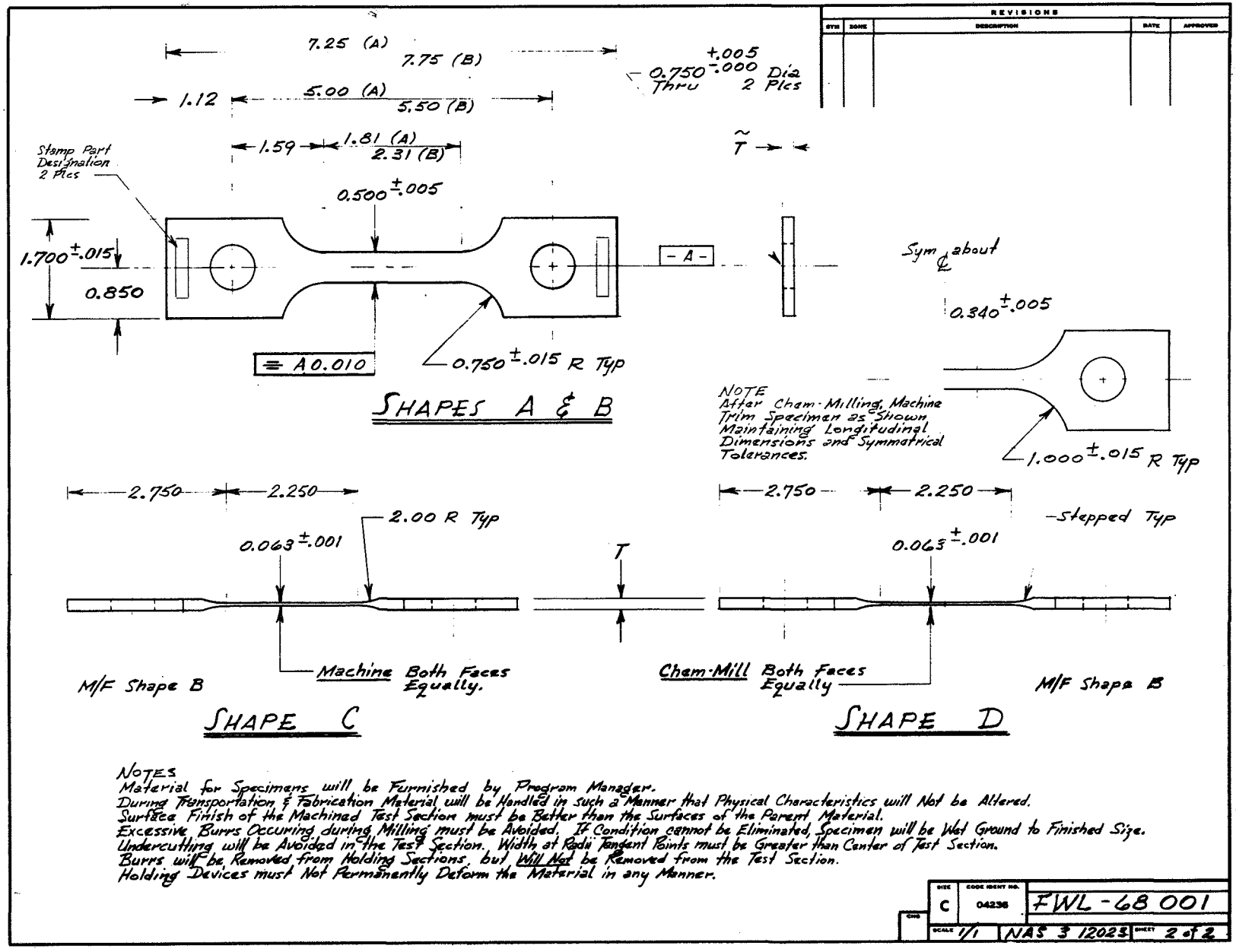

Figure 1.-Tensile Specimen Shapes

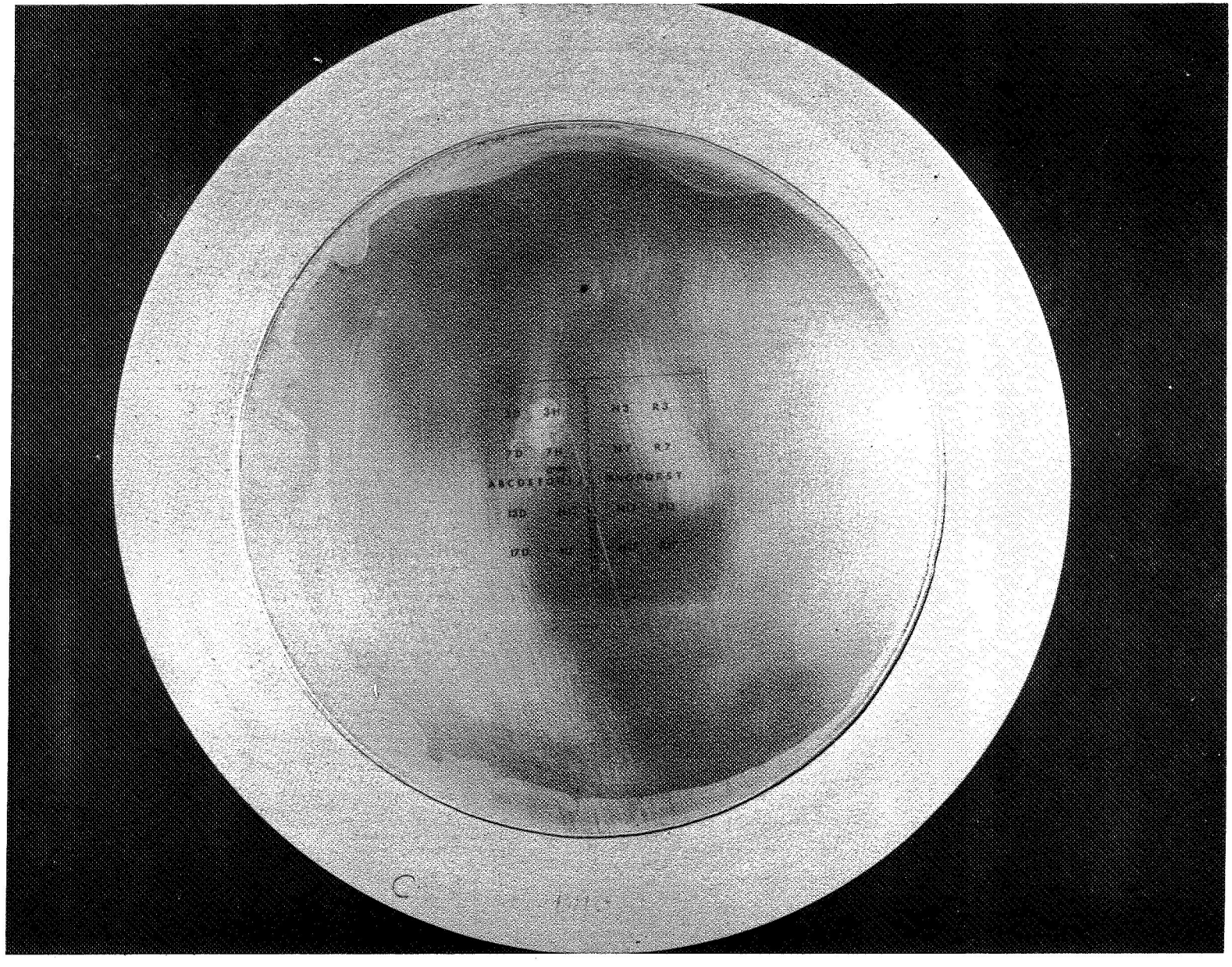

Figure 2.-Flat Biaxial Specimen (BHO)

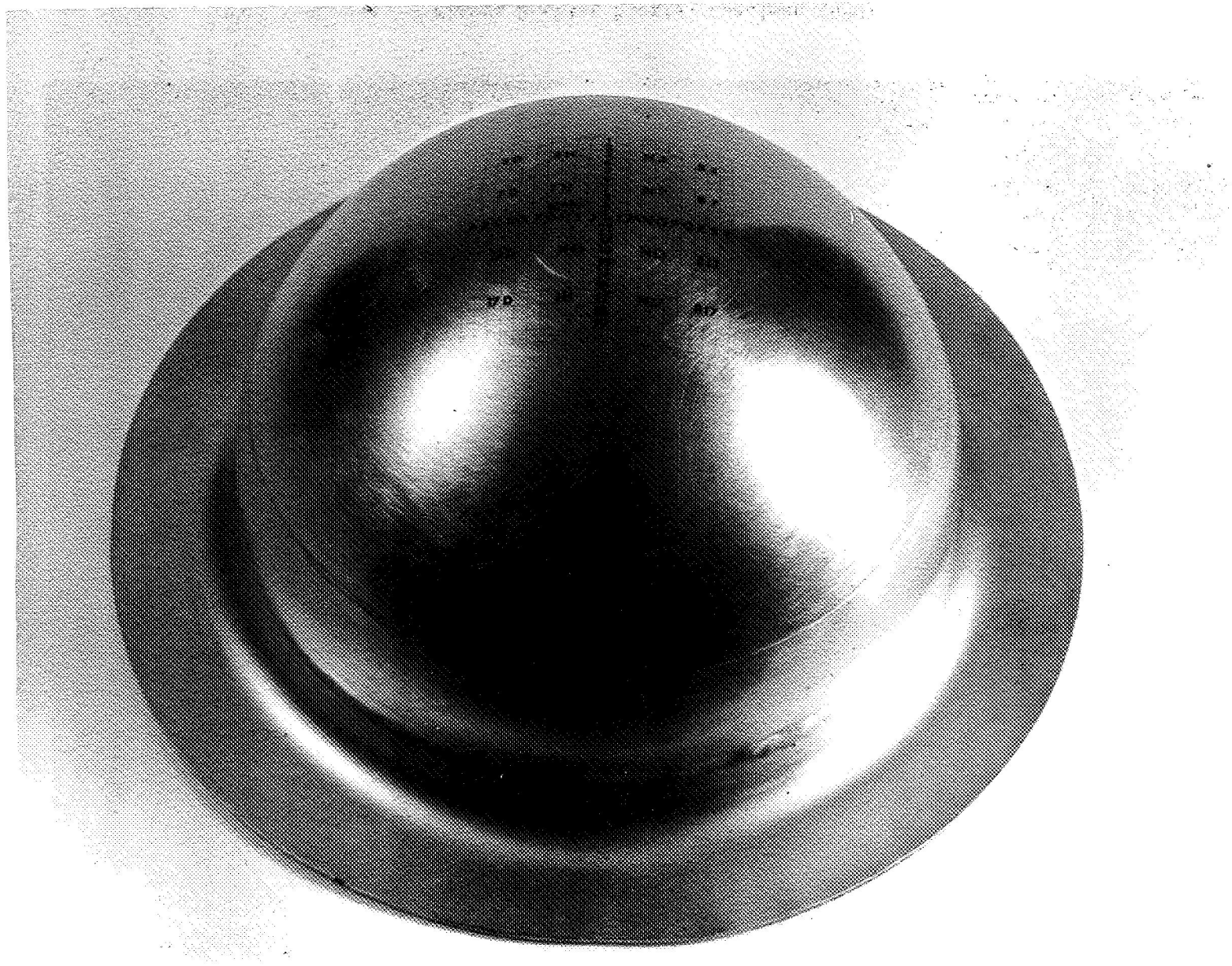

Figure 3.-Domed Biaxial Specimen

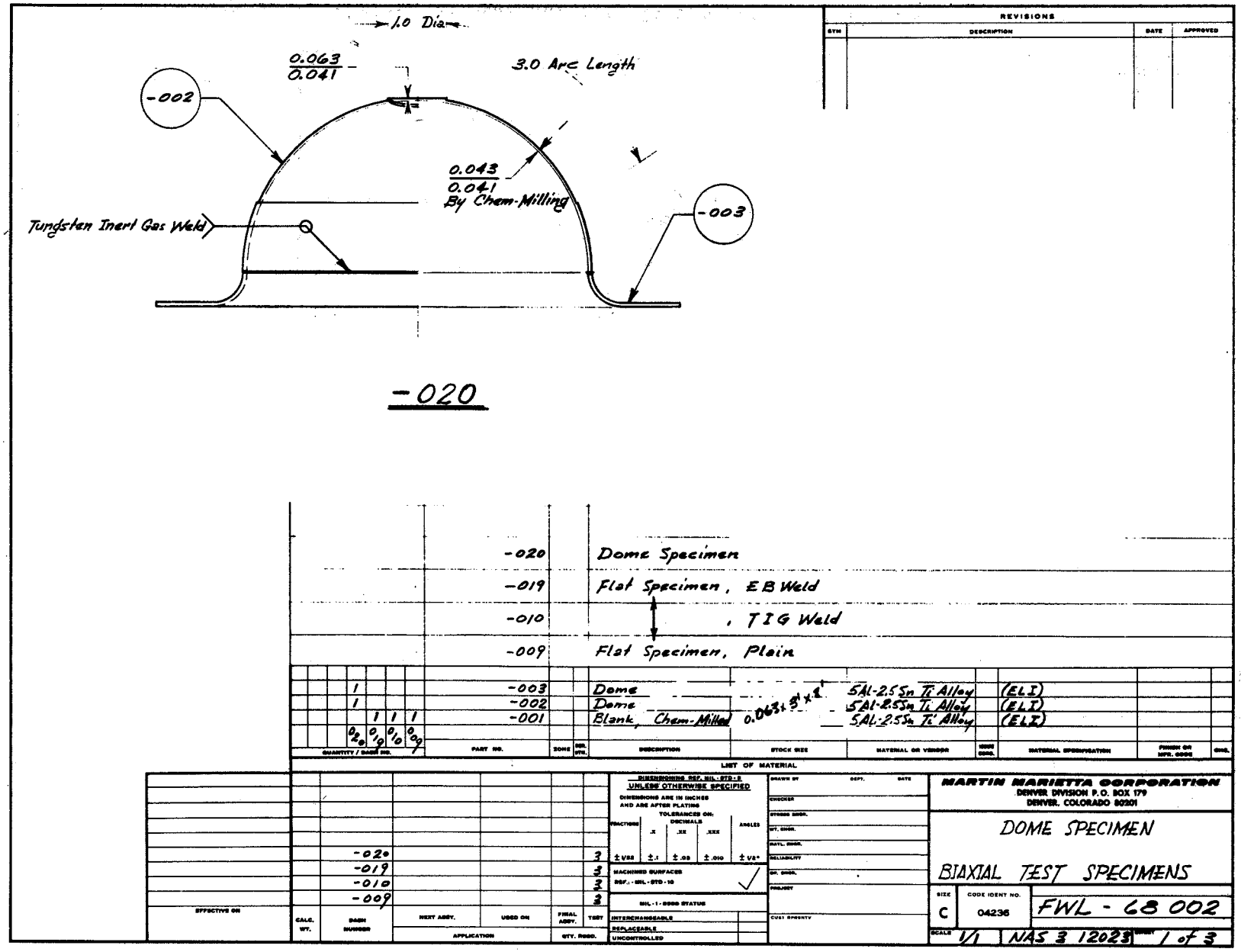

Figure 4.-Fabrication Drawing, Domed Biaxial Specimens

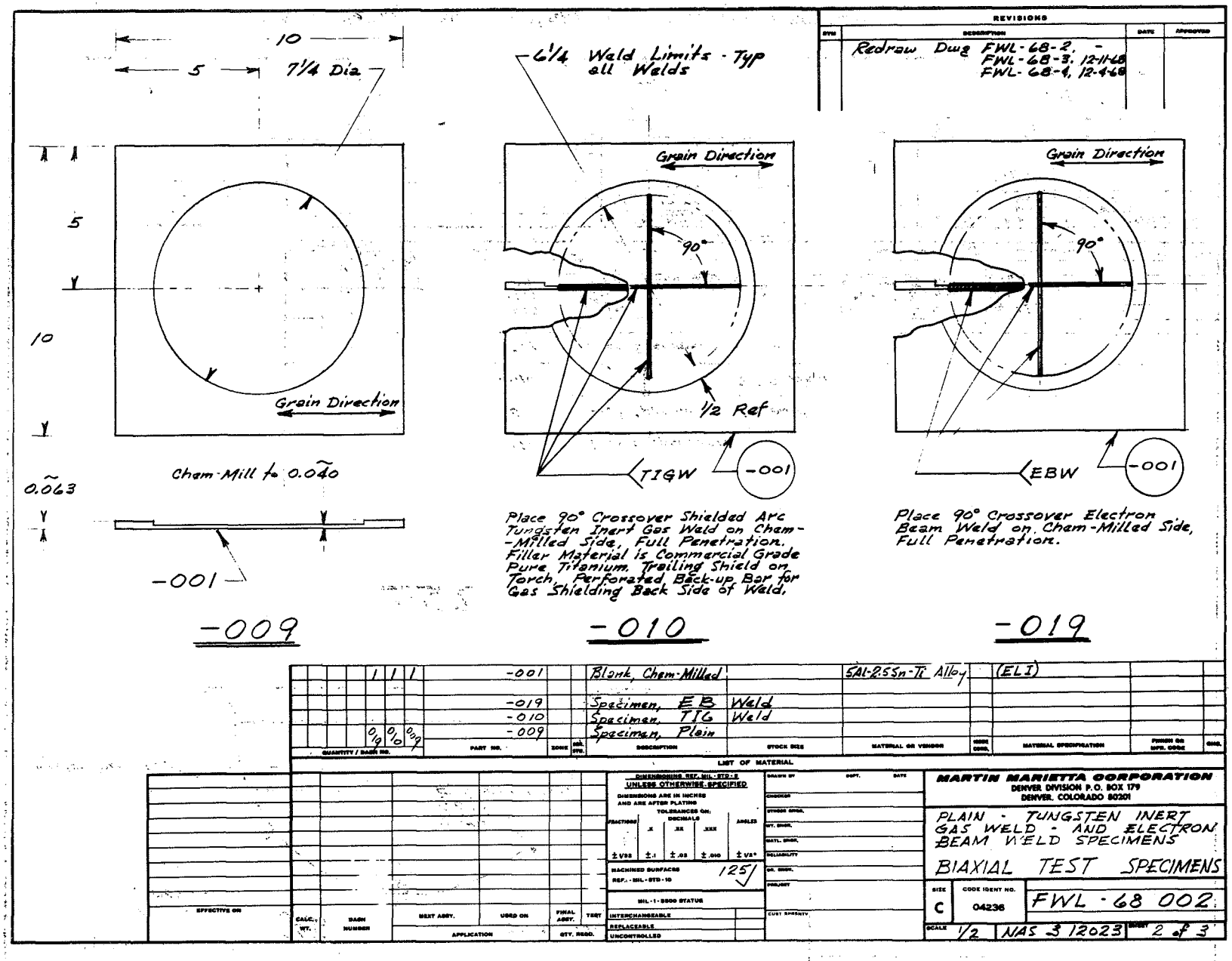

Figure 5.- Fabrication Drawing, Flat Biaxial Specimen Blanks

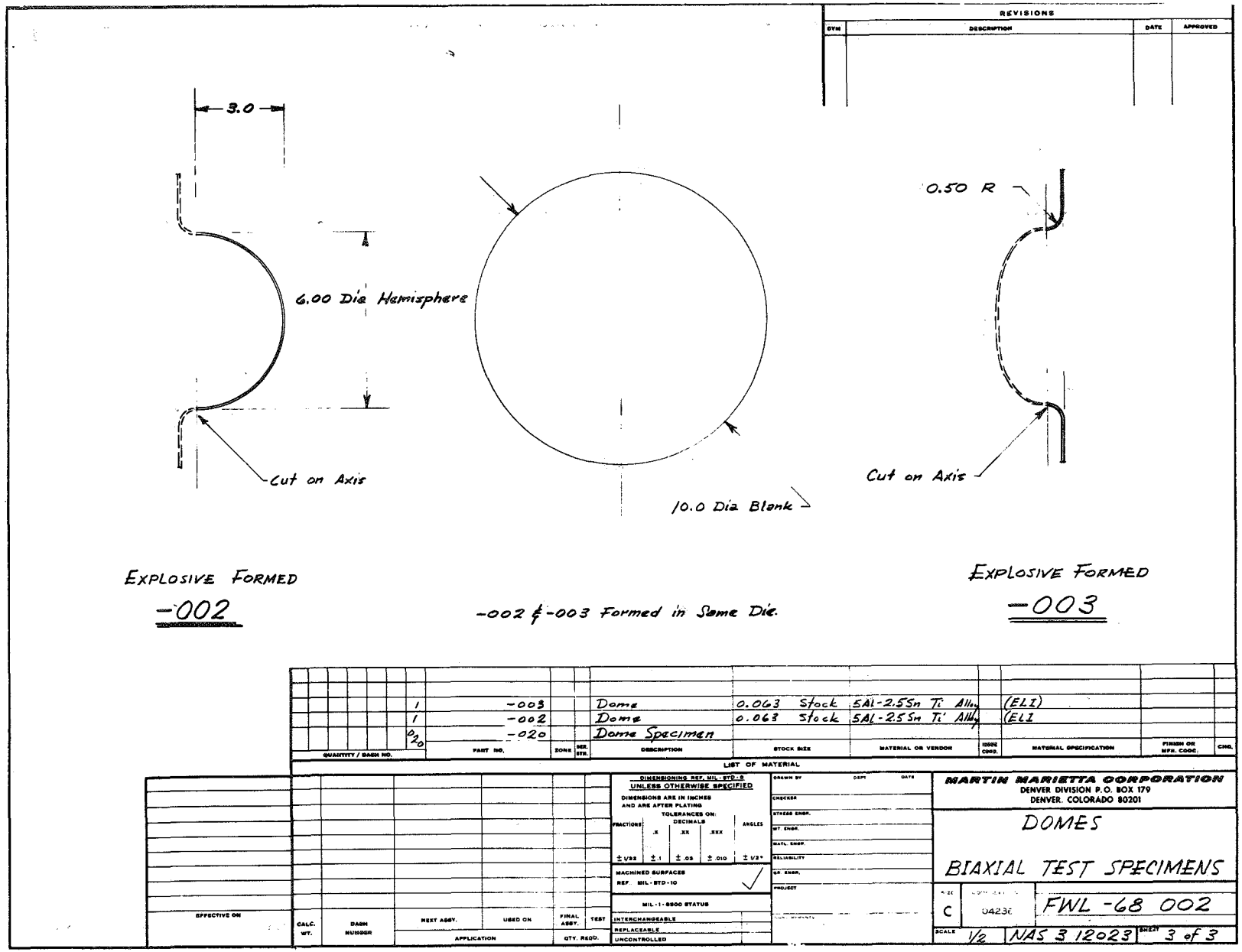

Figure 6.-Domed Biaxial Specimen Forming Guide

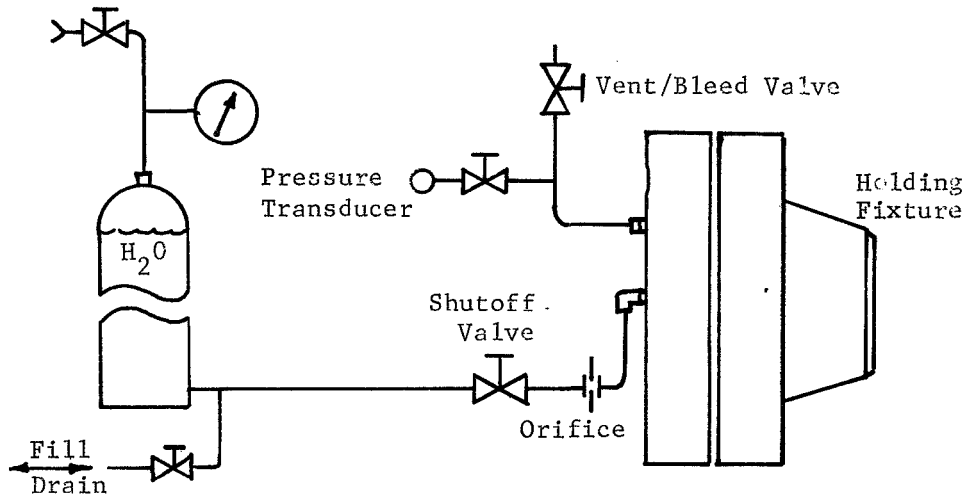

Figure 7.- Room Temperature Test Set-up, Biaxial Tests

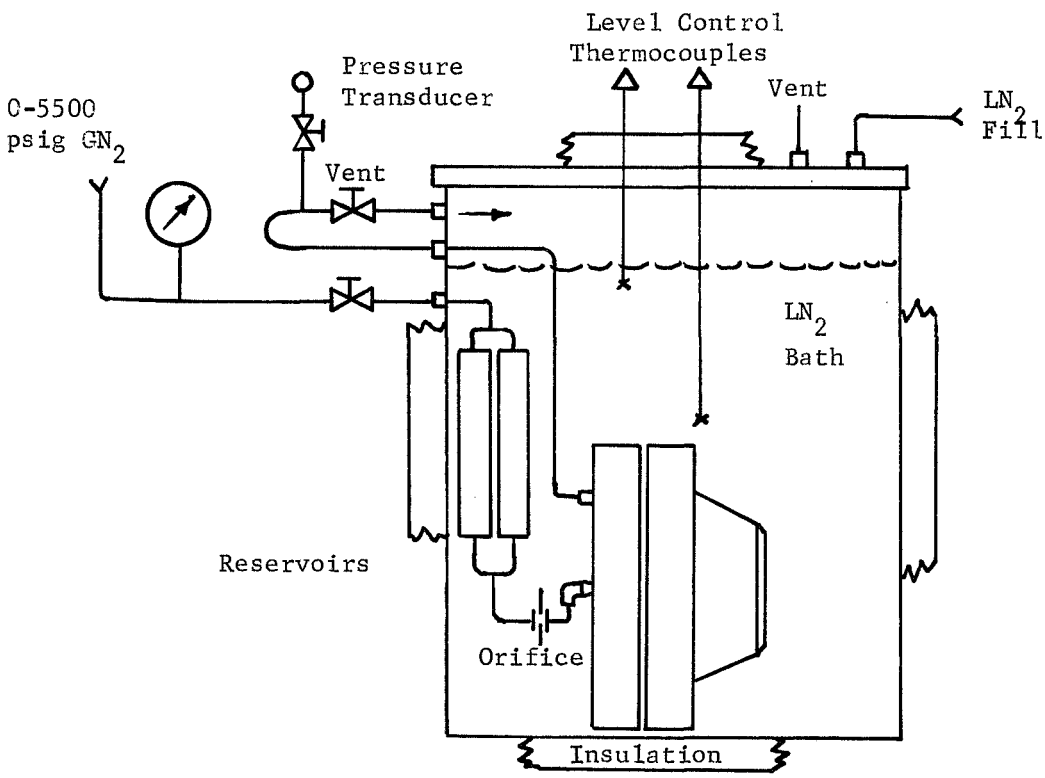

Figure 8.-LN_2 Temperature Test Set-Up, Biaxial Tests

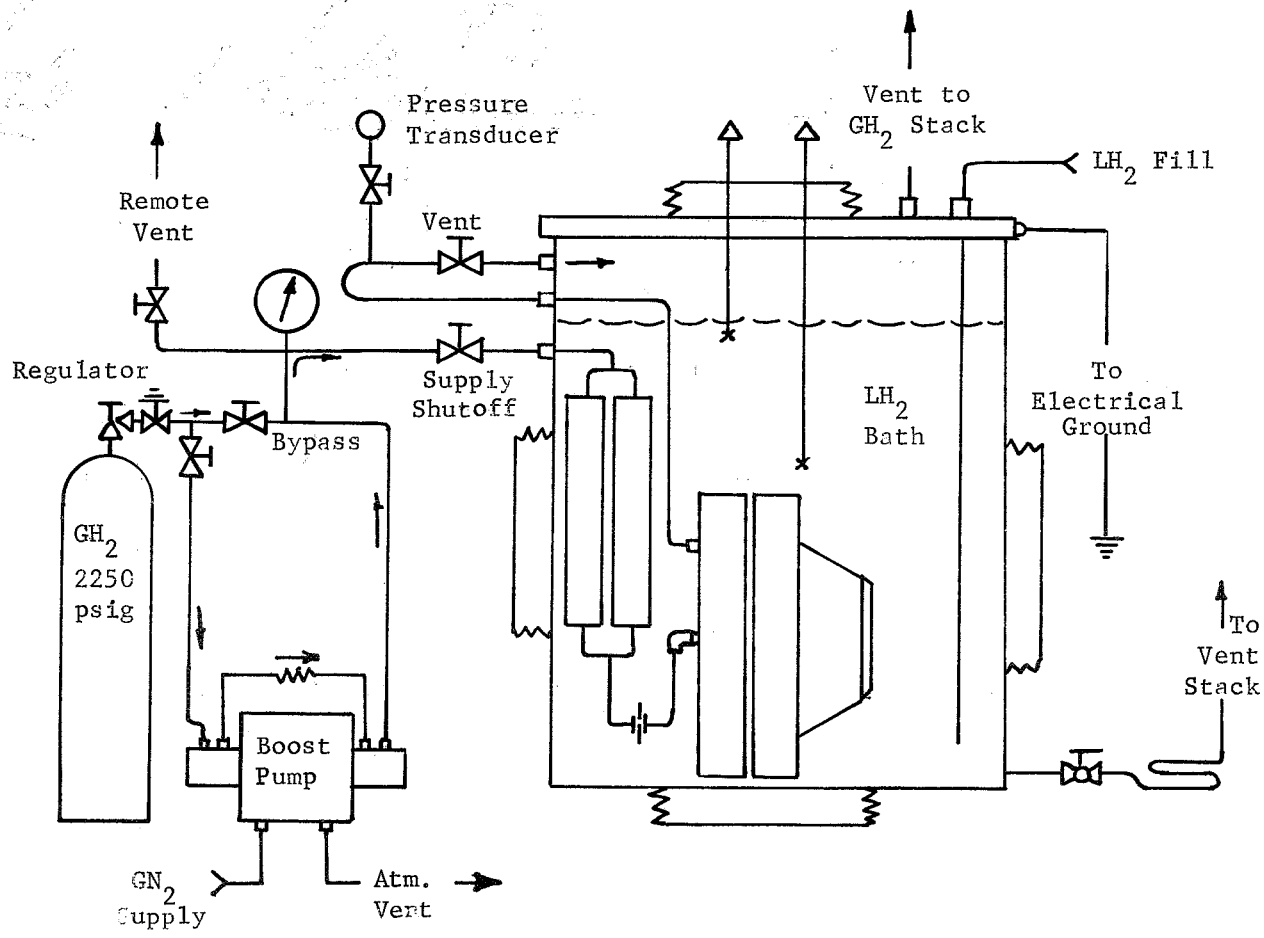

Figure 9. - LH_2 Temperature Test Set-up, Biaxial Tests

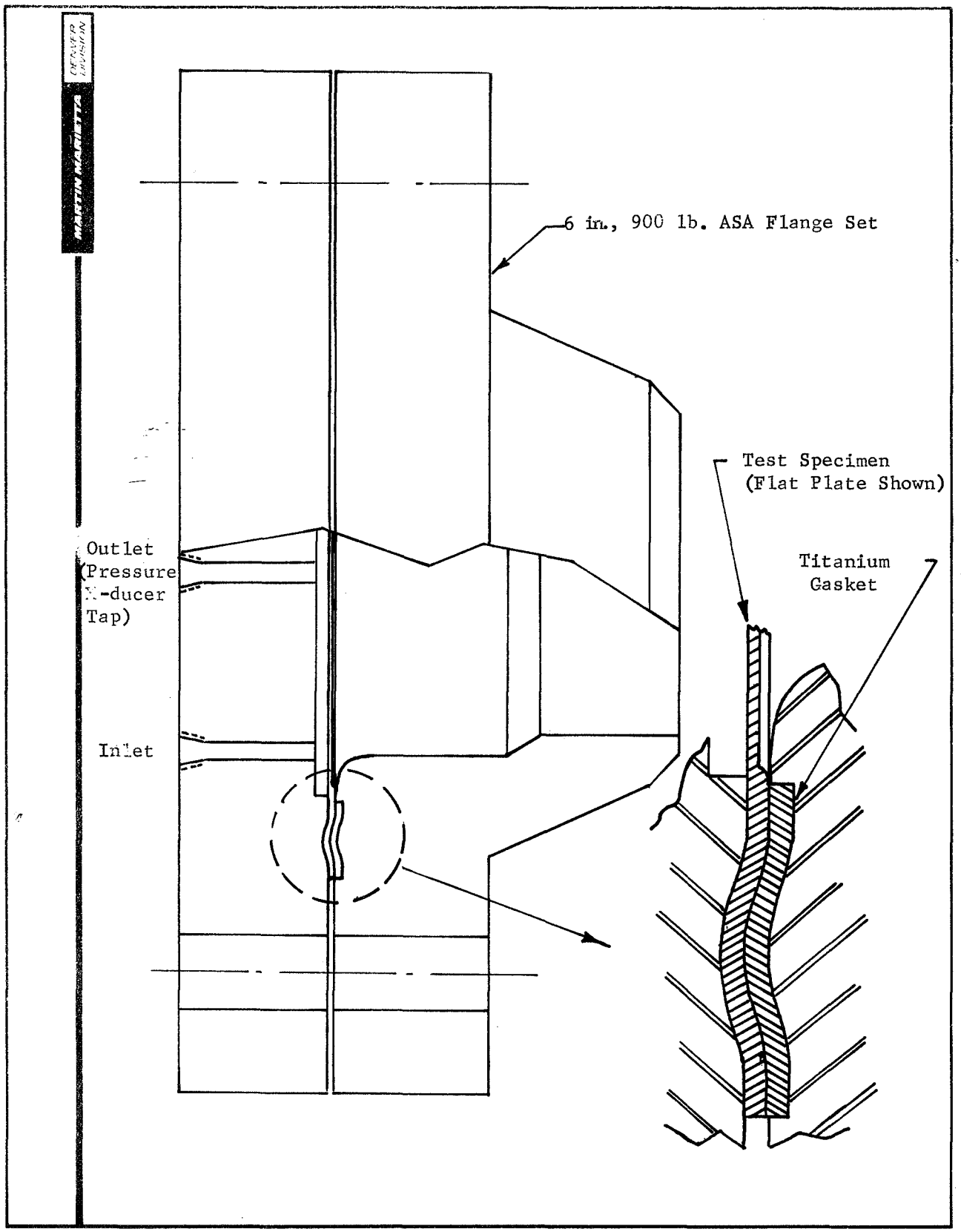

Figure 10. - Biaxial Test Specimen Holding Fixture

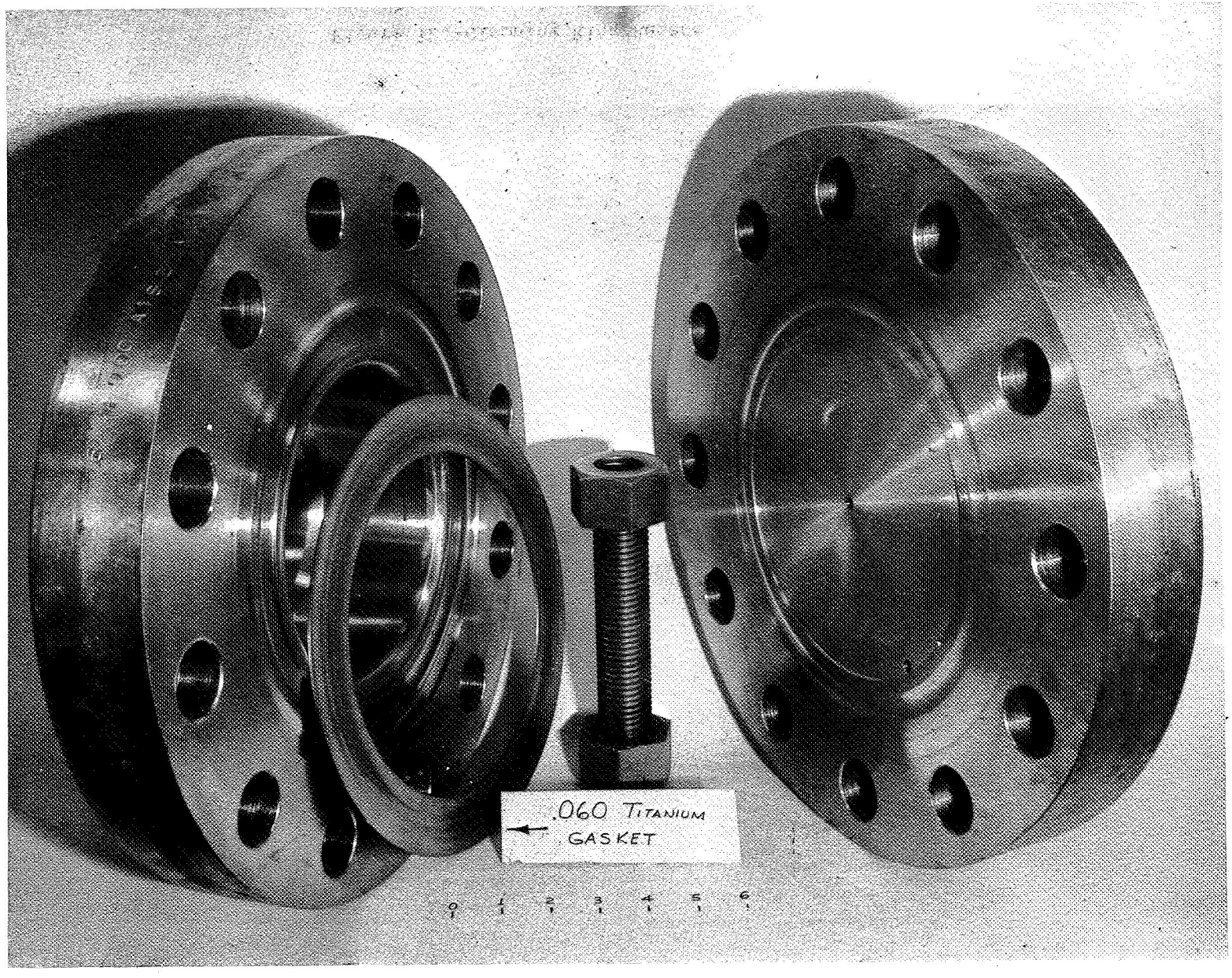

Figure 11.--Biaxial Test Specimen Holding Fixture

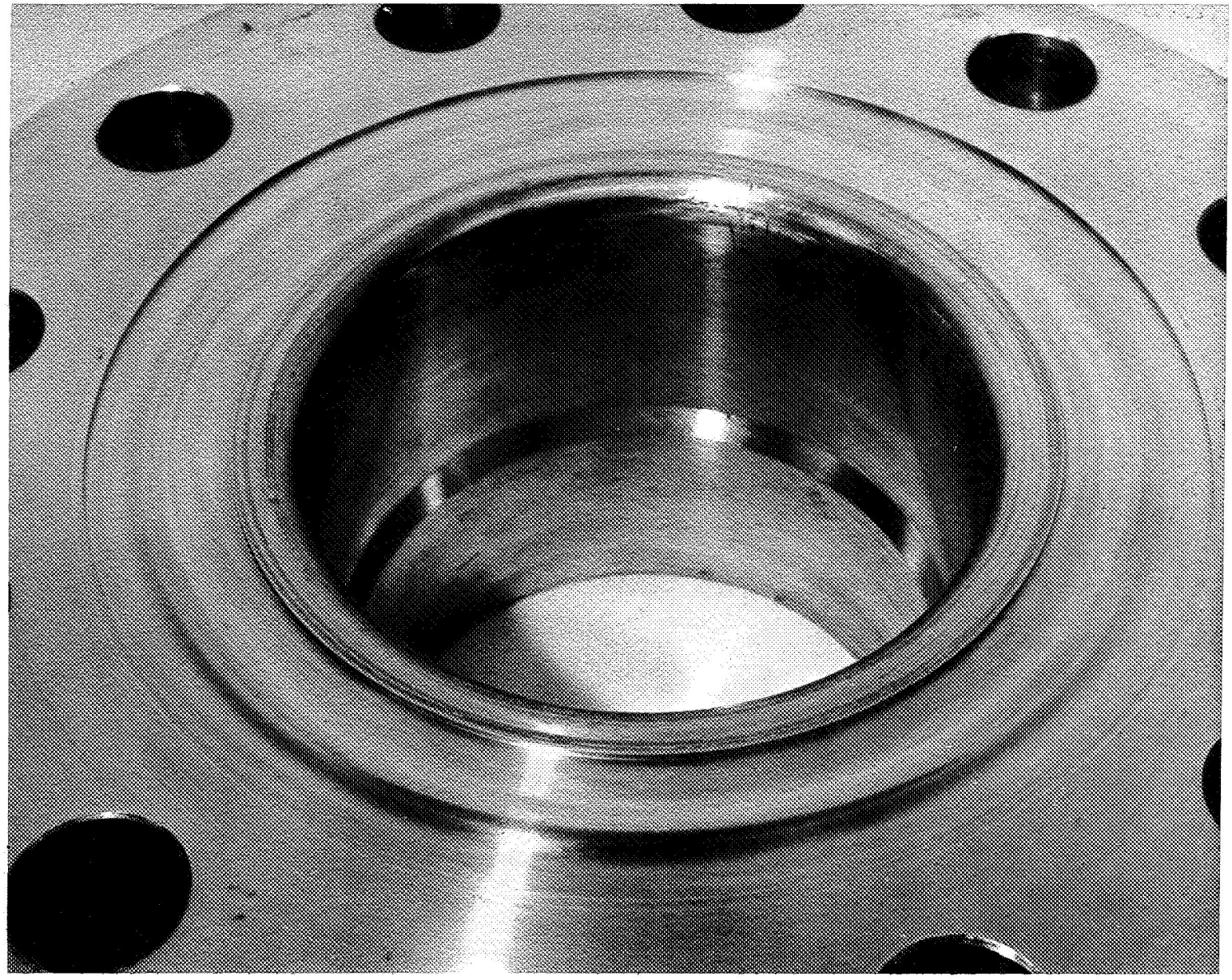

Figure 12.-Clamping Ring Recess

Figure 13.- Failed Specimen BRO, Top View

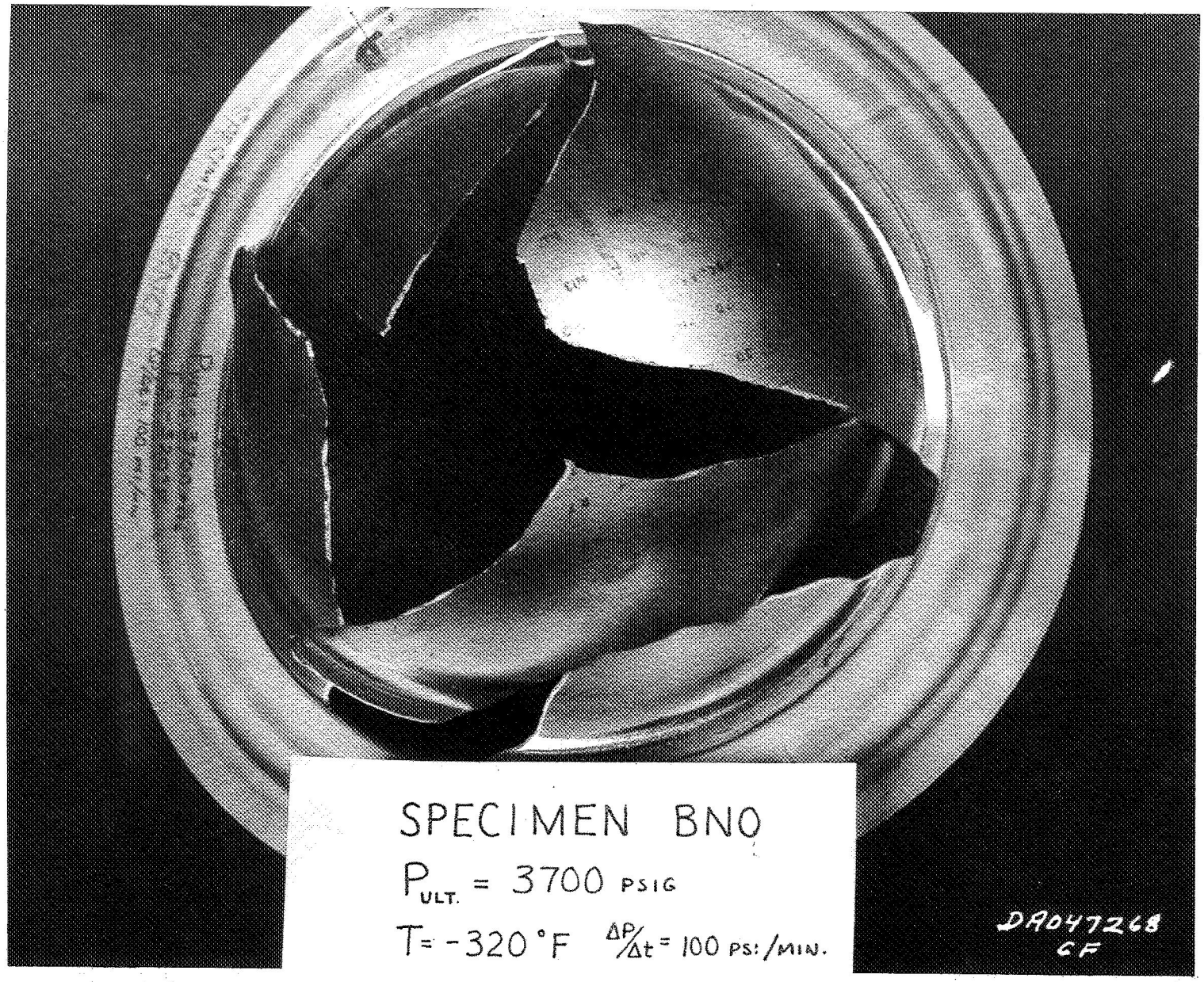

Figure 14.- Failed Specimen BNO, Top View

Figure 15.- Failed Specimen BHO, Side View

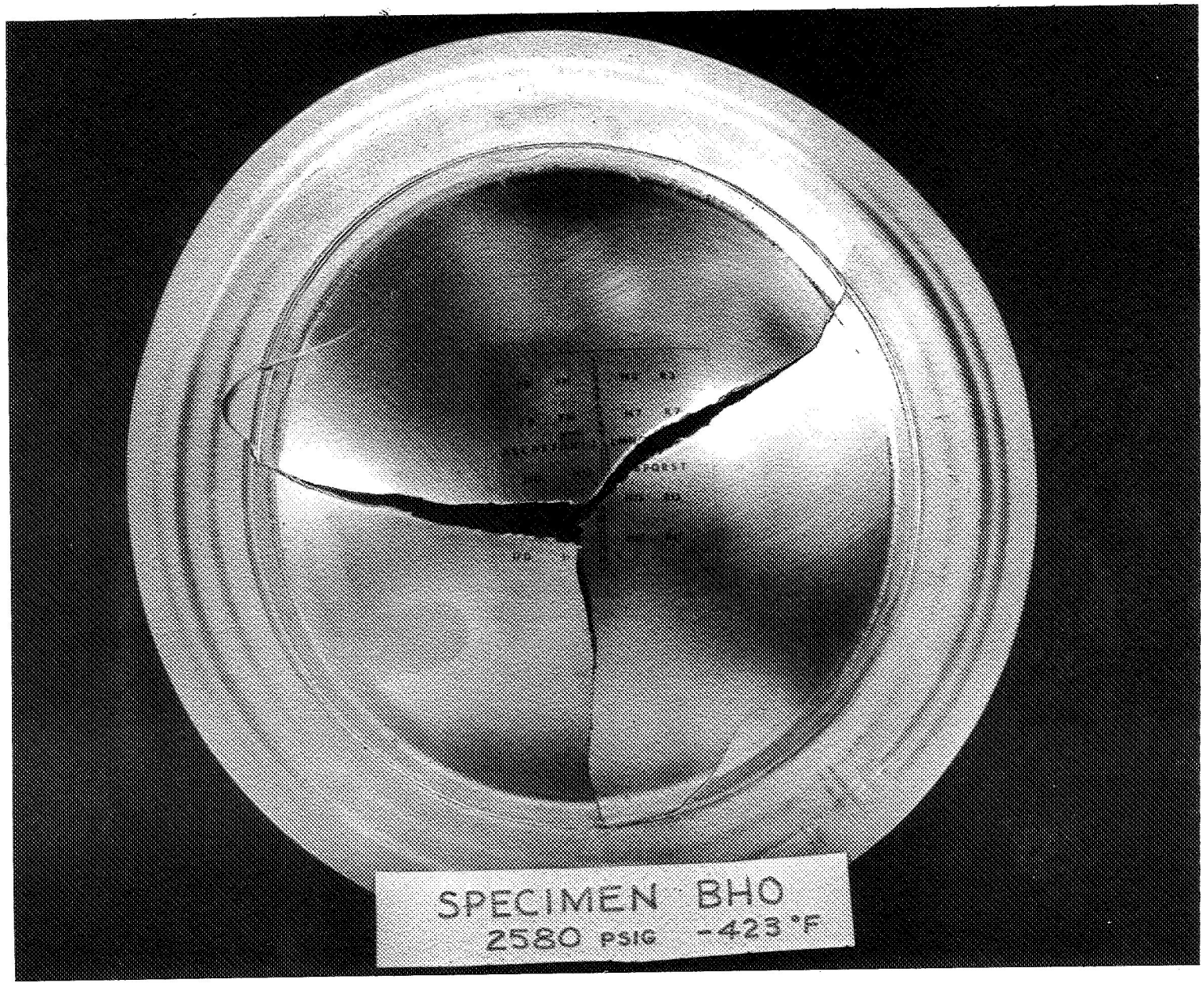

Figure 16.-Failed Specimen BHO, Top View

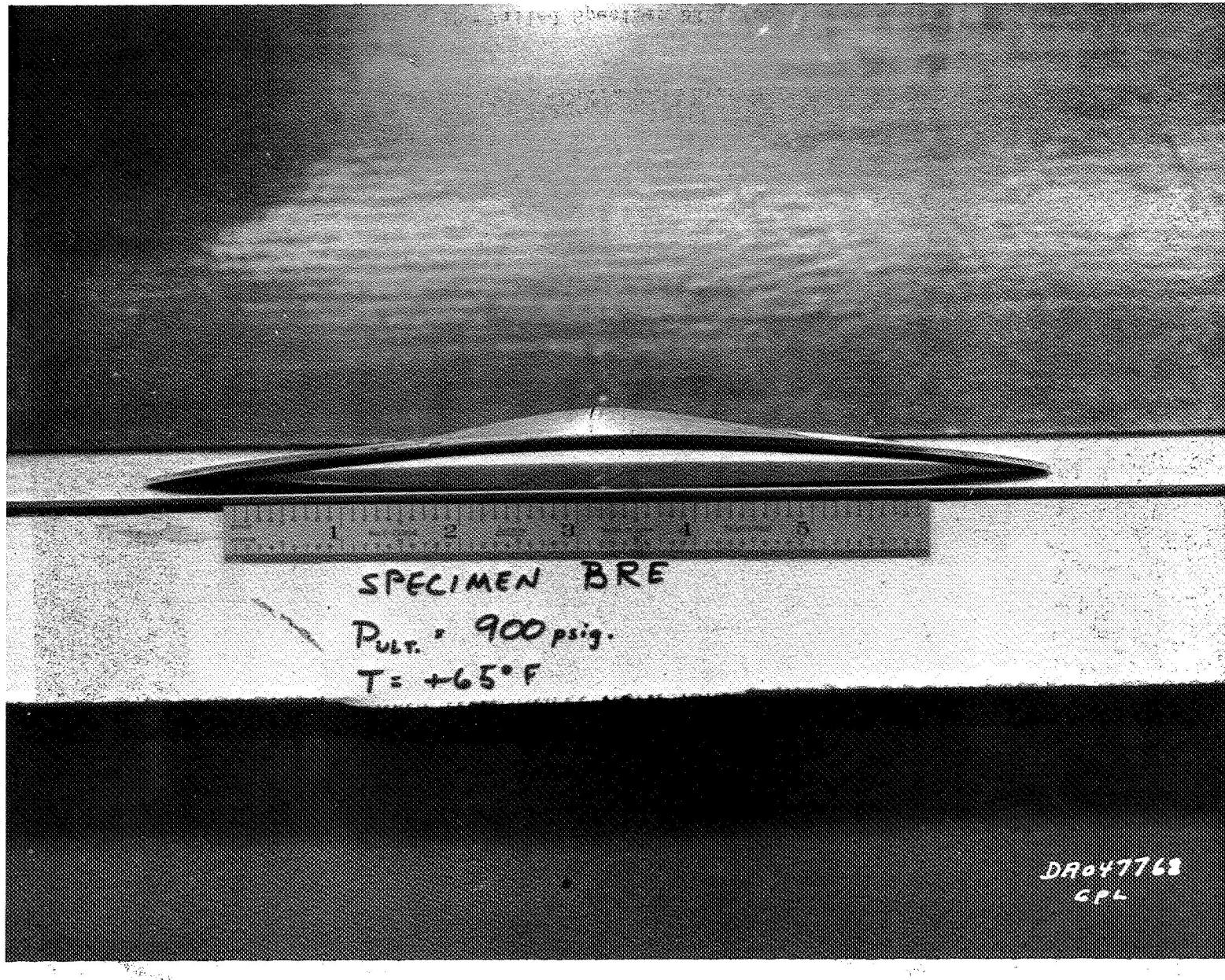

Figure 17.- Failed Specimen BRE, Edge View

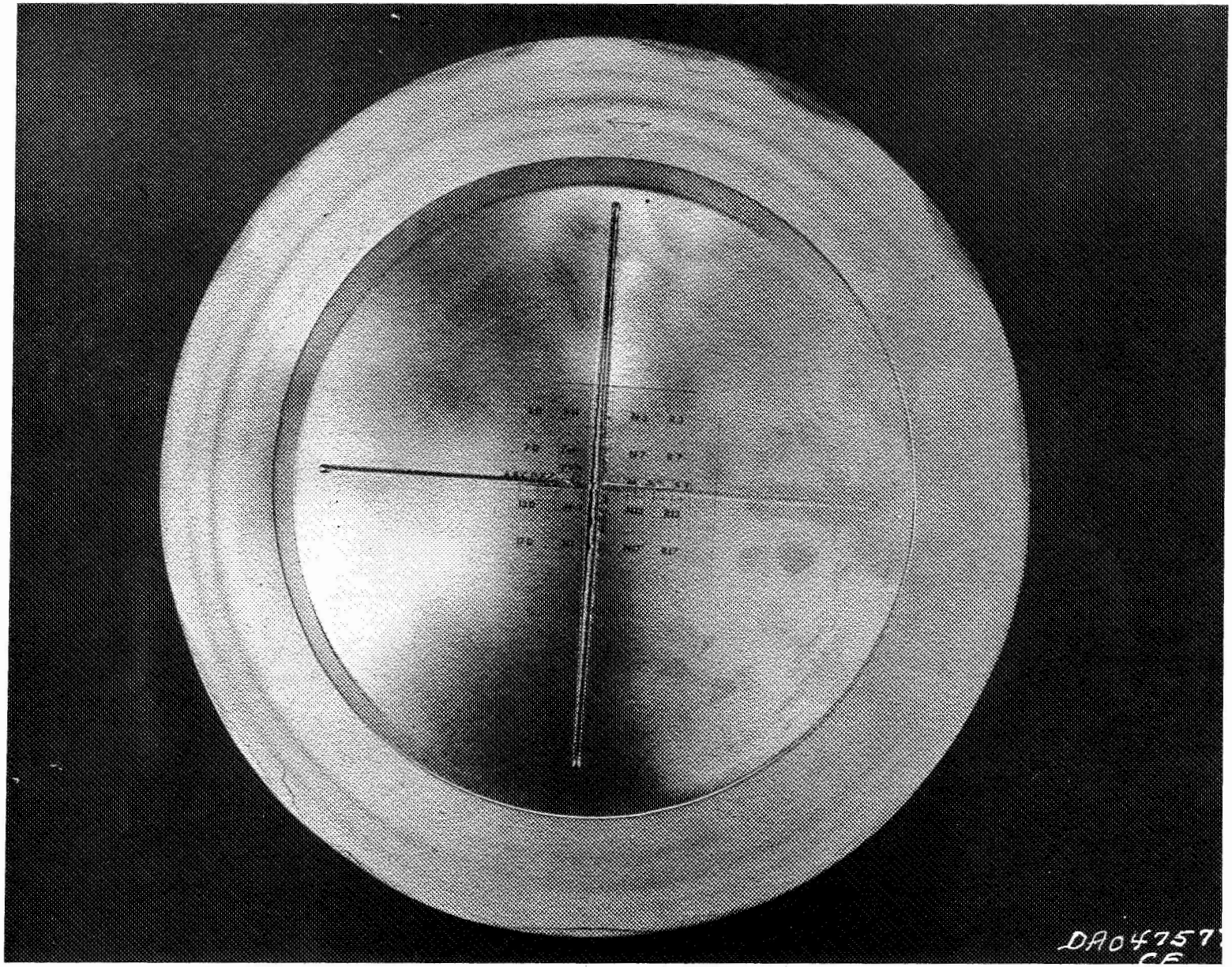

Figure 18.-Failed Specimen BRE, Top View

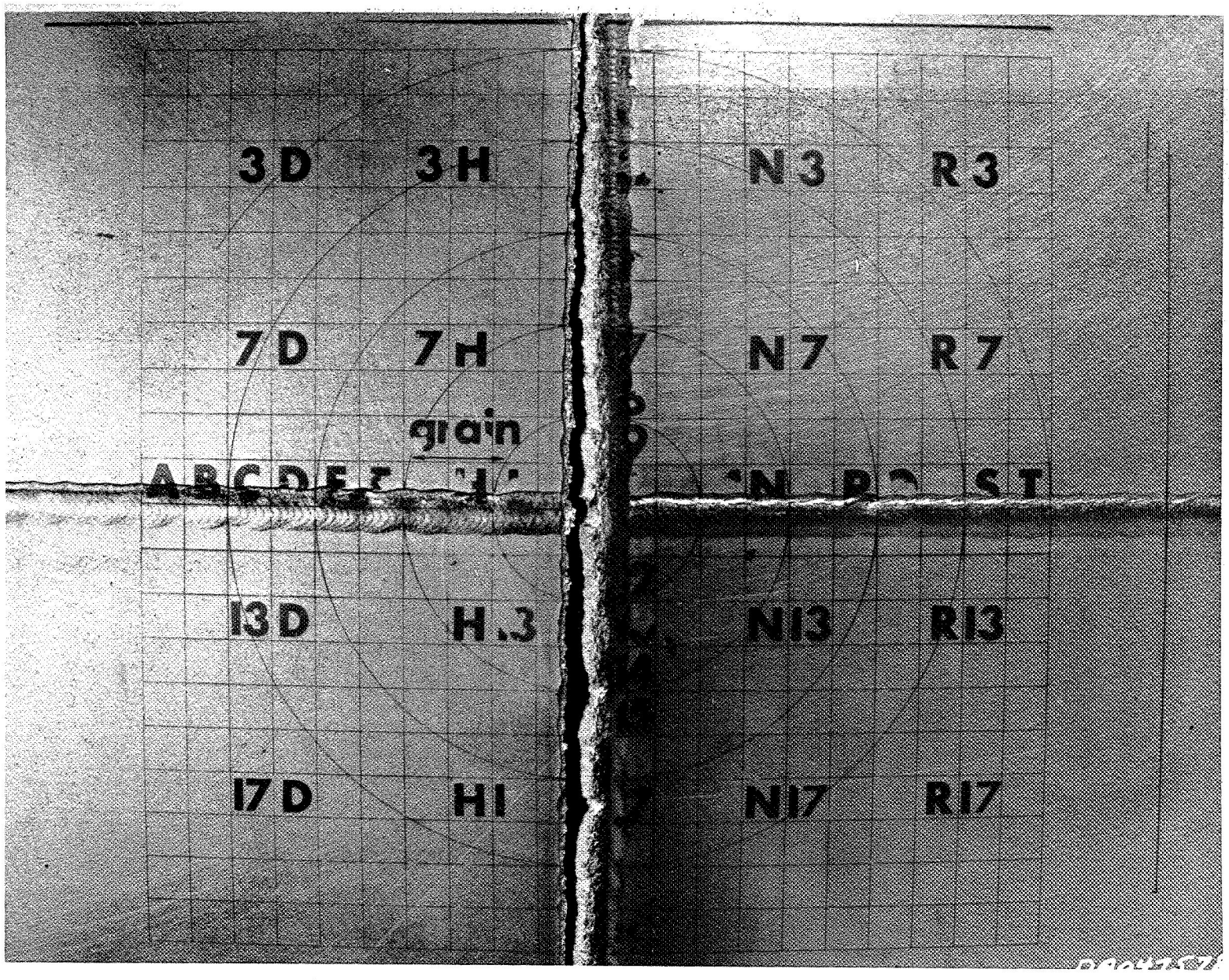

Figure 19.-Failed Specimen BRE, Close-Up of Gridded Area

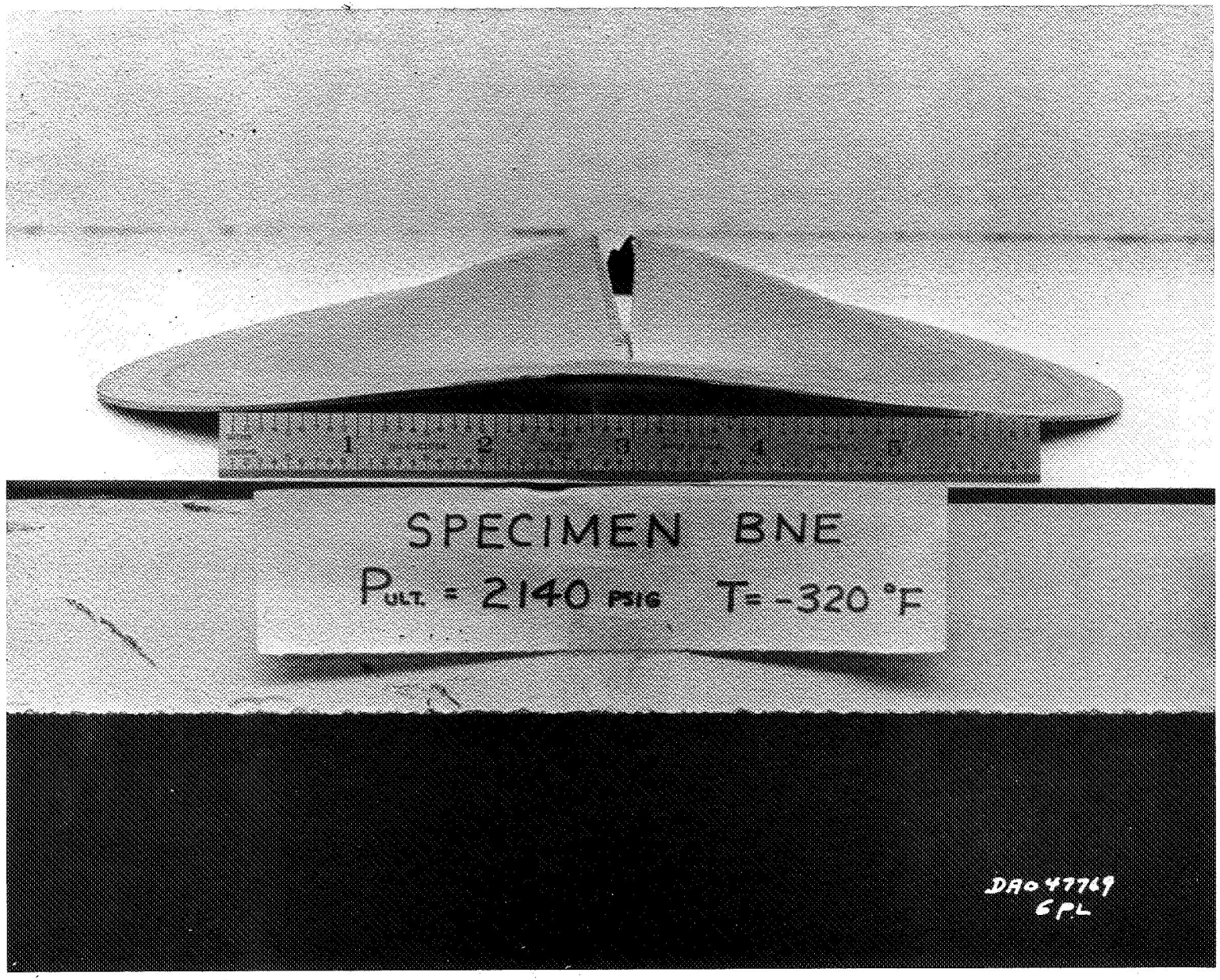

Figure 20.-Failed Specimen BNE, Edge View

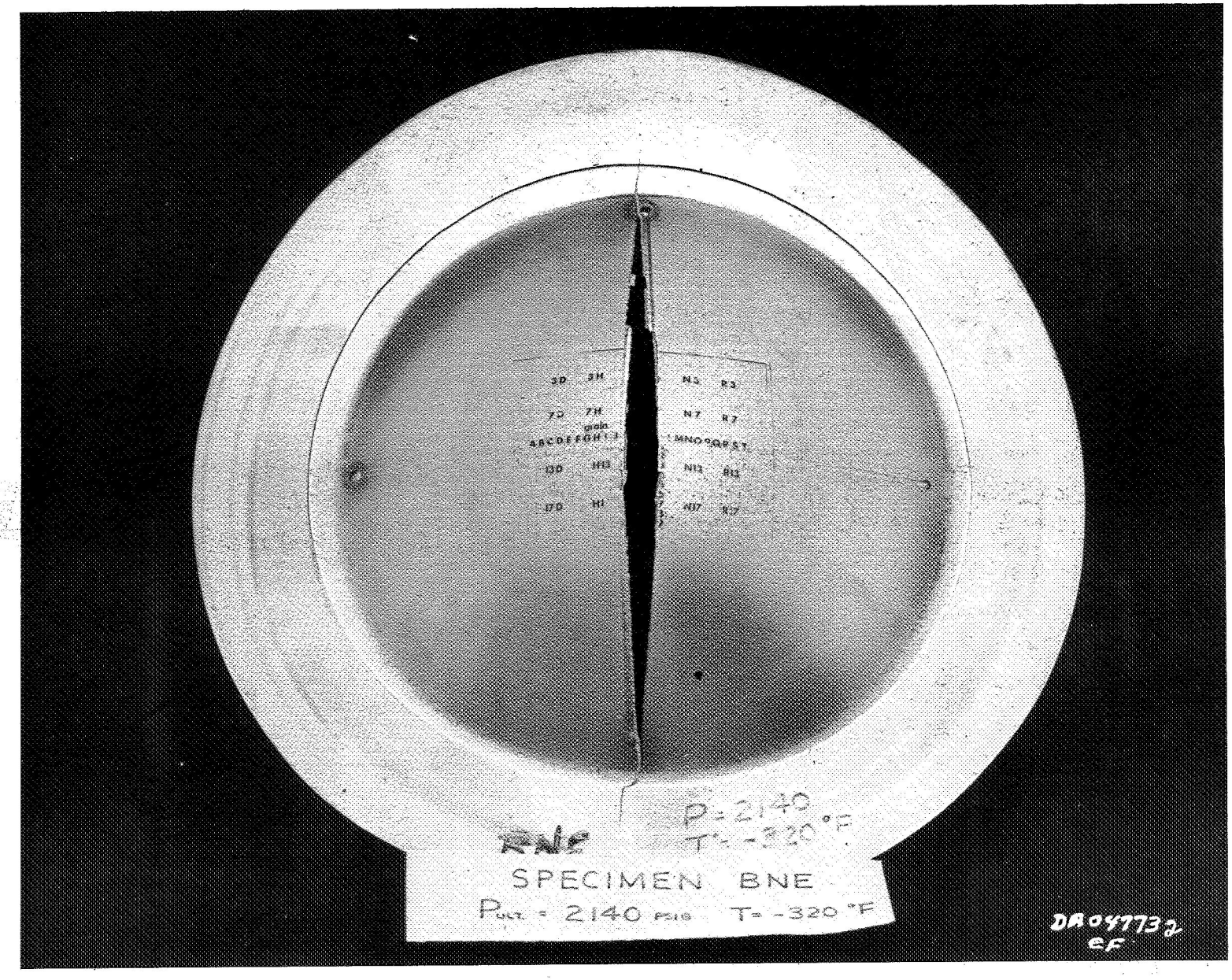

Figure 21.-Failed Specimen BNE, Top View

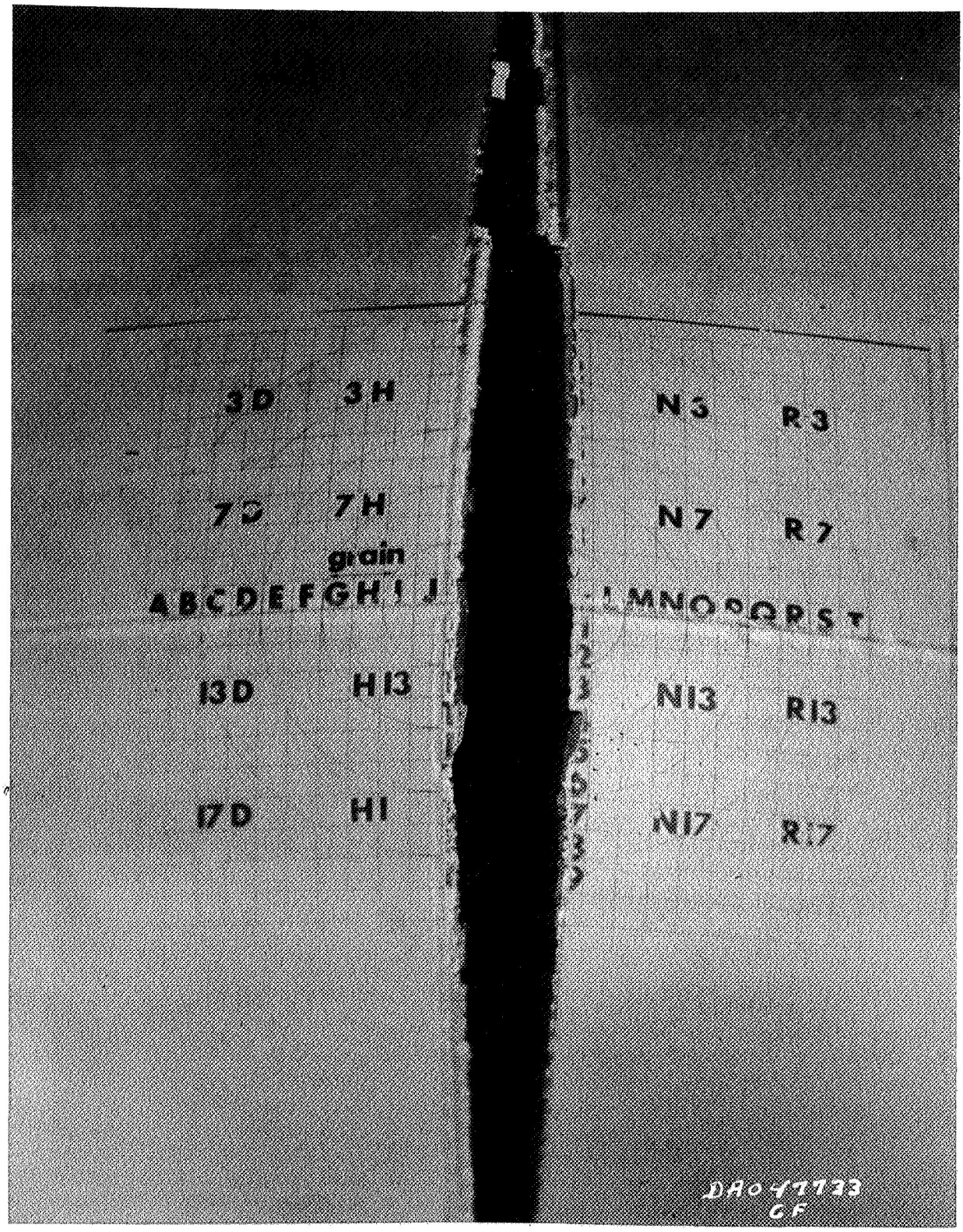

Figure 22.- Failed Specimen BNE, Close-Up

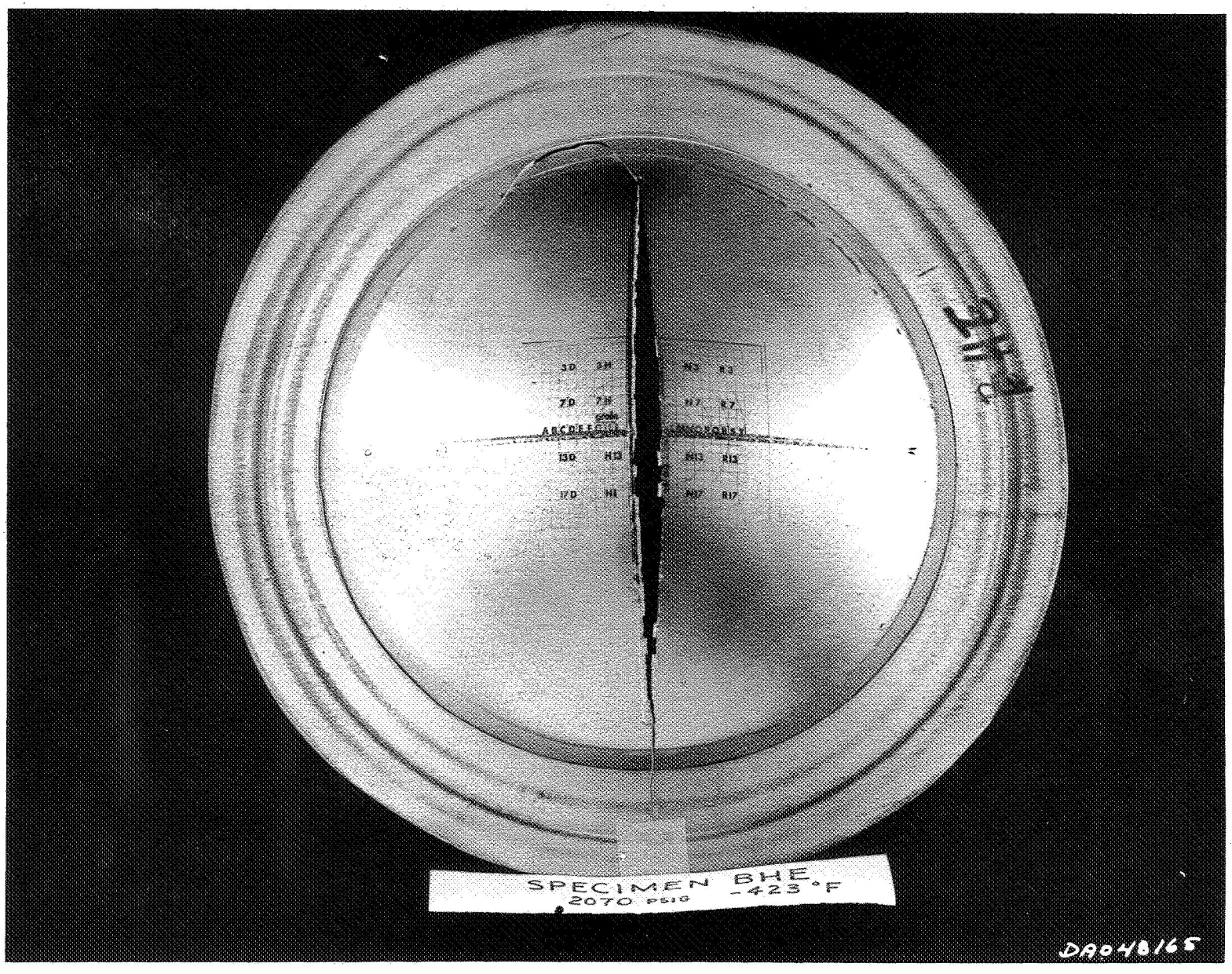

Figure 23.-Failed Specimen BHE, Top View

Figure 24.-Failed Specimen BHE, Side View

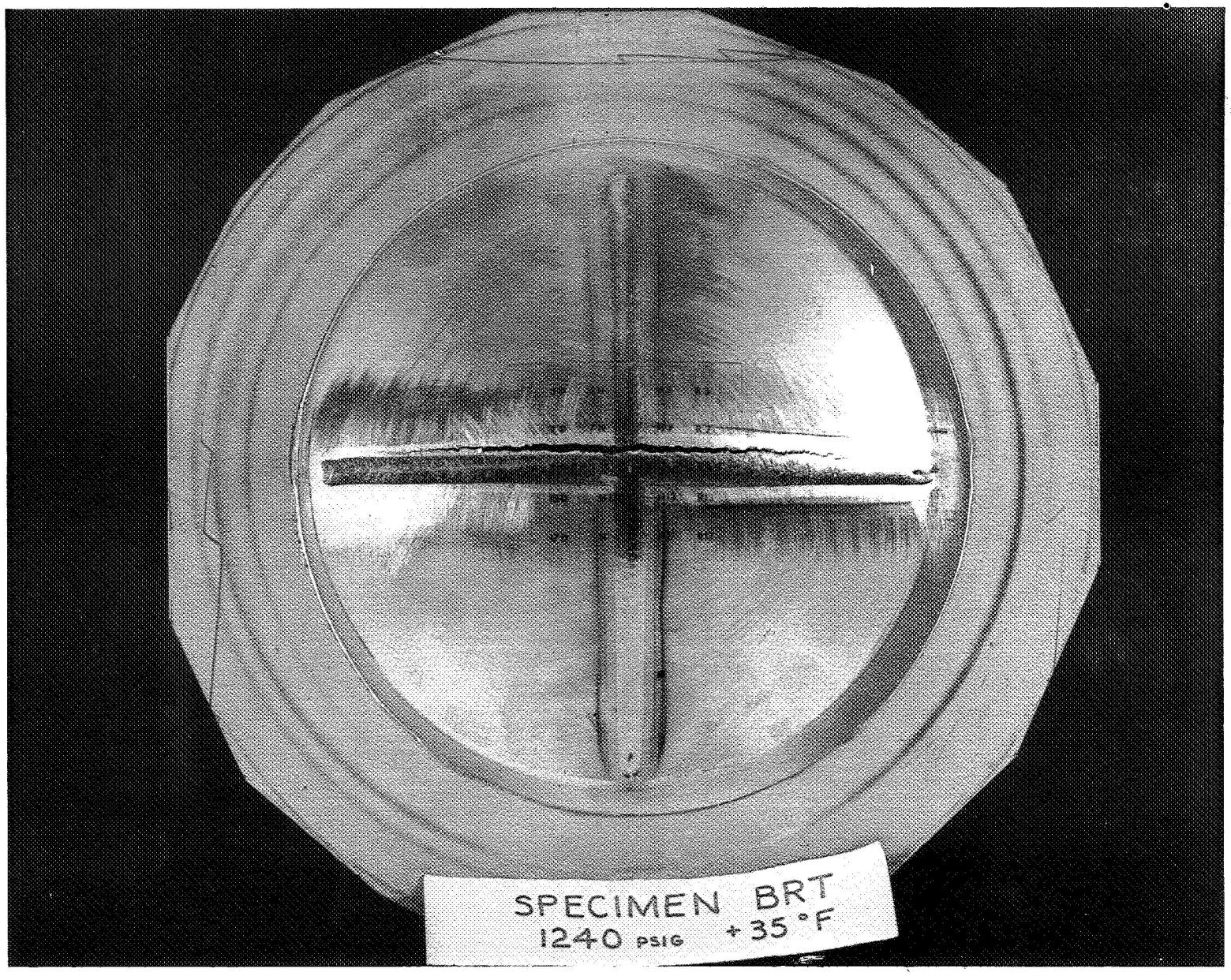

Figure 25.-Failed Specimen BRT, Top View

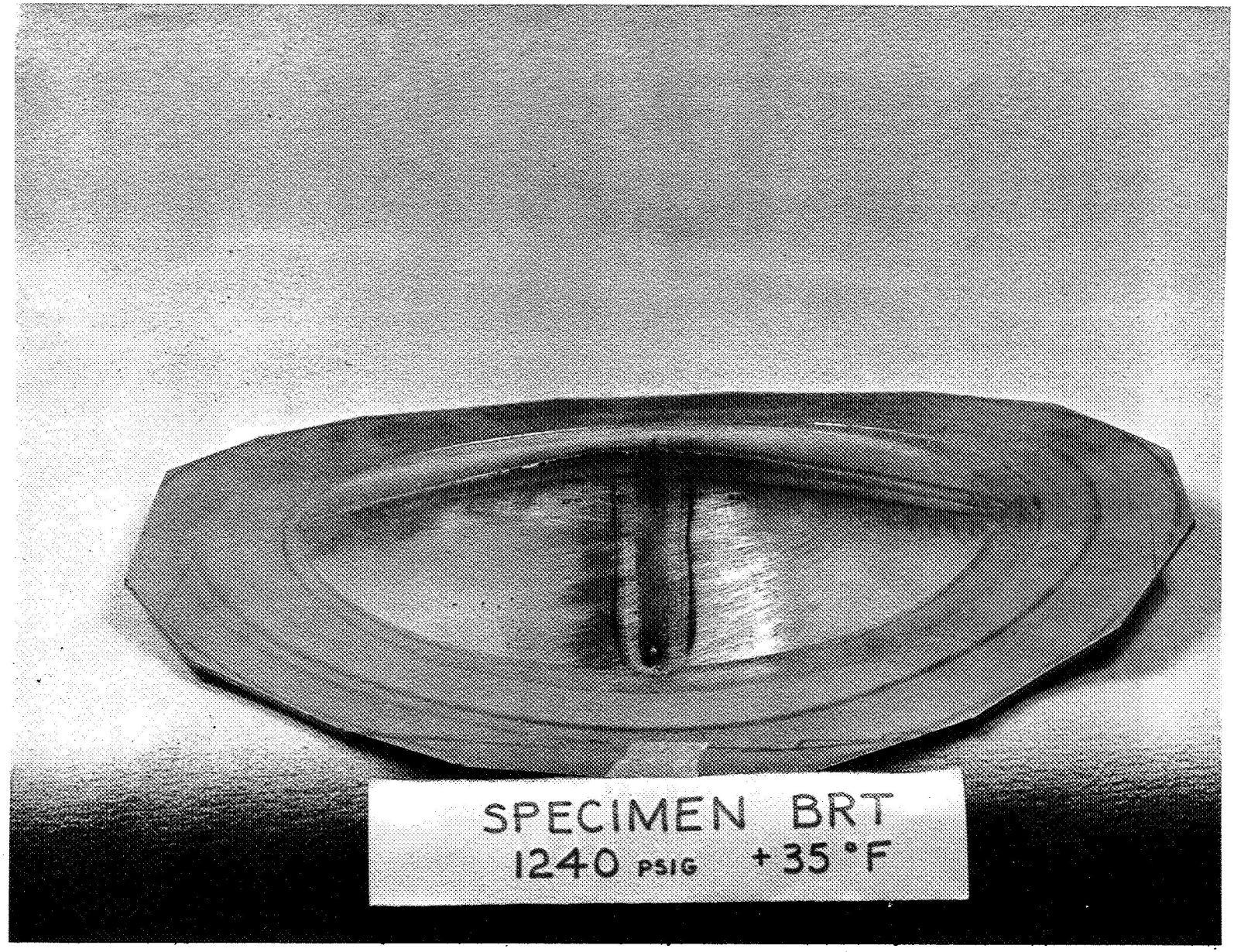

Figure 26.-Failed Specimen BRT, Side View

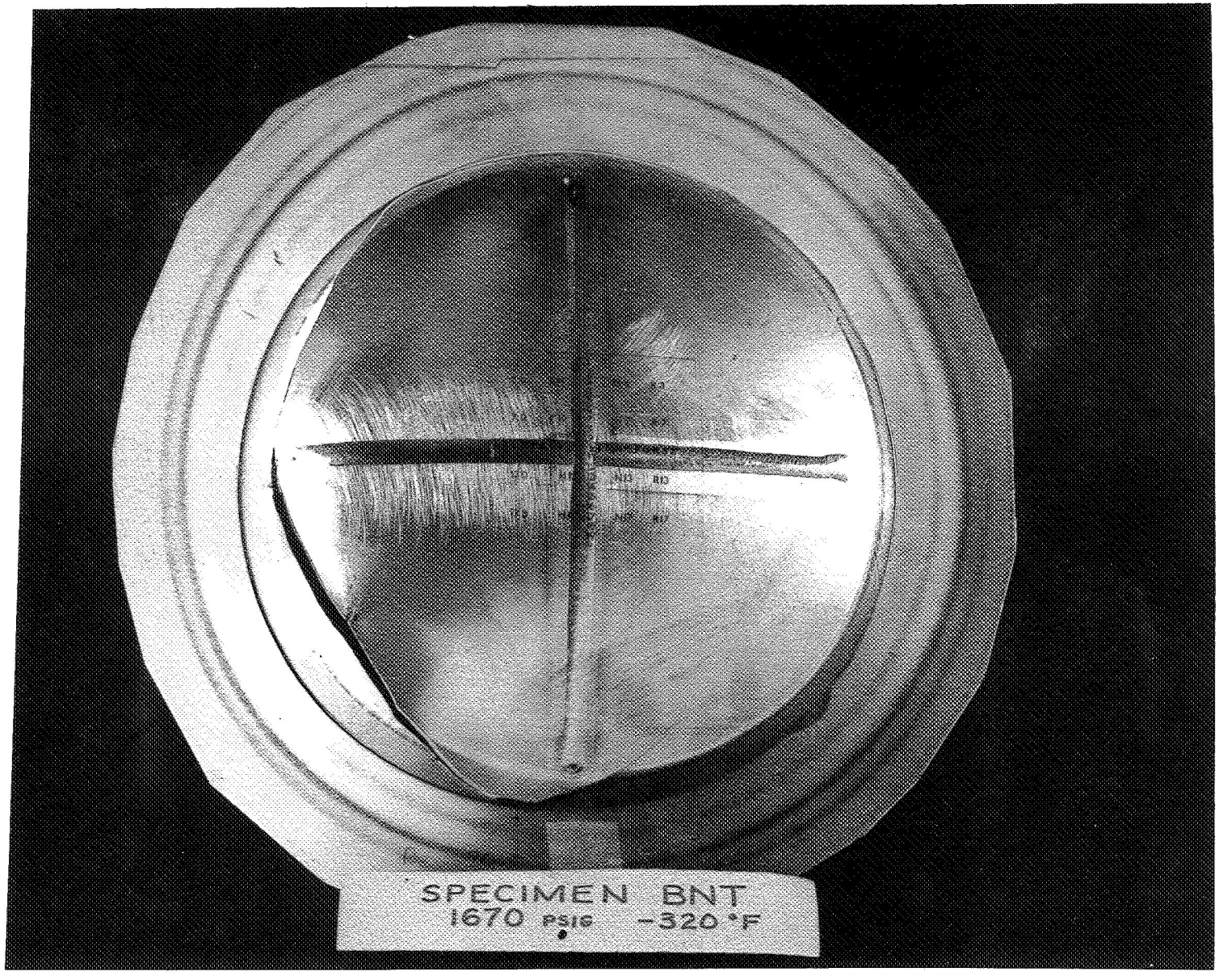

Figure 27.- Failed Specimen BNT, Top View

Figure 28.-Failed Specimen BNT, Side View

Figure 29.-Failed Specimen BHT, Top View

Figure 30.-Failed Specimen BHT, Side View

Figure 31.- Failed Specimen BRD

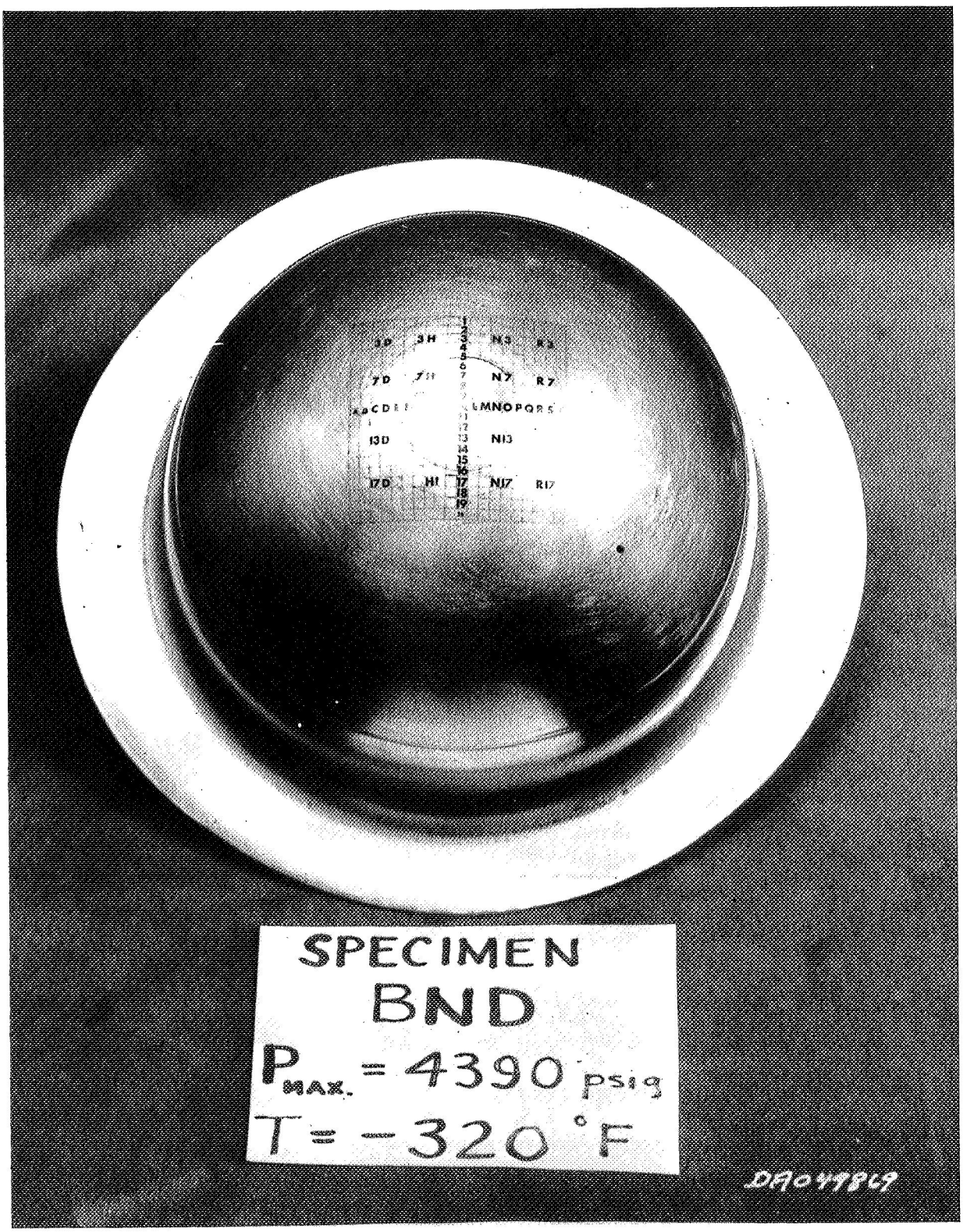

Figure 32.- Specimen BND After Test

Figure 33.-Failed Specimen BHD

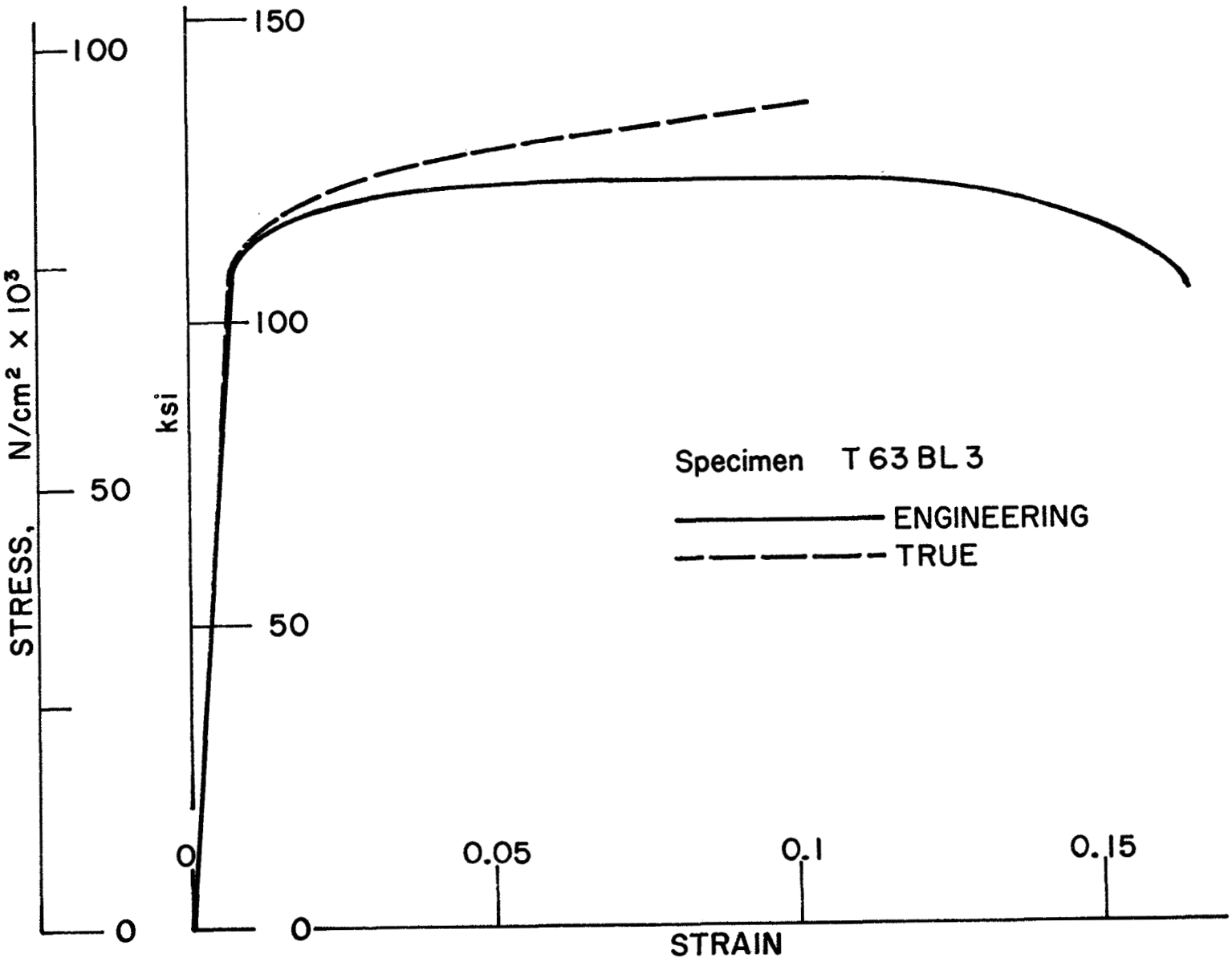

Figure 34.-Stress vs Strain for Specimen T63BL3, Arithmetic Coordinates

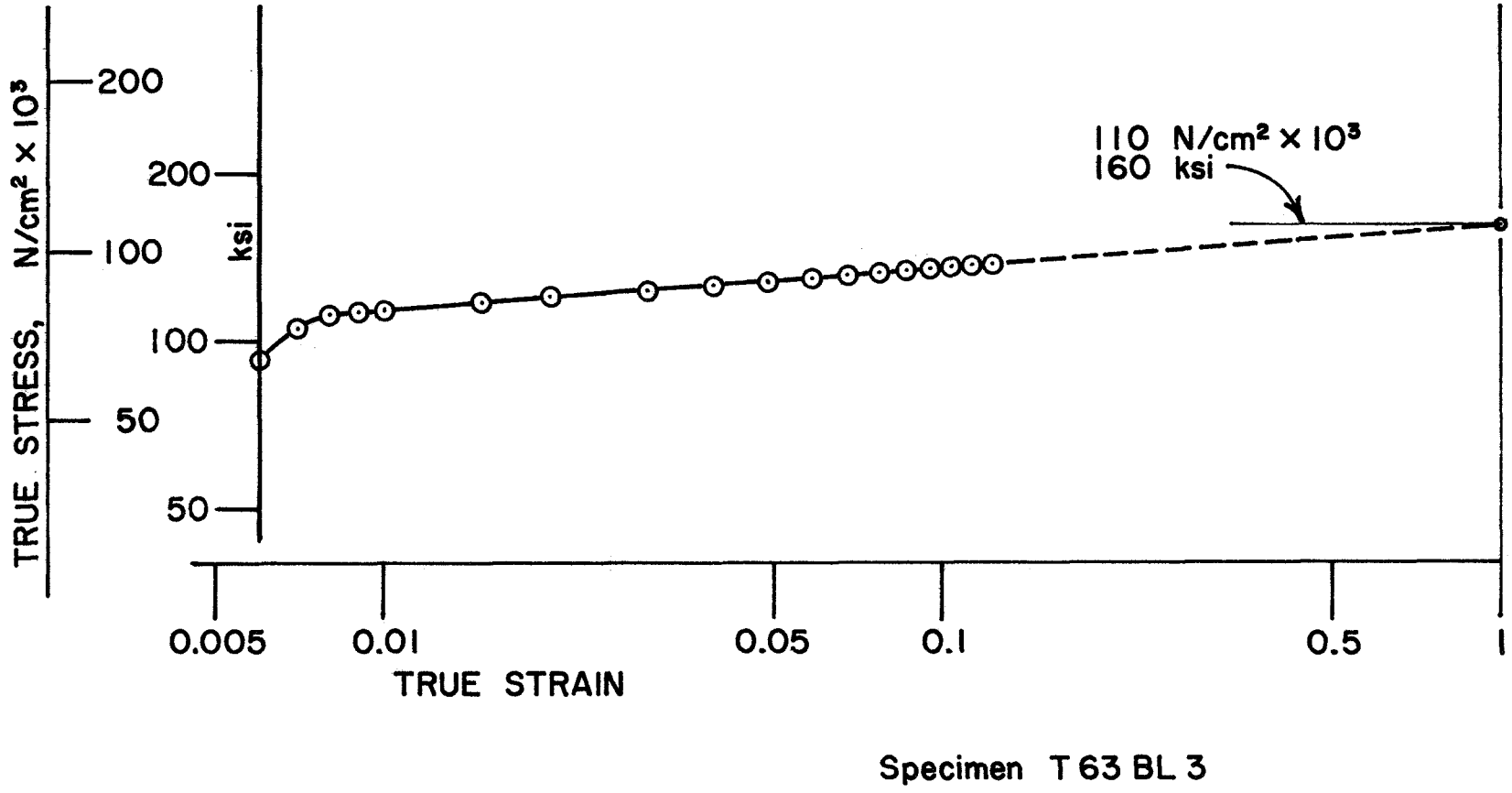

Figure 35.-True Stress vs True Strain for Specimen T63BL3, Logarithmic Coordinates

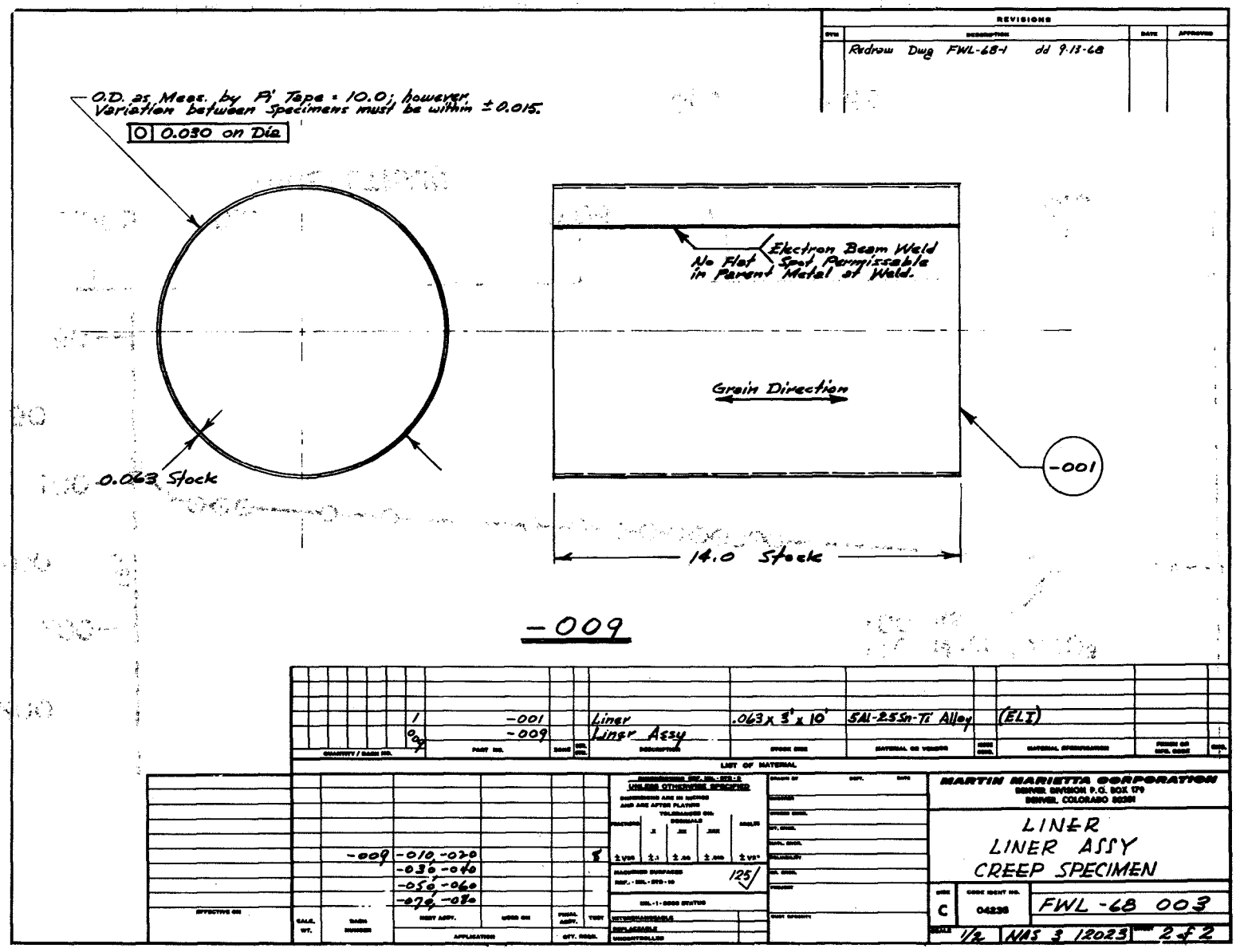

Figure 36.-Fabrication Plan for Creep Specimen Blanks

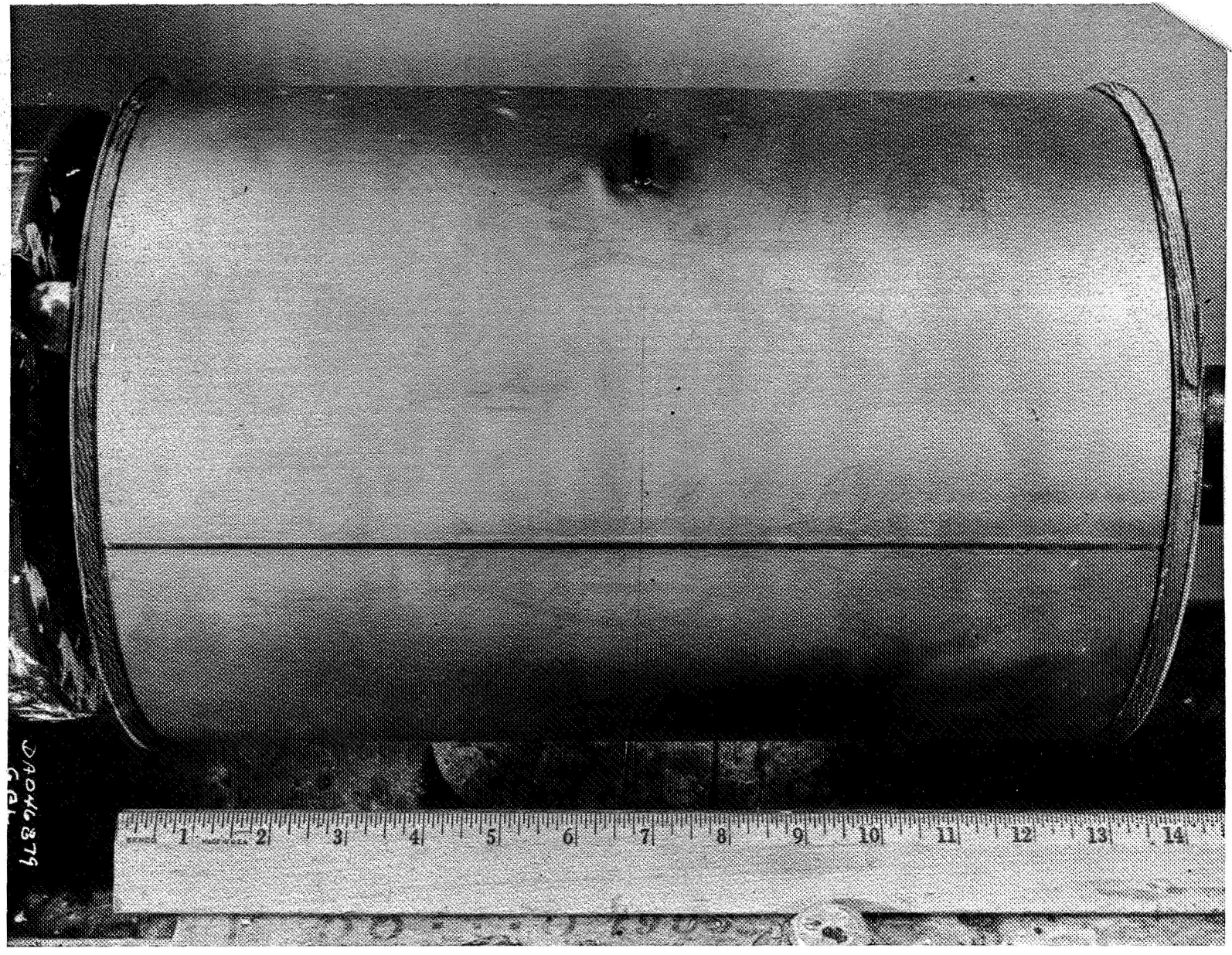

Figure 37. - Creep Specimen before Wrapping

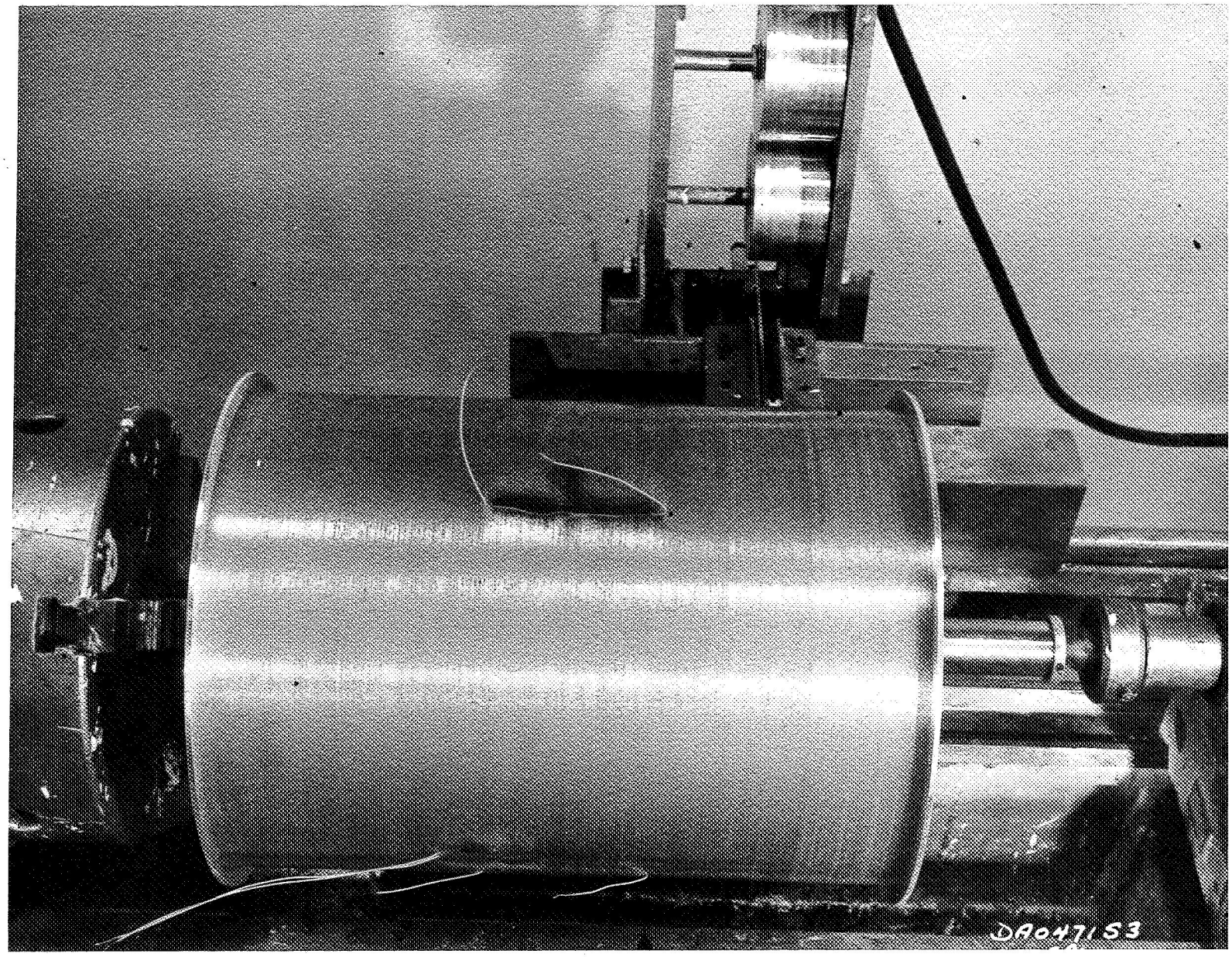

Figure 38.-Creep Specimen Being Overwrapped

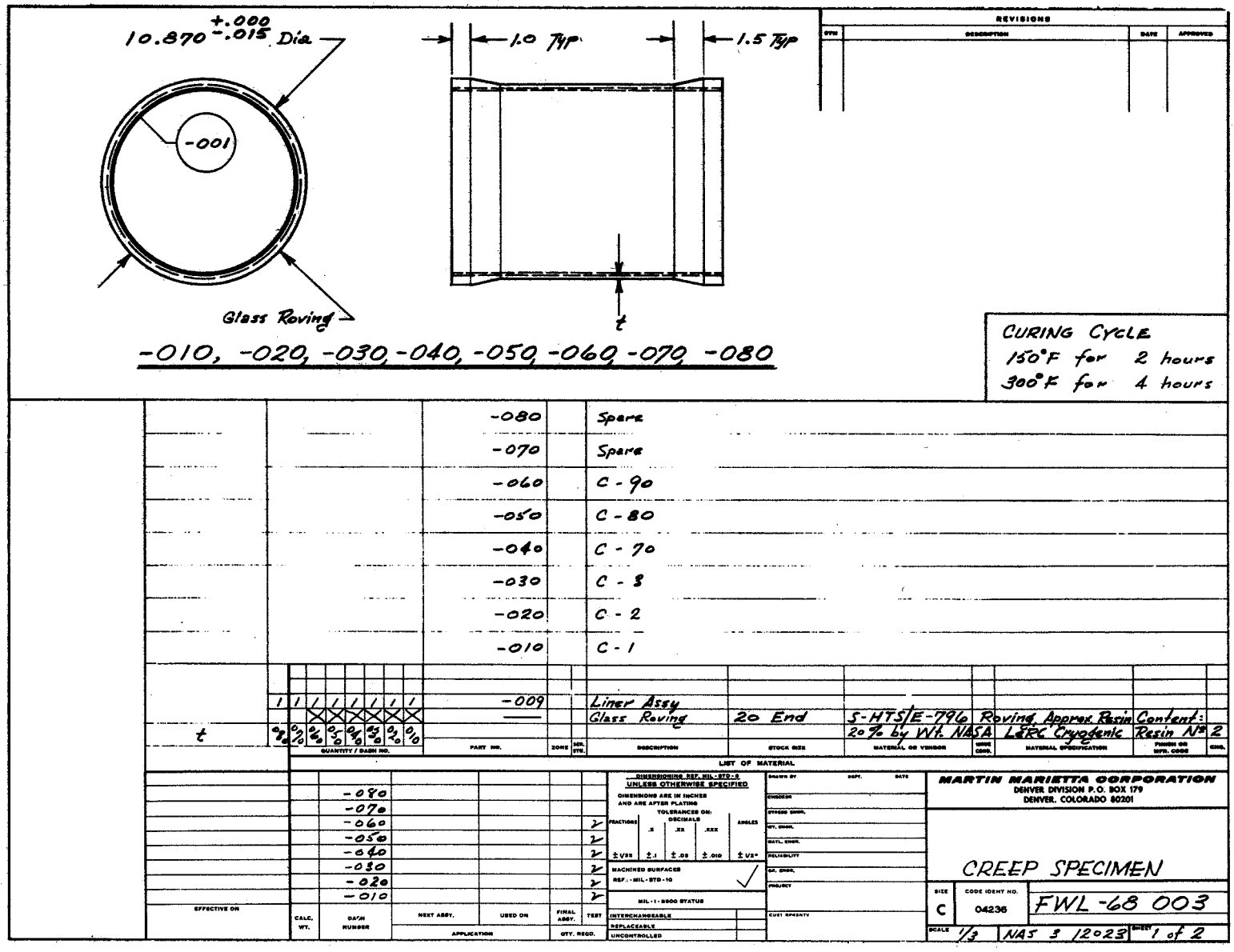

Figure 39.- Plan for Overwrapped Creep Specimens

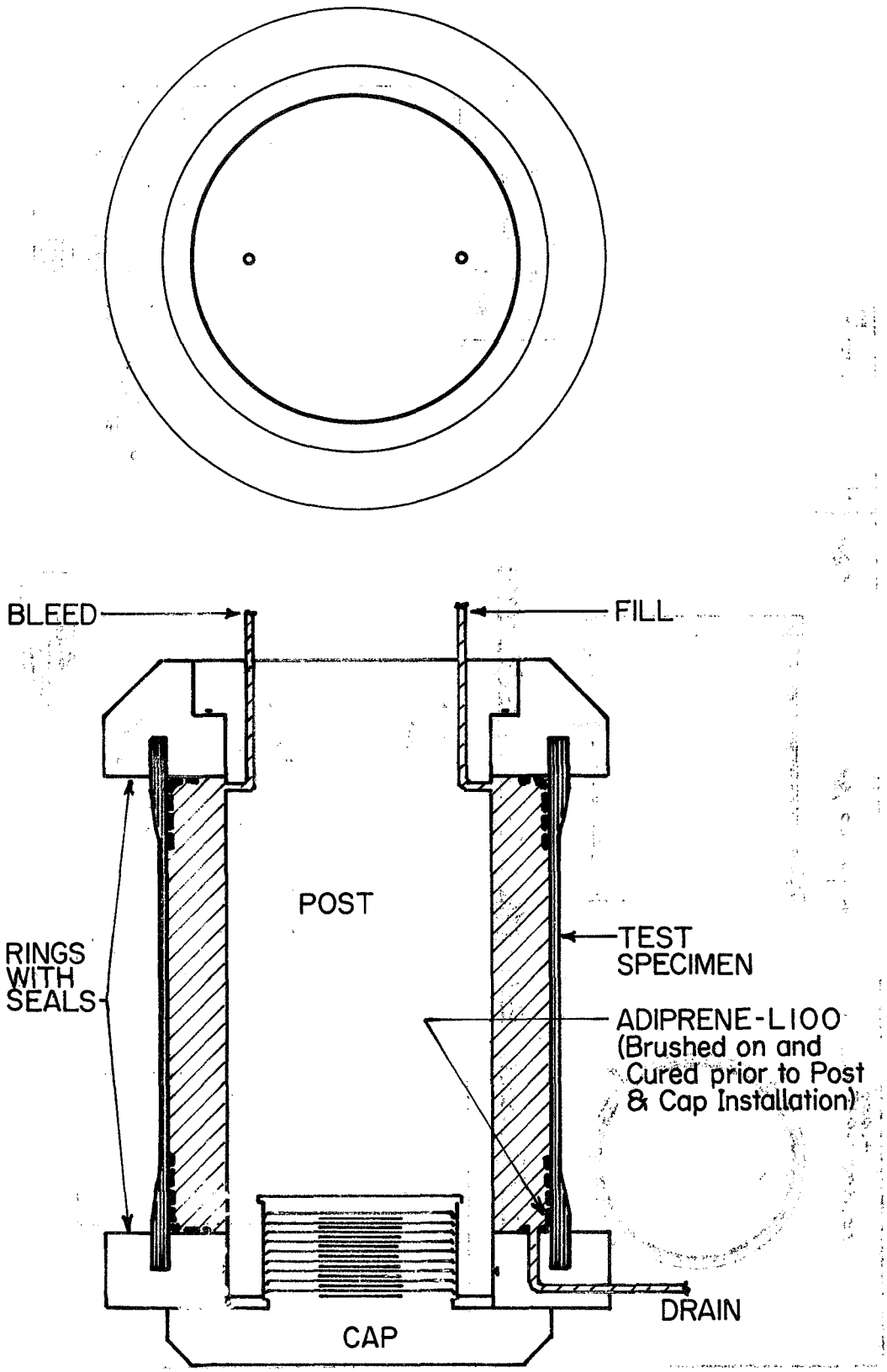

Figure 40.-Creep Test Setup

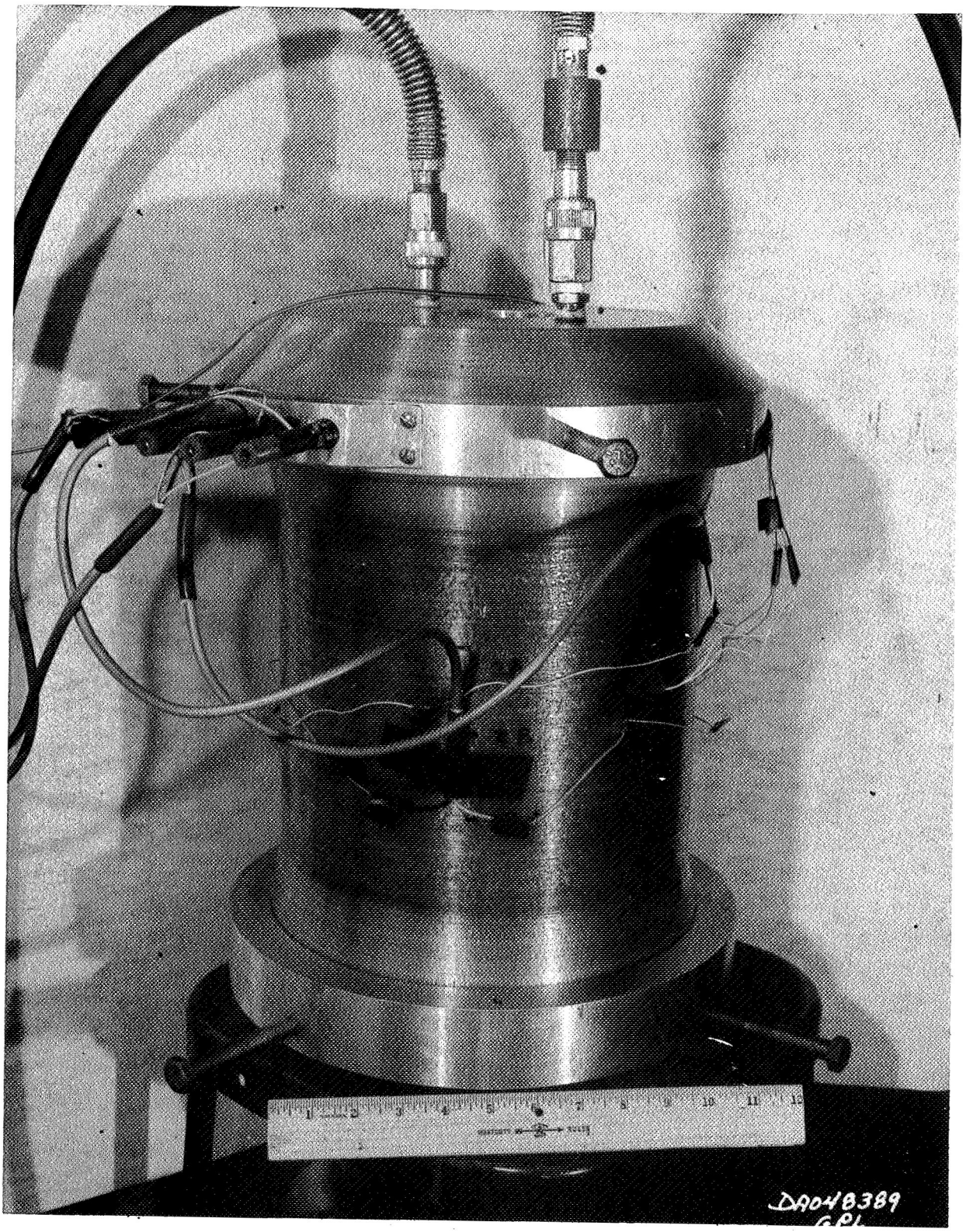

Figure 41.-Assembled Creep Test Fixture with Specimen

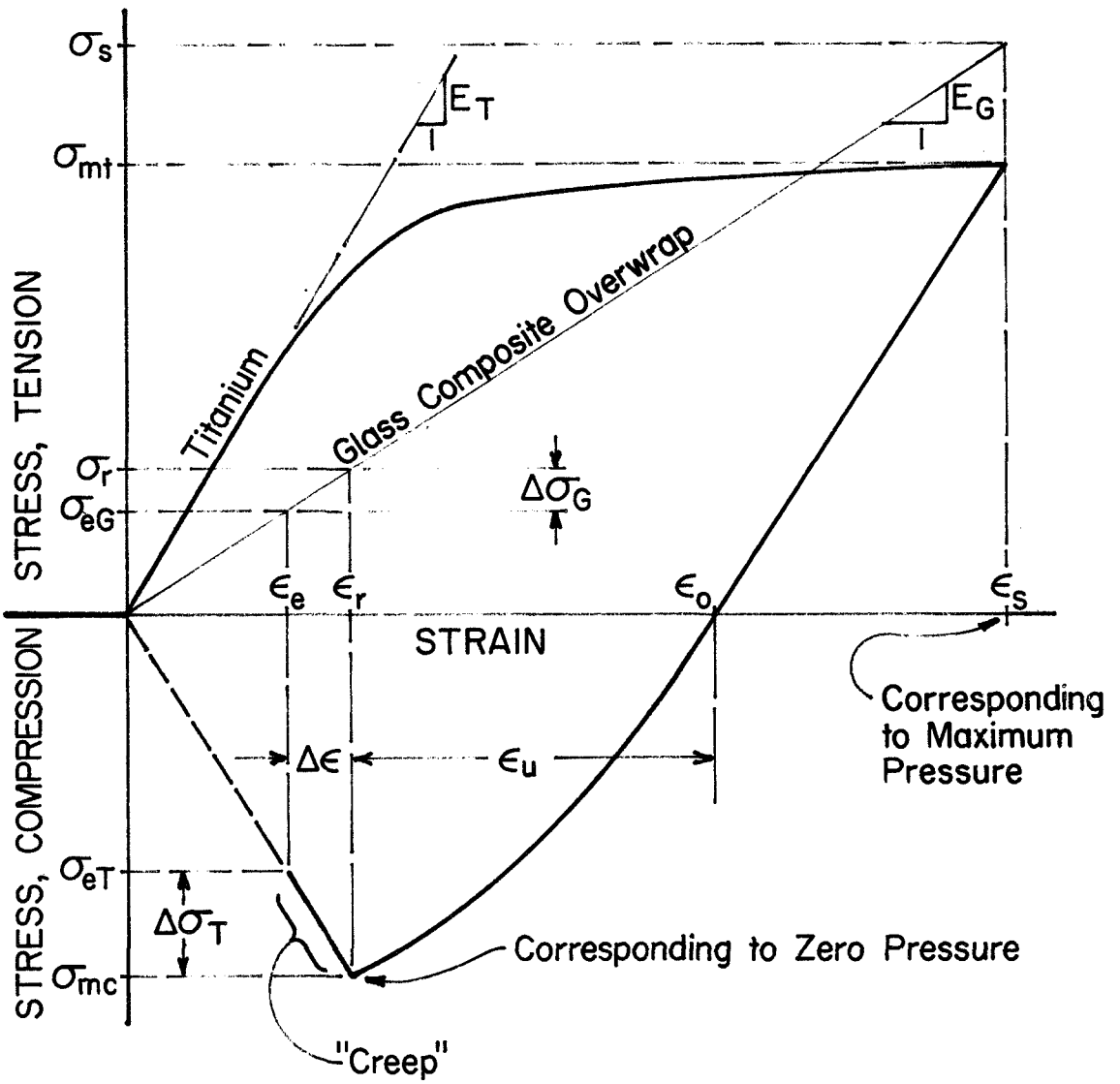

Figure 42.-Stress-Strain Characteristics of Titanium and Fiberglass, Defining Symbols

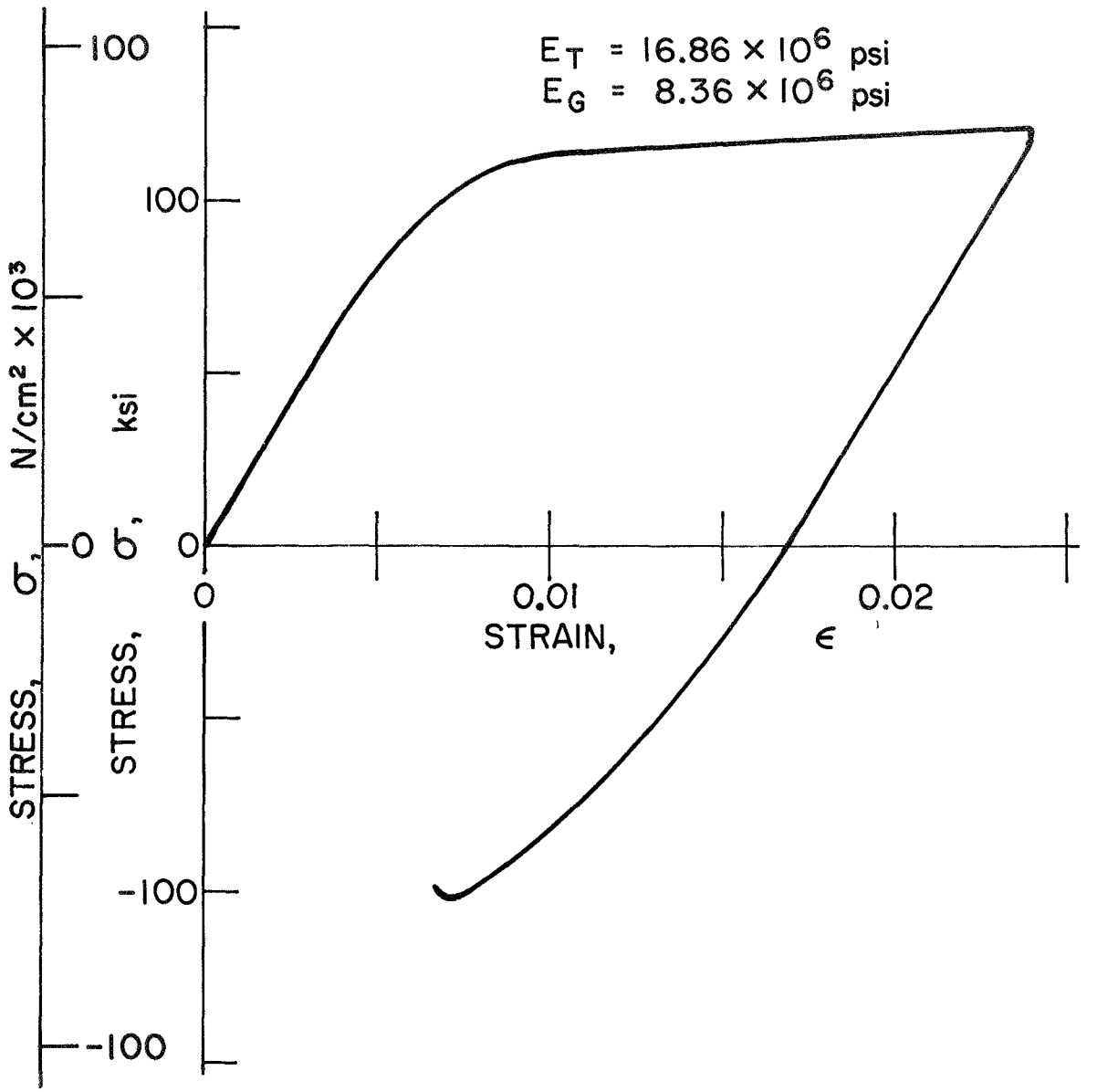

Figure 43.-Computed Stress vs Strain for Specimen C-1

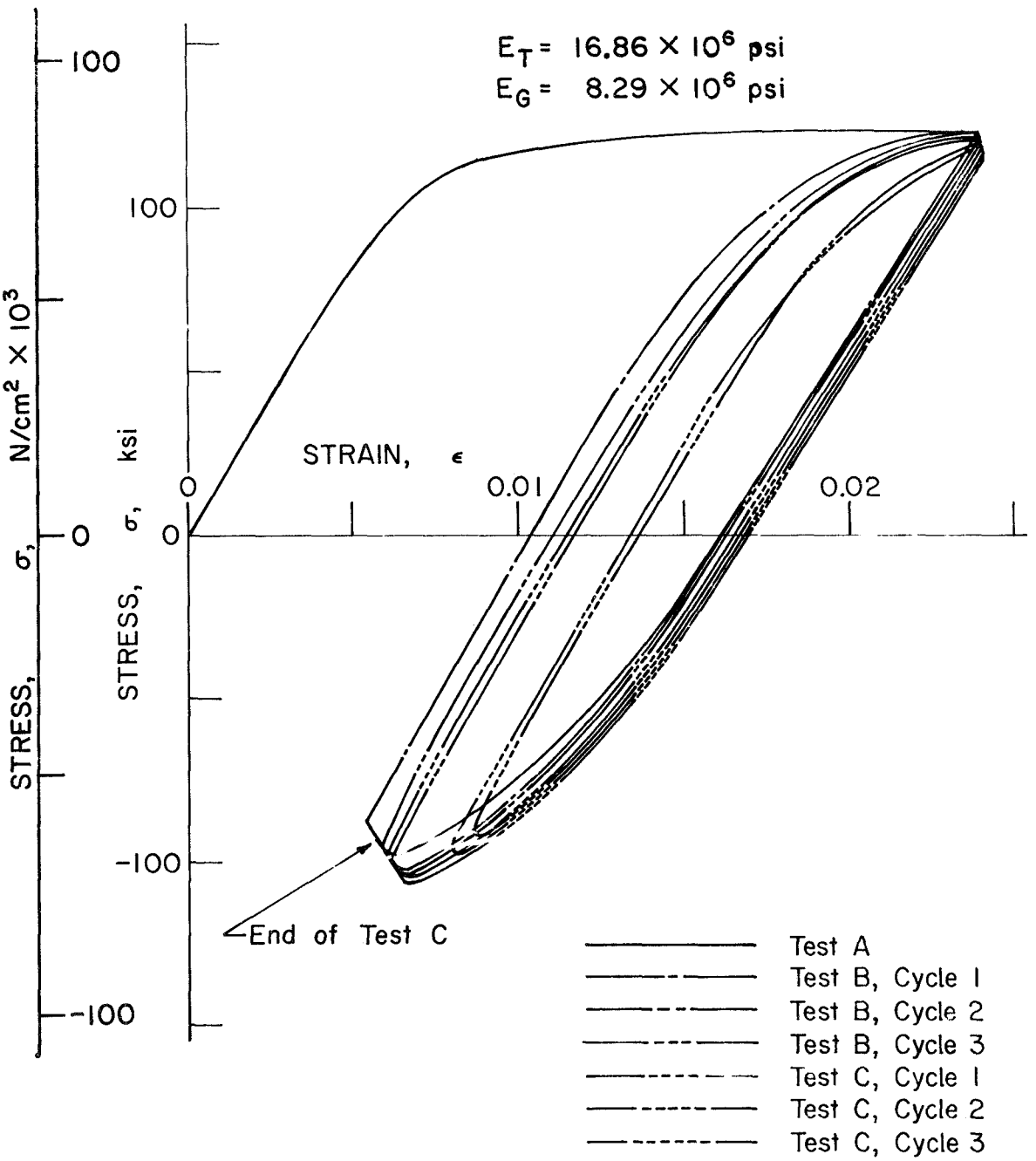

Figure 44.-Computed Stress vs Strain for Specimen C-2

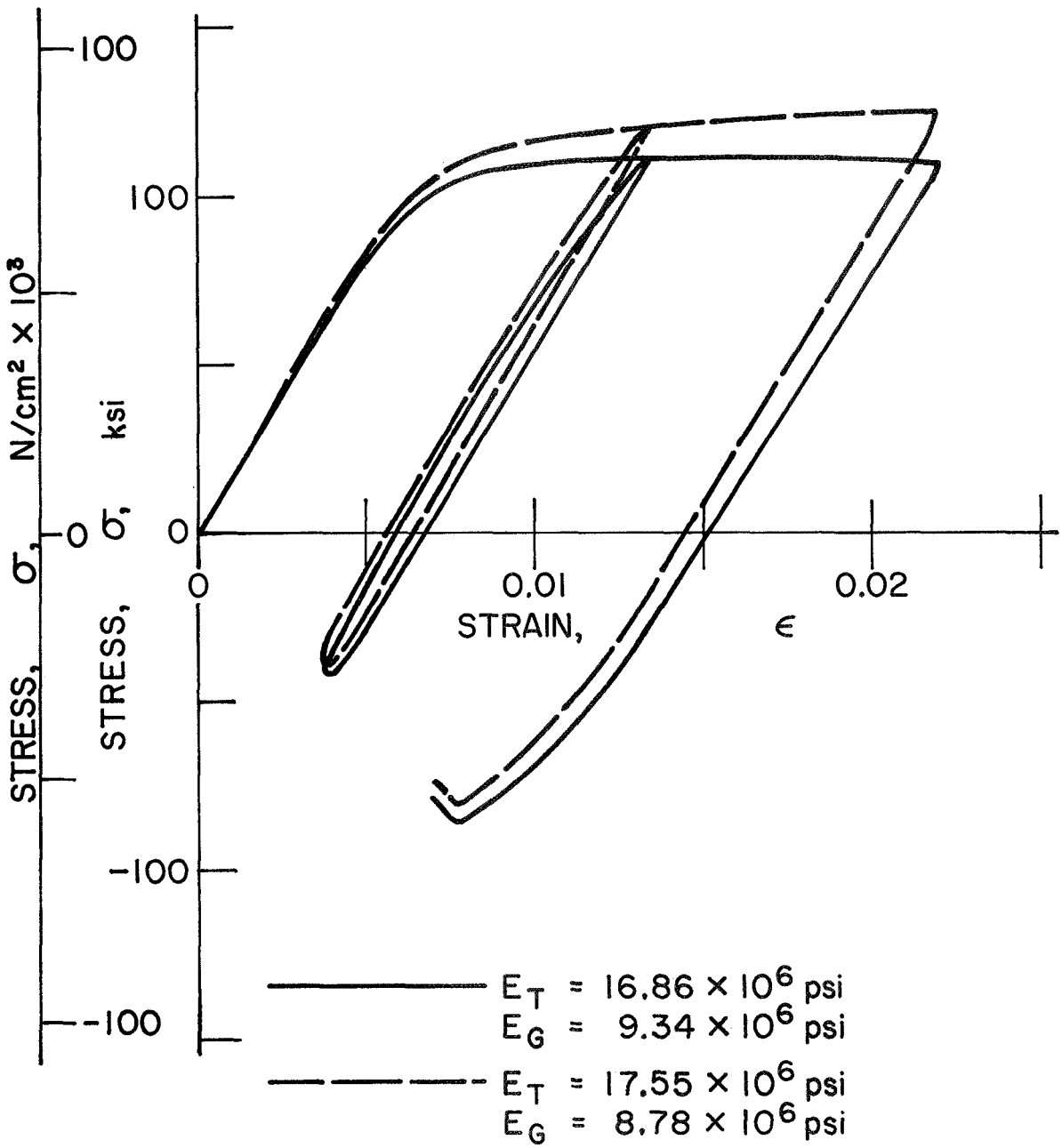

Figure 45.-Computed Stress vs Strain for Specimen C-90

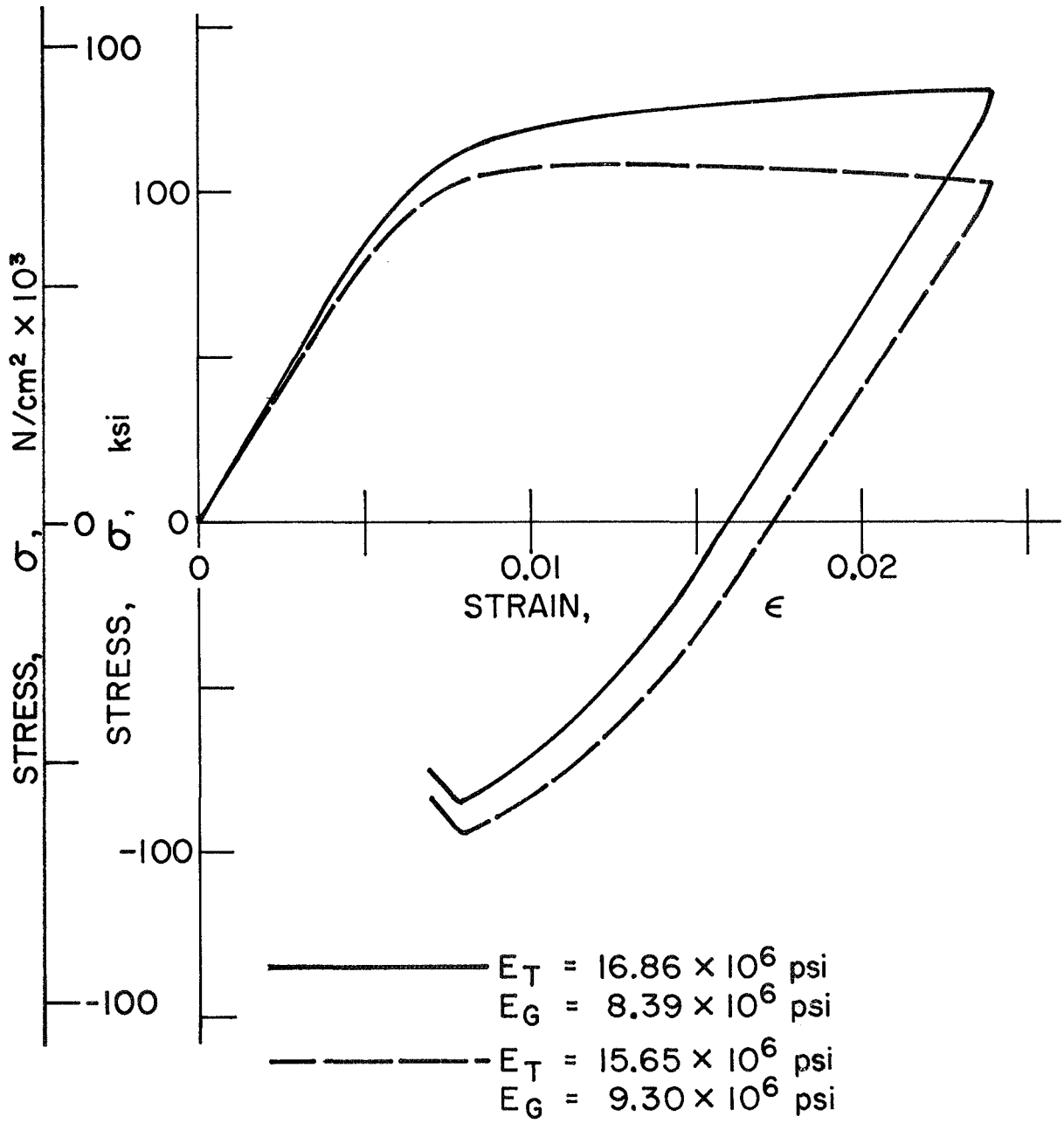

Figure 46.-Computed Stress vs Strain for Specimen C-80

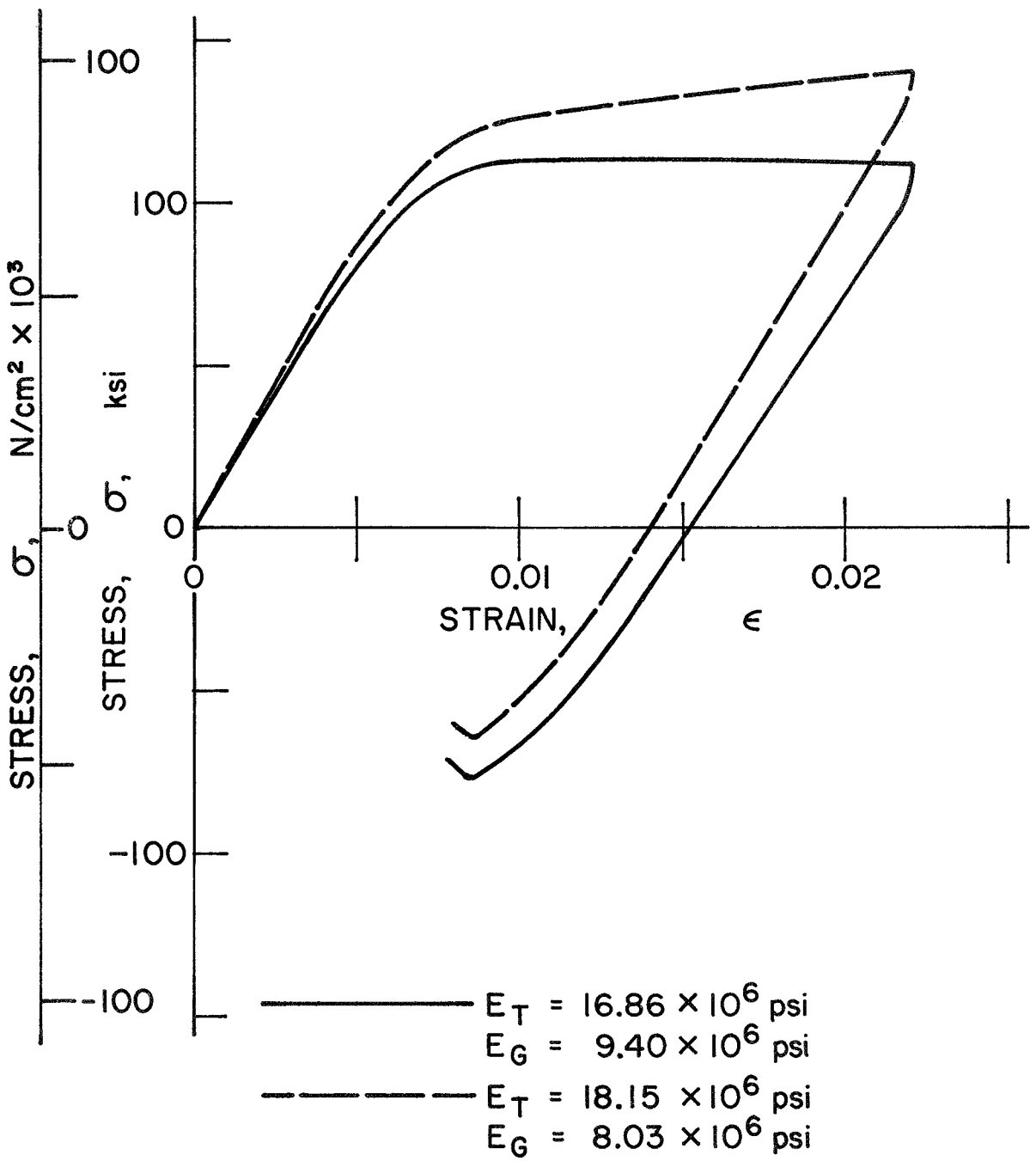

Figure 47.-Computed Stress vs Strain for Specimen C-70

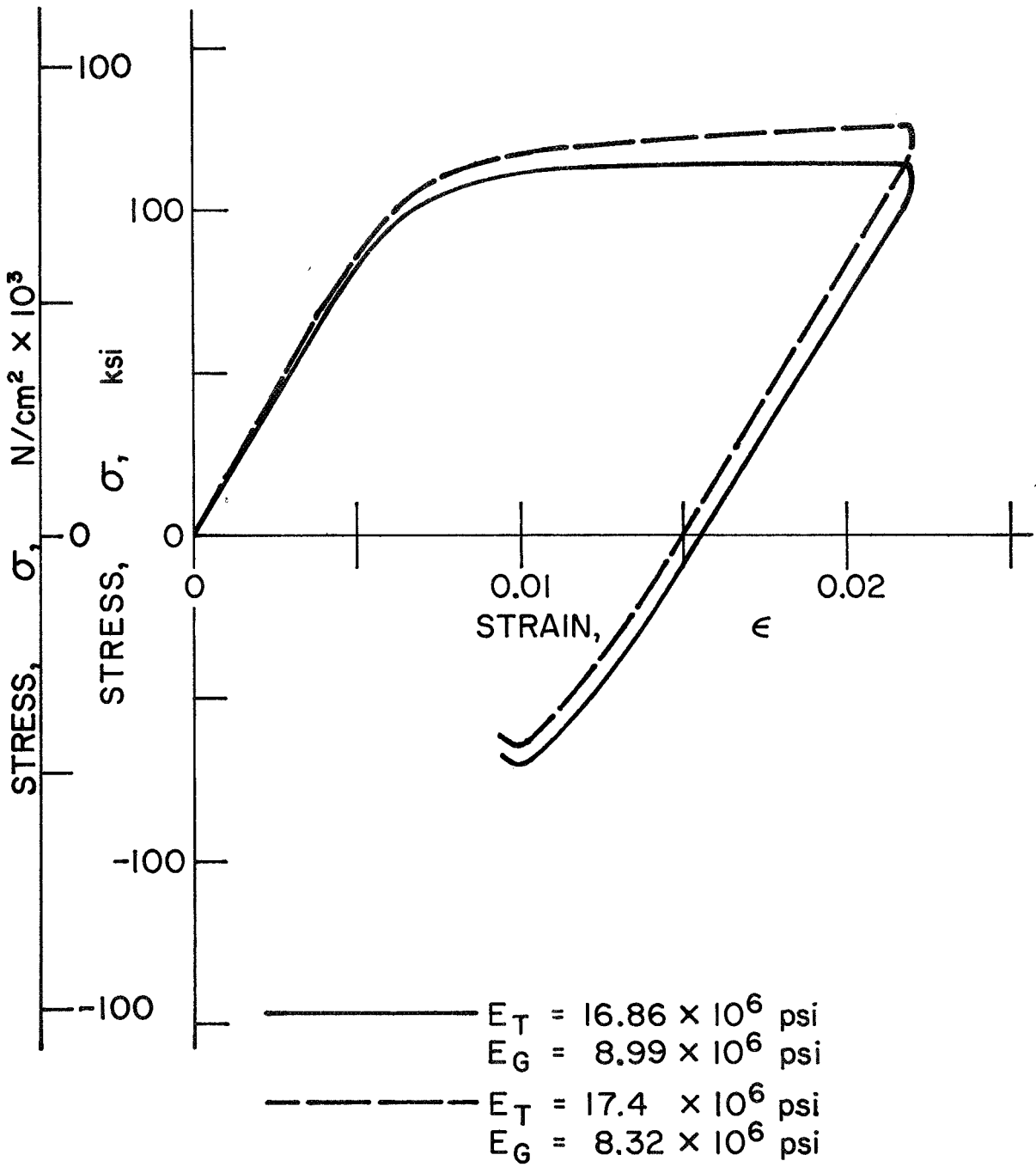

Figure 48.-Computed Stress vs Strain for Specimen C-X1

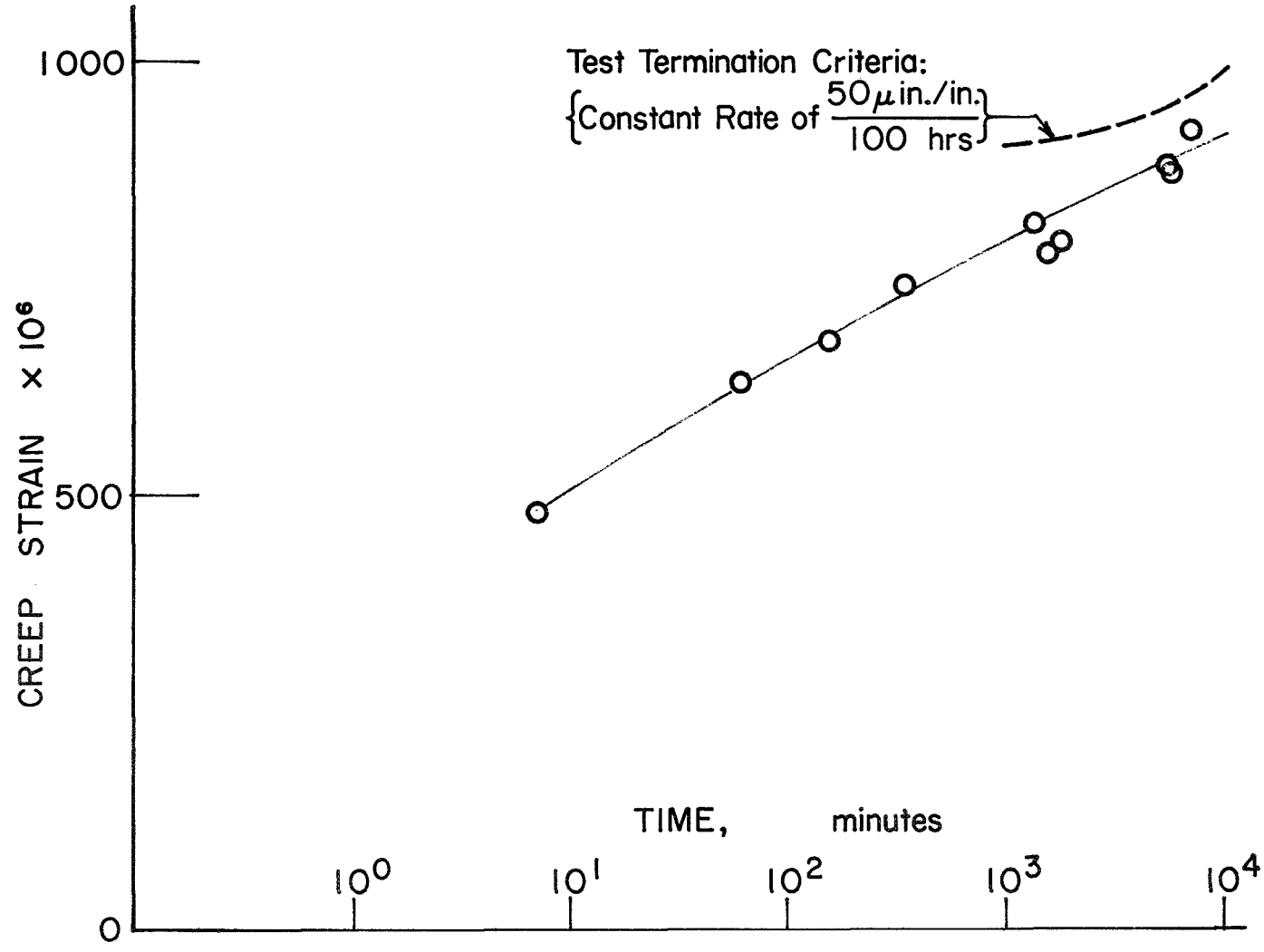

Figure 49.- Strain vs Time for Specimen C-2

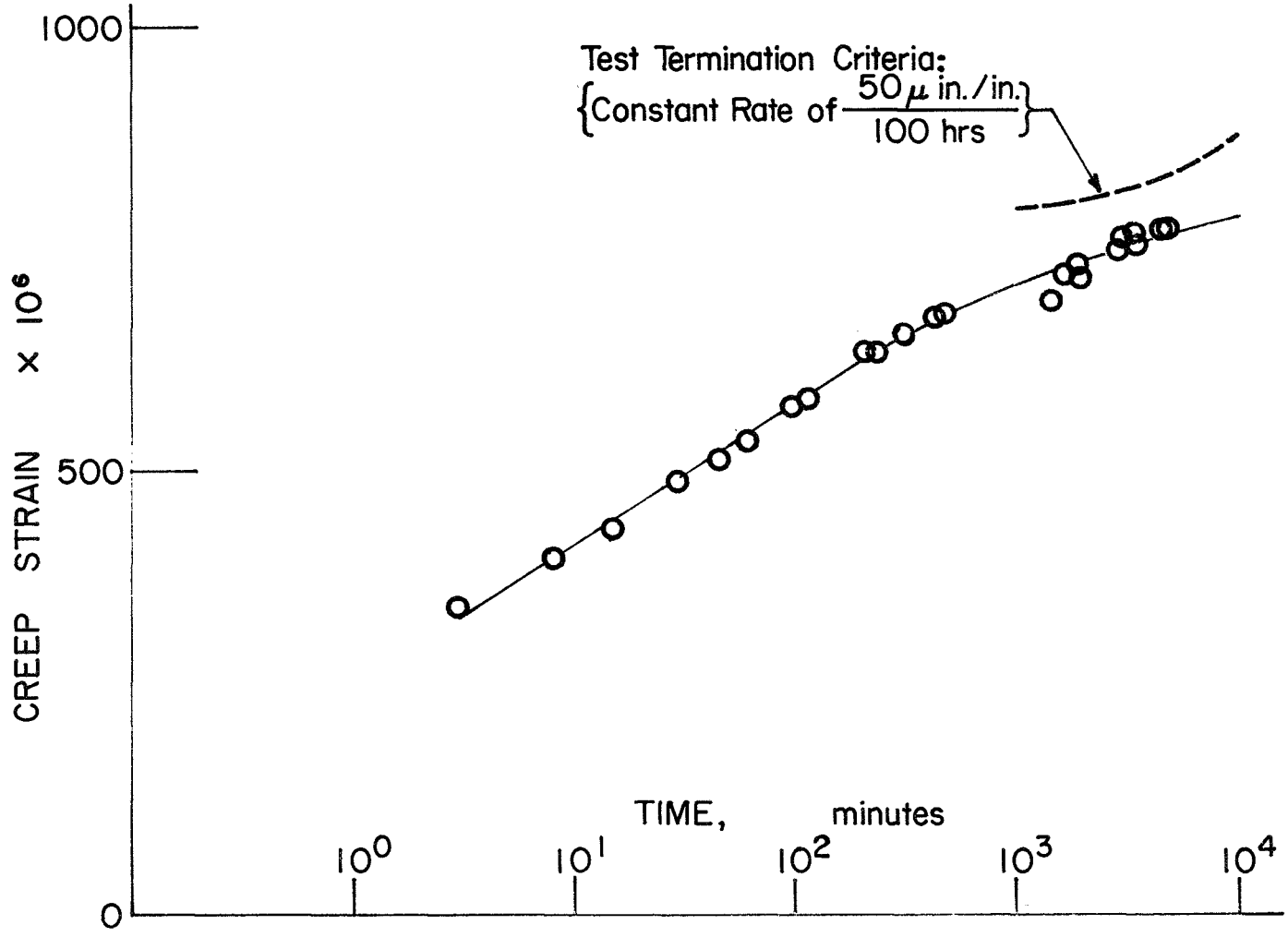

Figure 50.- Strain vs Time for Specimen C-90

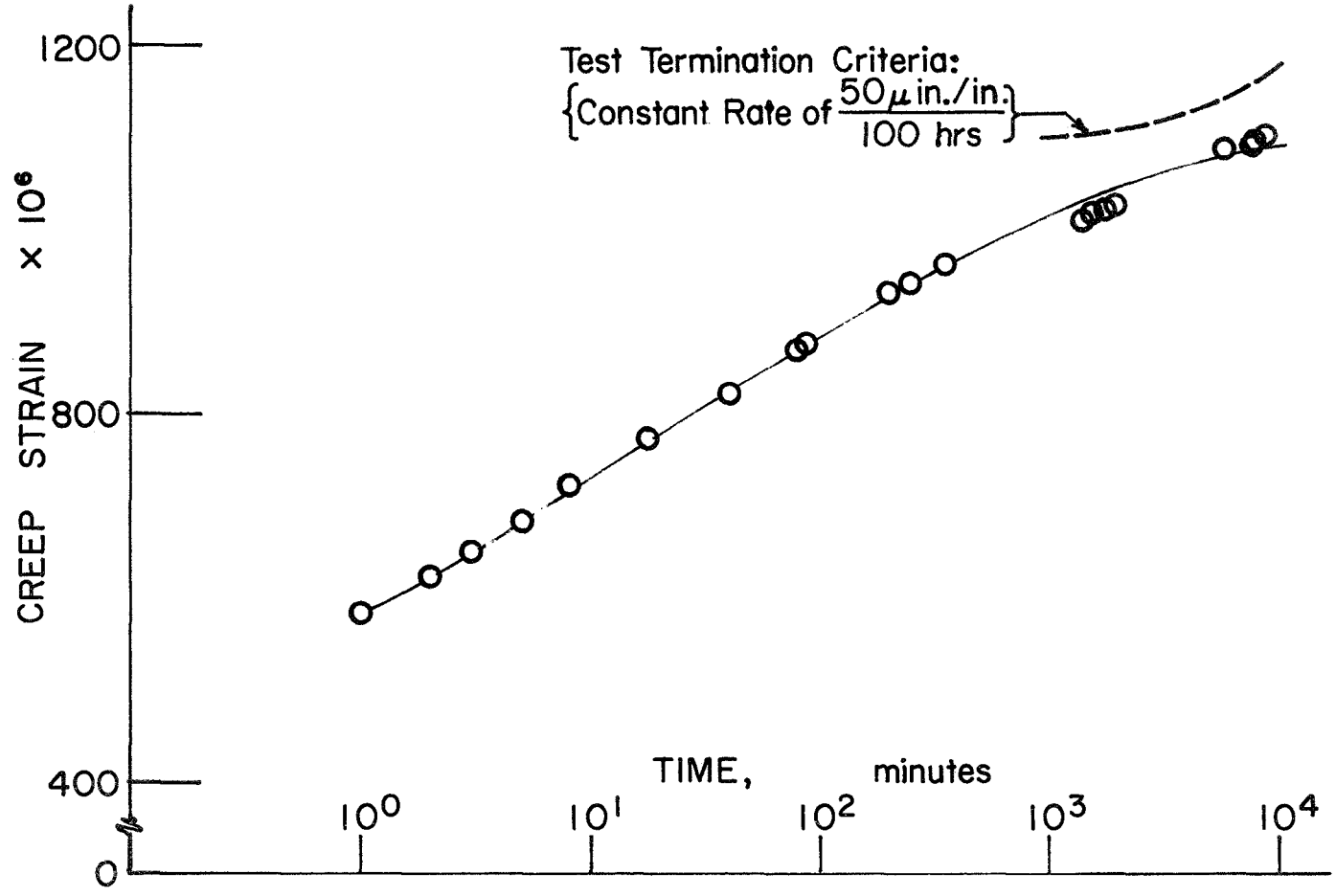

Figure 51.-Strain vs Time for Specimen C-80

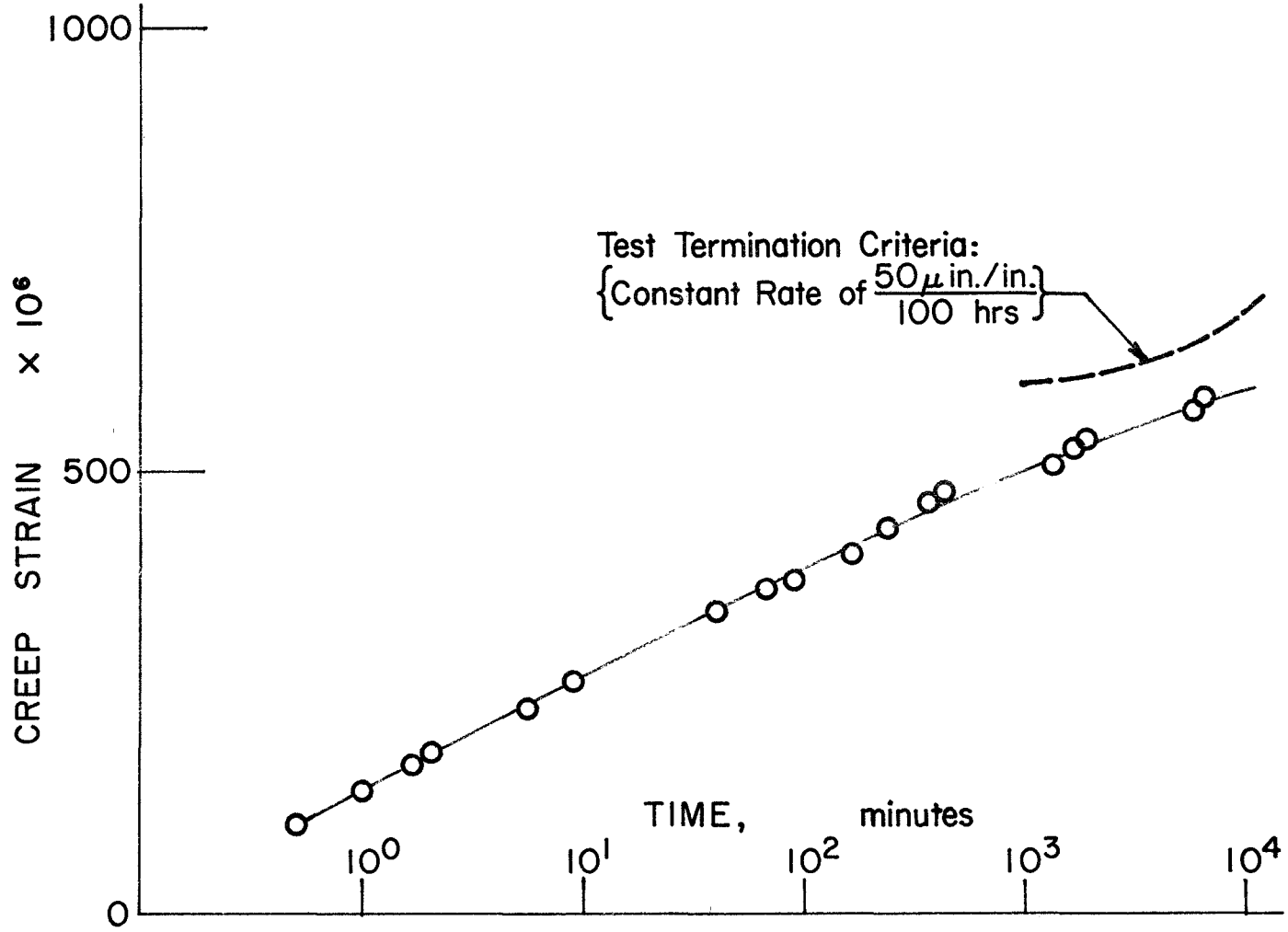

Figure 52. Strain vs Time for Specimen C-70

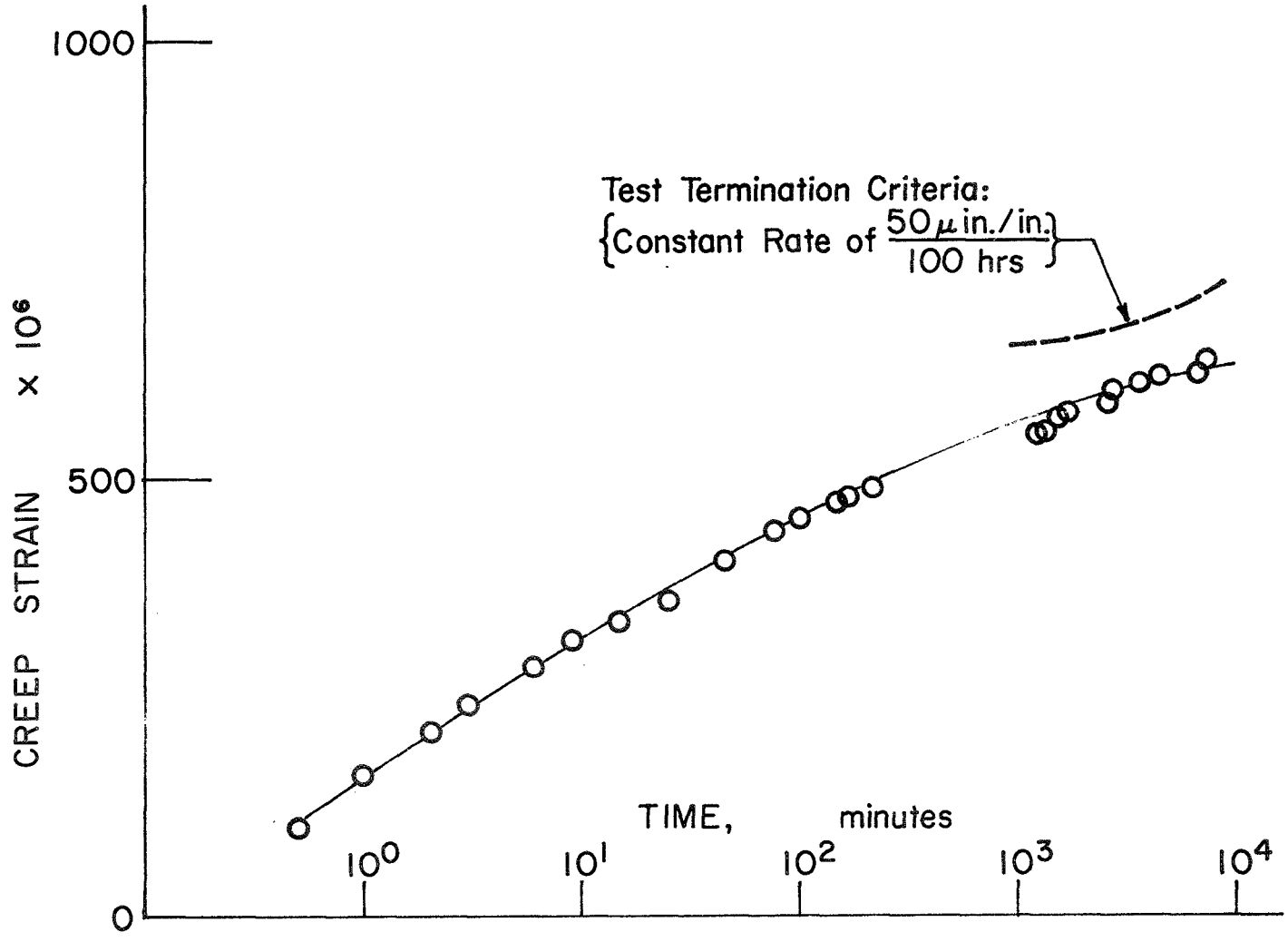

Figure 53.-Strain vs Time for Specimen C-X1

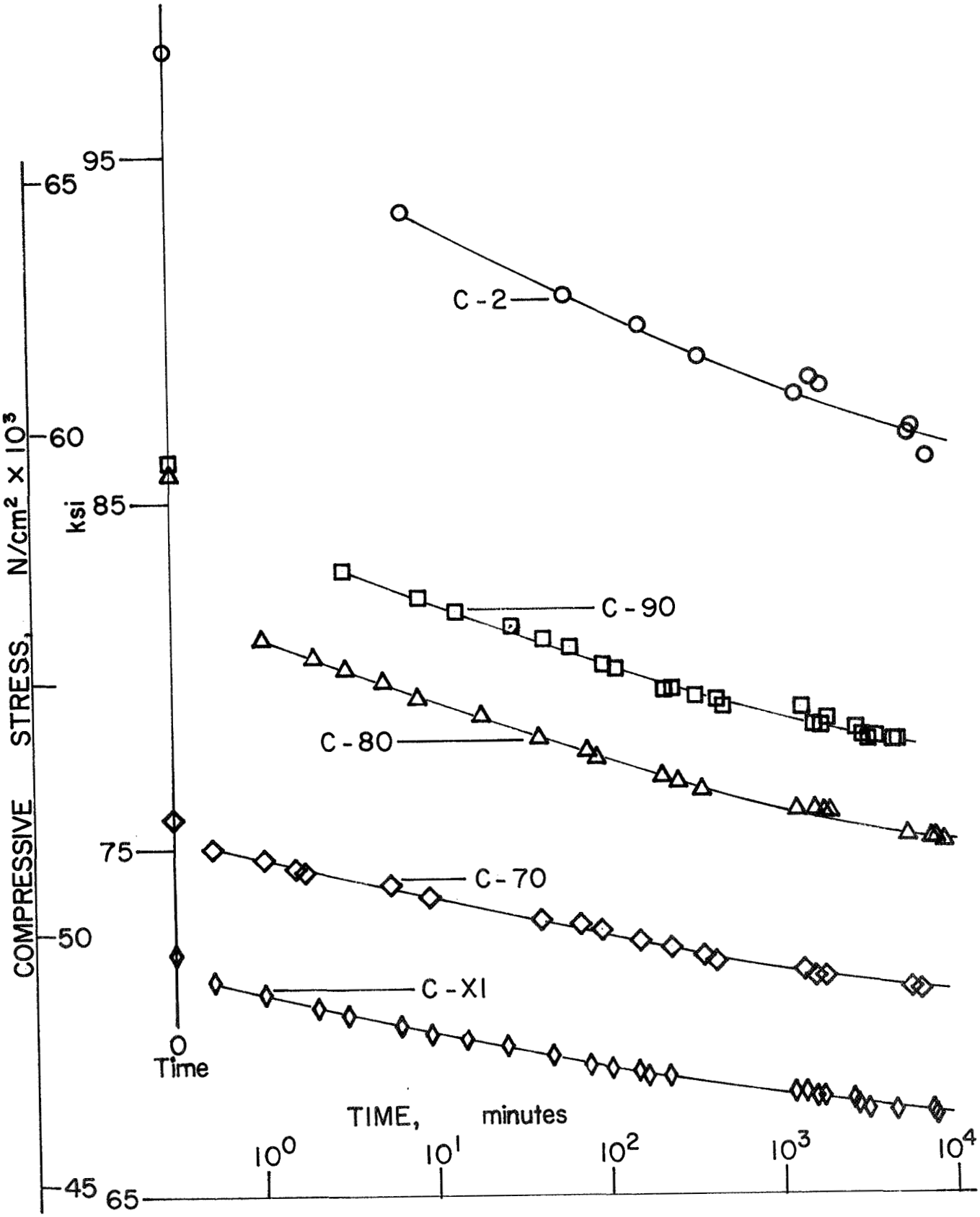

Figure 54.--Stress vs Time During Creep Tests

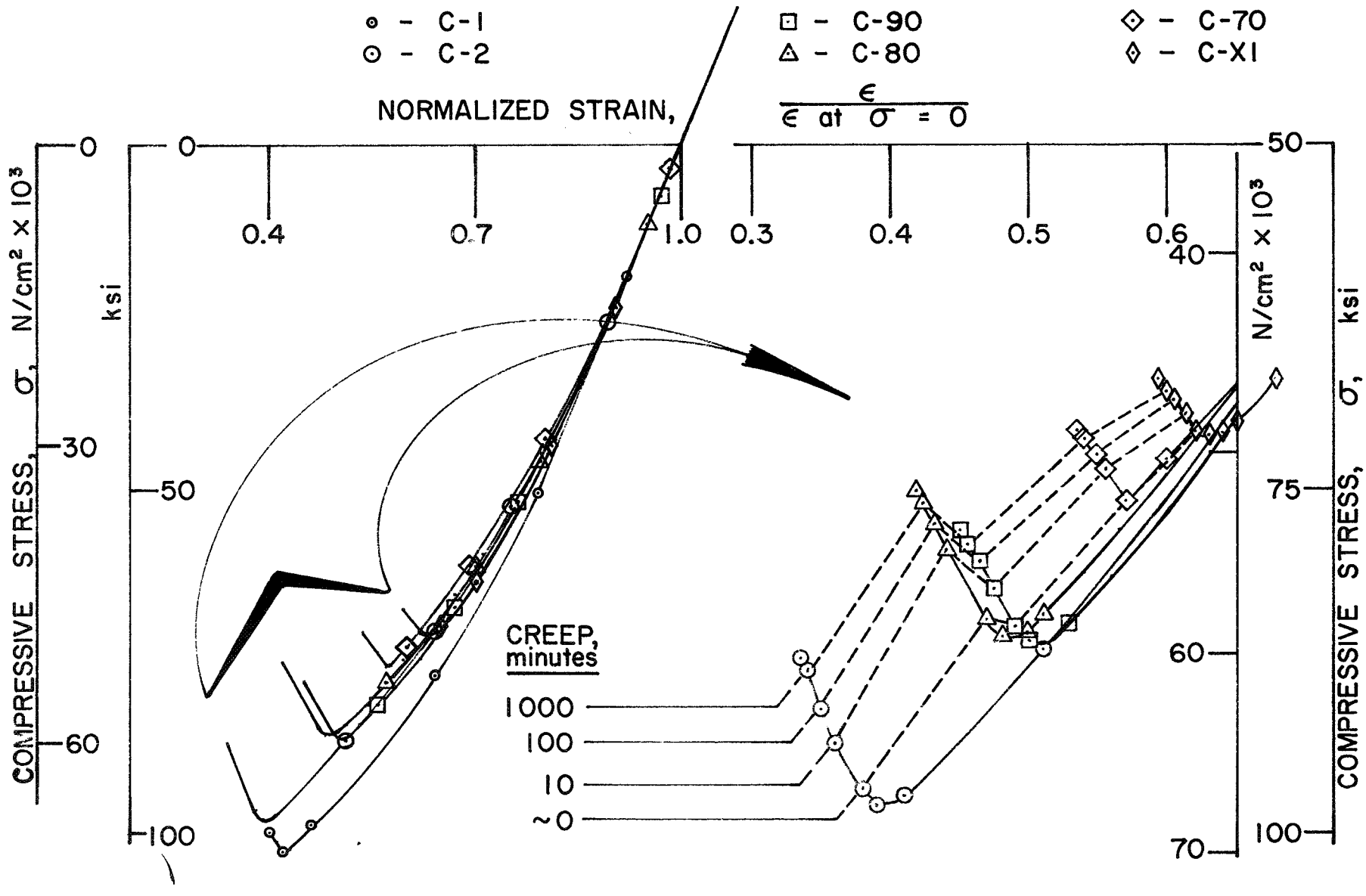

Figure 55.-Normalized Compression Stress-Strain Diagrams

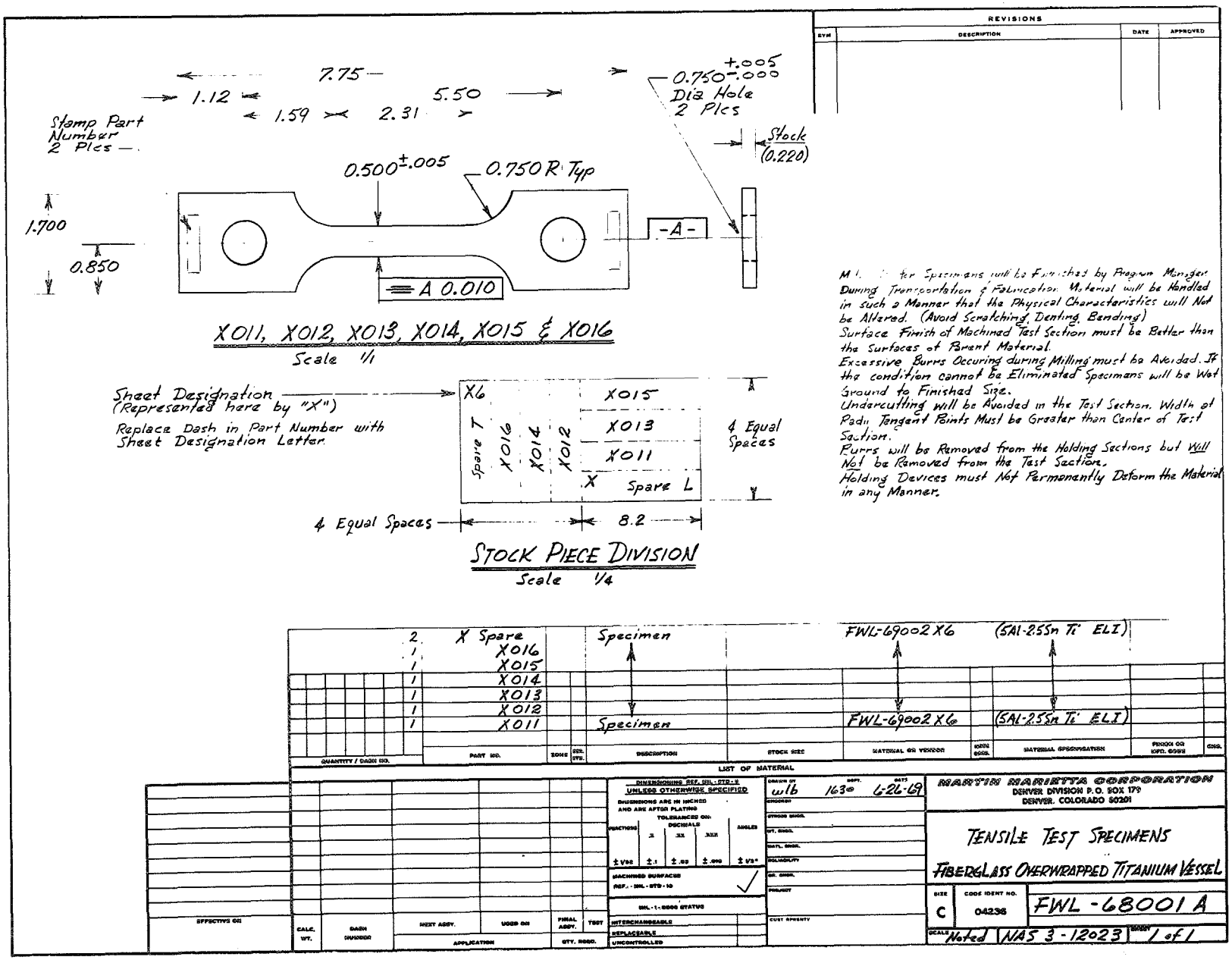

Figure 56. -Arrangement and Shape of Liner Tension Coupons

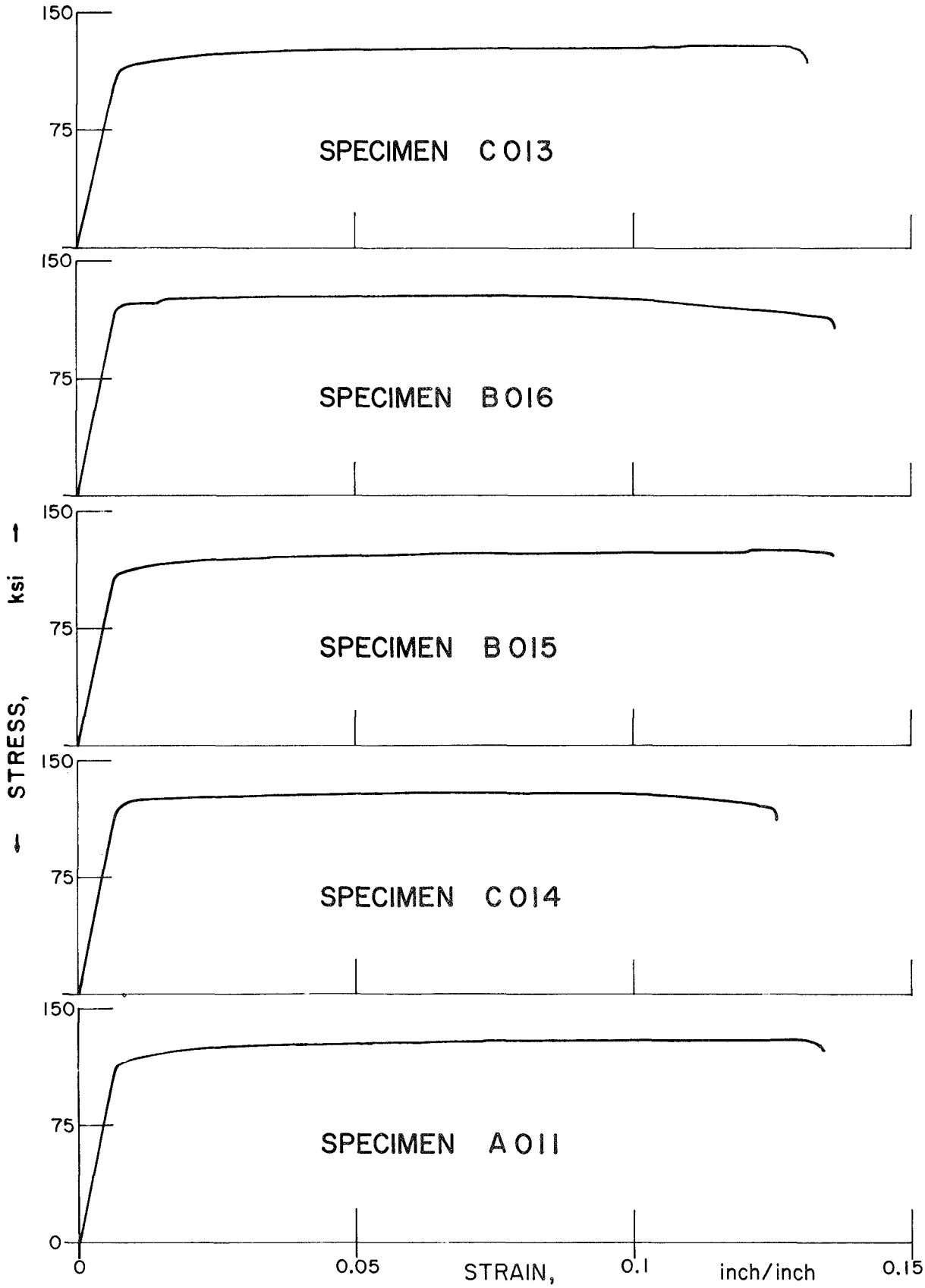

Figure 57.- Stress-Strain Relations for Specimens Cut From Liner Material Plates.

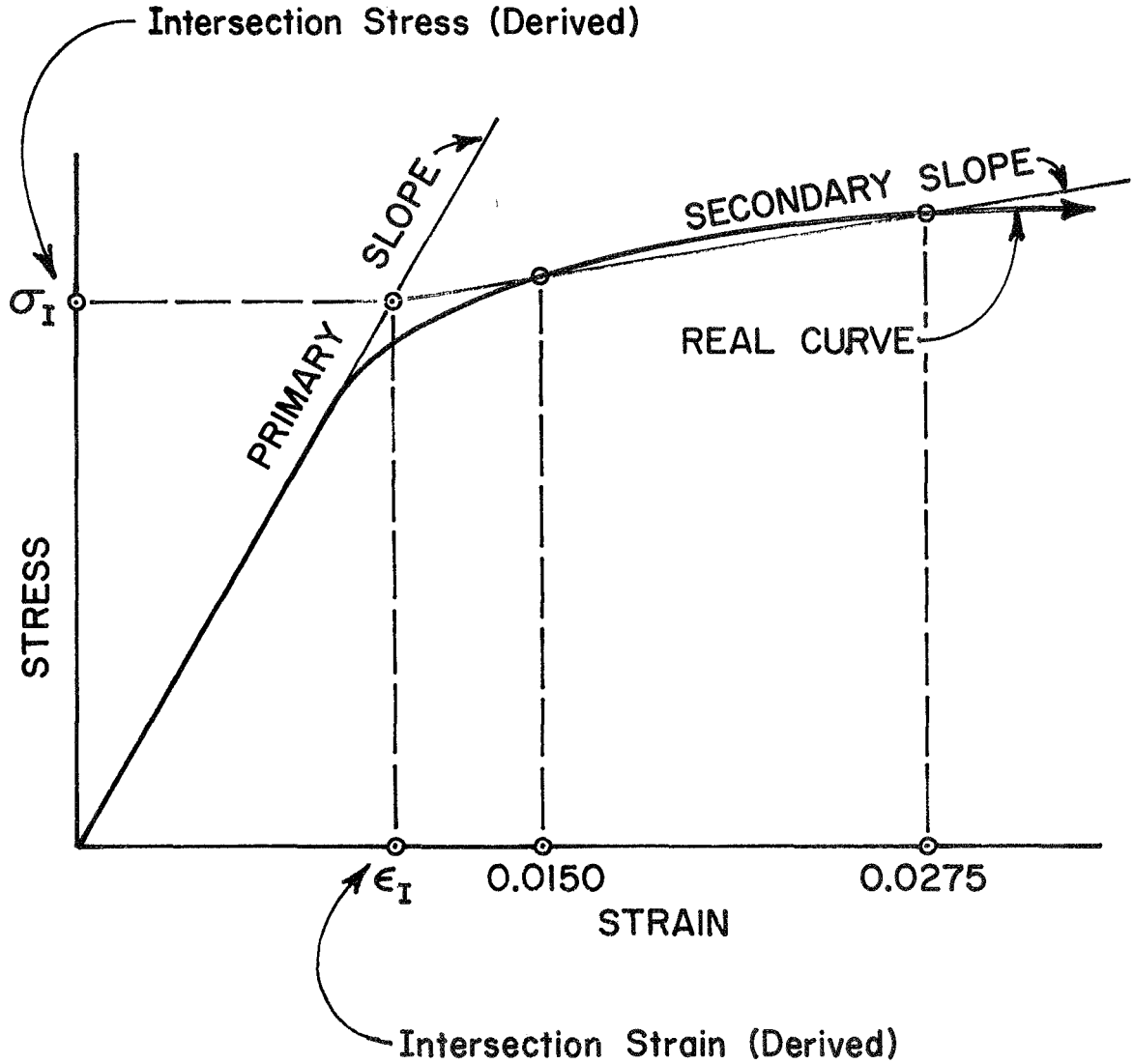

Figure 58.-Scheme for Determining Inelastic Slope

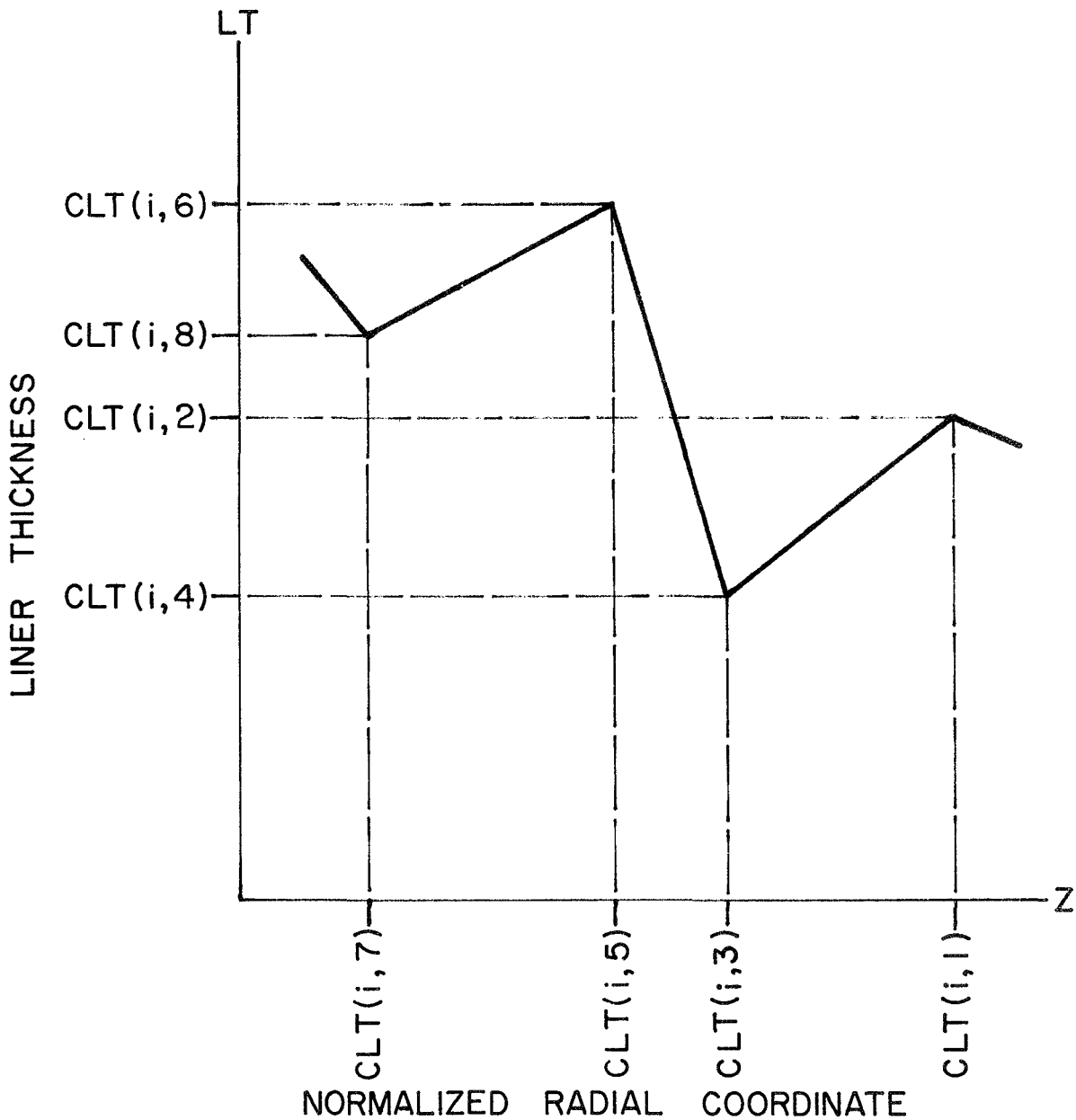

Figure 59.-Piecewise Linear Liner Thickness Variation

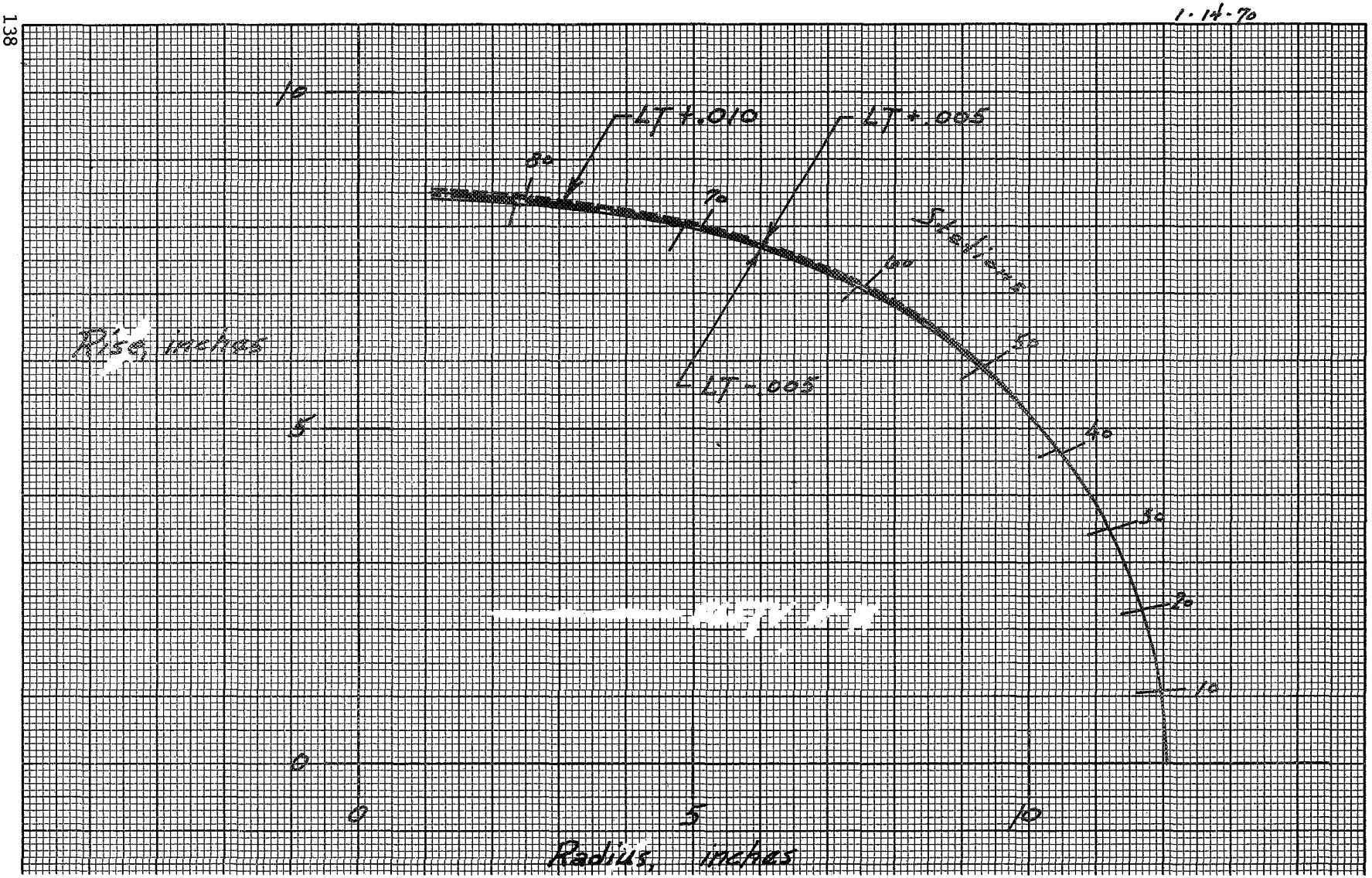

Figure 60.--Head Shape of Final Design

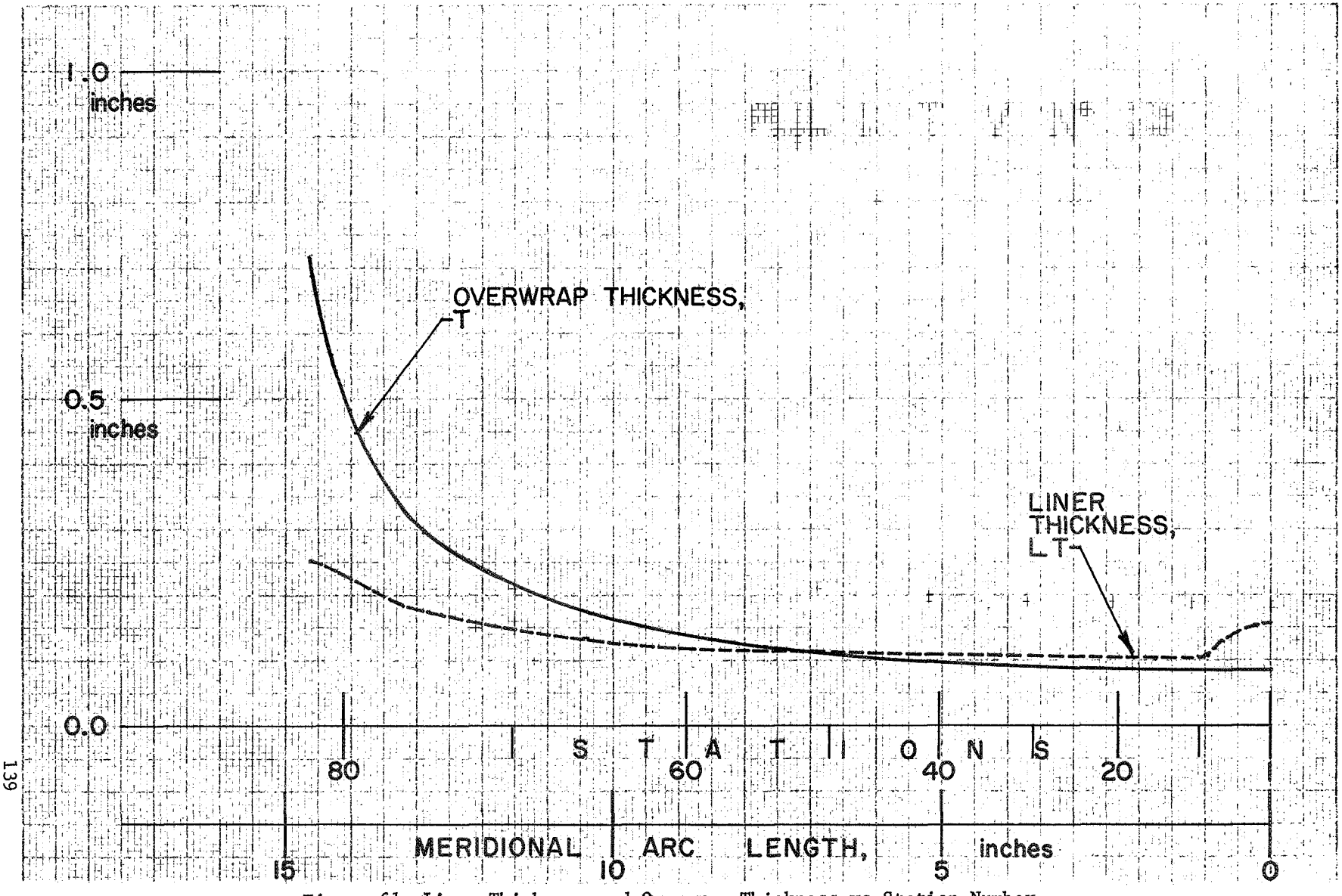

Figure 61.--Liner Thickness and Overwrap Thickness vs Station Number

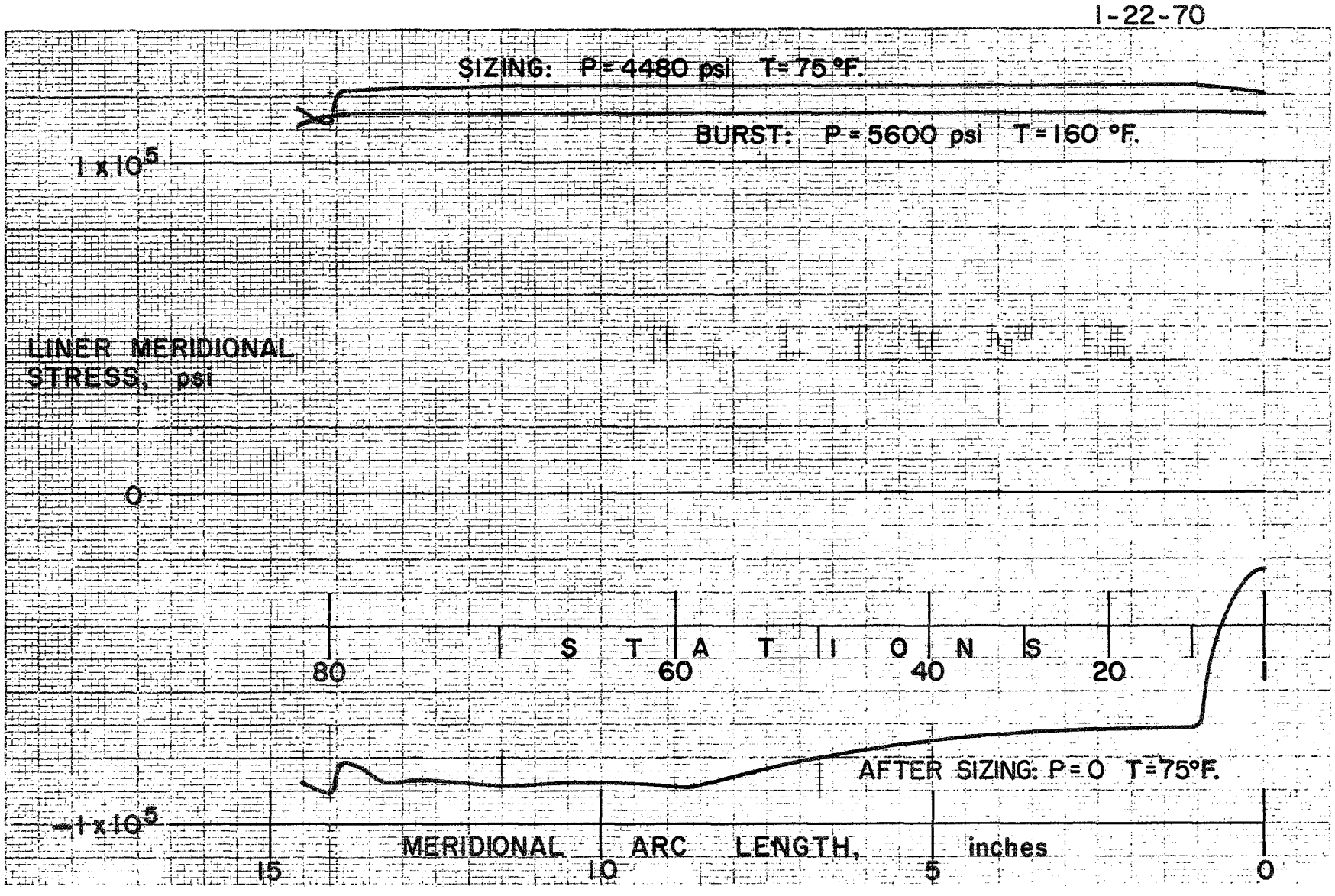

Figure 62.-Meridional Stress vs Station Number

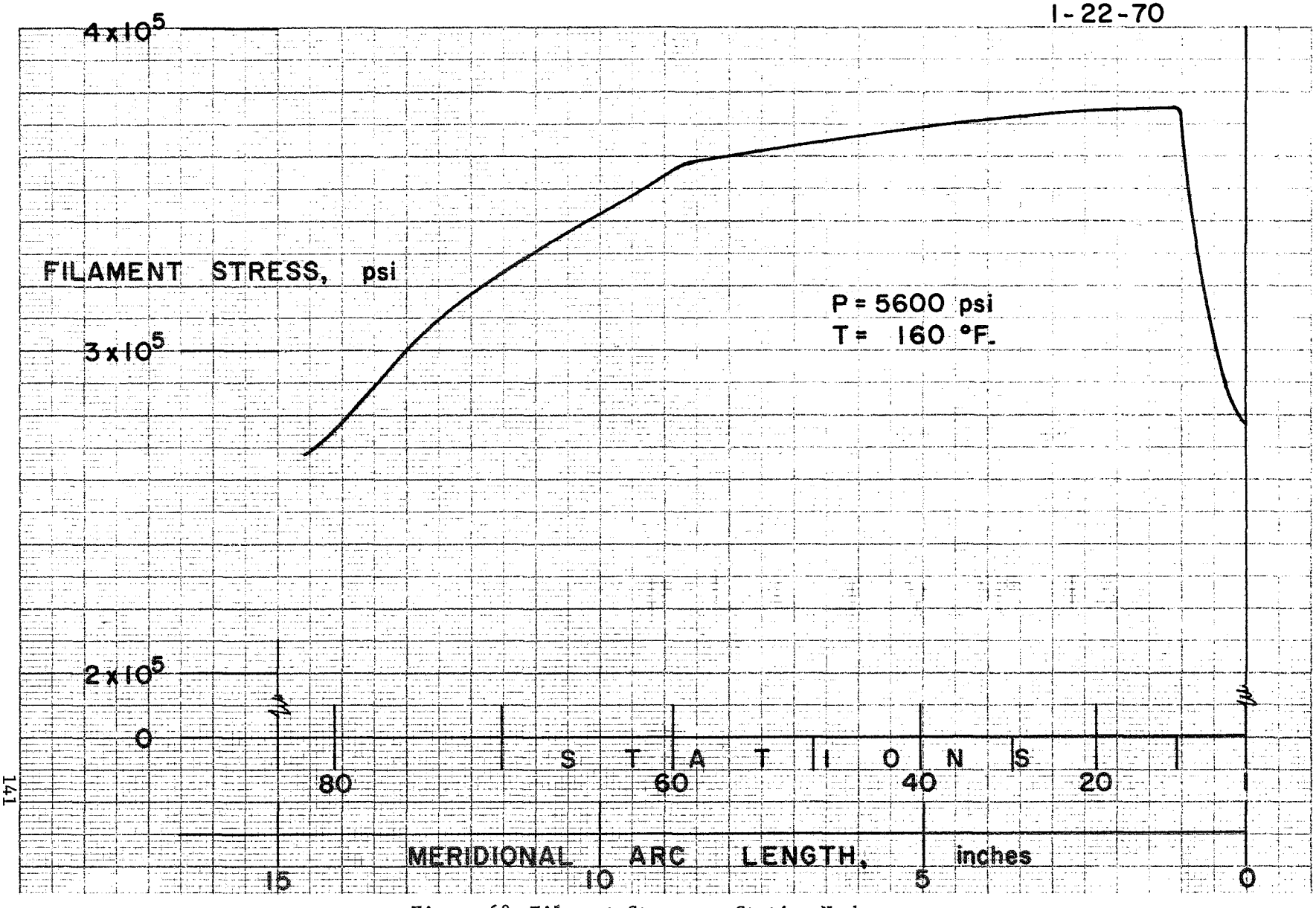

Figure 63.-Filament Stress vs Station Number

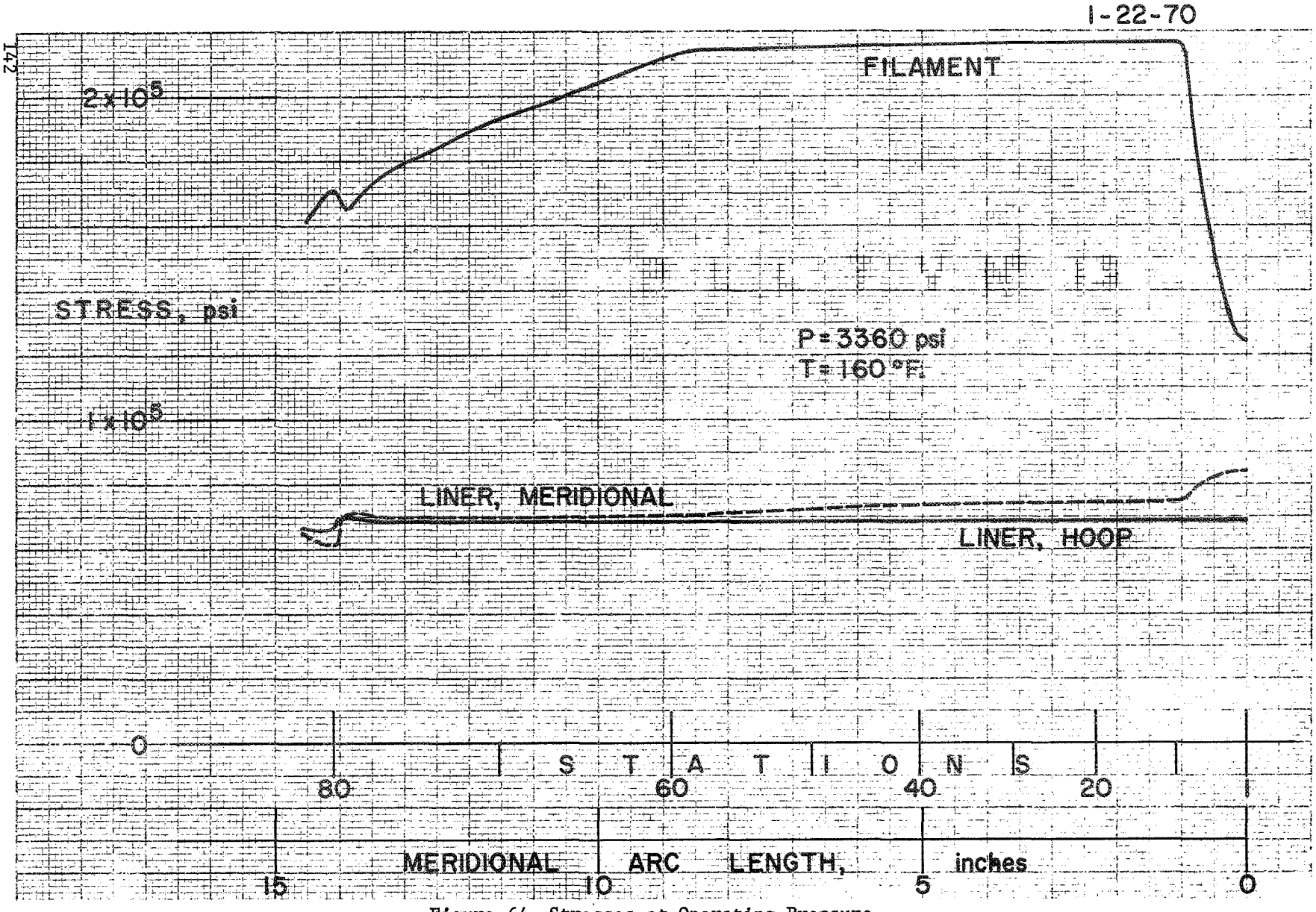

Figure 64.-Stresses at Operating Pressure

OVERWRAP PROCEDURE

Layer	Hoop Wrap Cyl Length	Polar Wrap Nº Ribbons	Polar Wrap Ribbon Width	Polar Wrap Wrap Angle	Ends per Inch per Layer	Total Ends per Inch	Weight of Wrap Mat'l, Pounds	Remarks
1 & 2		36	2.1	10° 15'	480	960	6.4	
3 & 4		36	2.1	10° 15'	480	960	6.4	
5 & 6		36	2.1	10° 15'	480	960	6.4	
7-25	5.0				440	8360	8.0	
26	5.0				560	560	0.5	
							27.7	

REVISIONS

SYM	DESCRIPTION	DATE	APPROVED
	Rev Table		

NOTES:
1. Verify Vessel & Parts Designations and Log. See Marking Note, Sheet 2
2. Weigh Liner (-019) Prior to Wrapping and Log.

3. Overwrapping will be as Specified in above Table and in Accord with NASA-CR-54855

4. Cure Wound Vessel at 150°F for 2 Hours and then at 300°F for 4 Hours in Programer-Controlled Oven, during which Vessel will be Supported in Curing Fixture.
5. Size Vessel by Pressurizing to 4480 psi.

LIST OF MATERIAL

Quantity / Dash No.			Part No.	Description	Stock Size	Material or Vendor
	X			Roving, Glass, 20 End, S994/HTS Finish Preimpregnated w/ EPON 828/DSA/EMPOL 1040 BDMA (100/115.9/20/1)		
	2		-005	End Boss	See Sheet 7	
	1		X403, X503	Cylinder Section	M/F X4, X5	
	2		X111, X221, X331	Dome	M/F X11, X22, X33	
		1	019	Liner		
019	009		009	Vessel		

MARTIN MARIETTA CORPORATION
DENVER DIVISION P.O. BOX 179
DENVER, COLORADO 80201

Drawn: W/b 1630 1-13-70

FIBERGLASS OVERWRAPPED TITANIUM VESSEL

Size	Code Ident No.	
C	04236	FWL-69002
Scale: -	NAS 3-12023	Sheet 1 of 7

Figure 65.- Final Vessel Design - Page 1

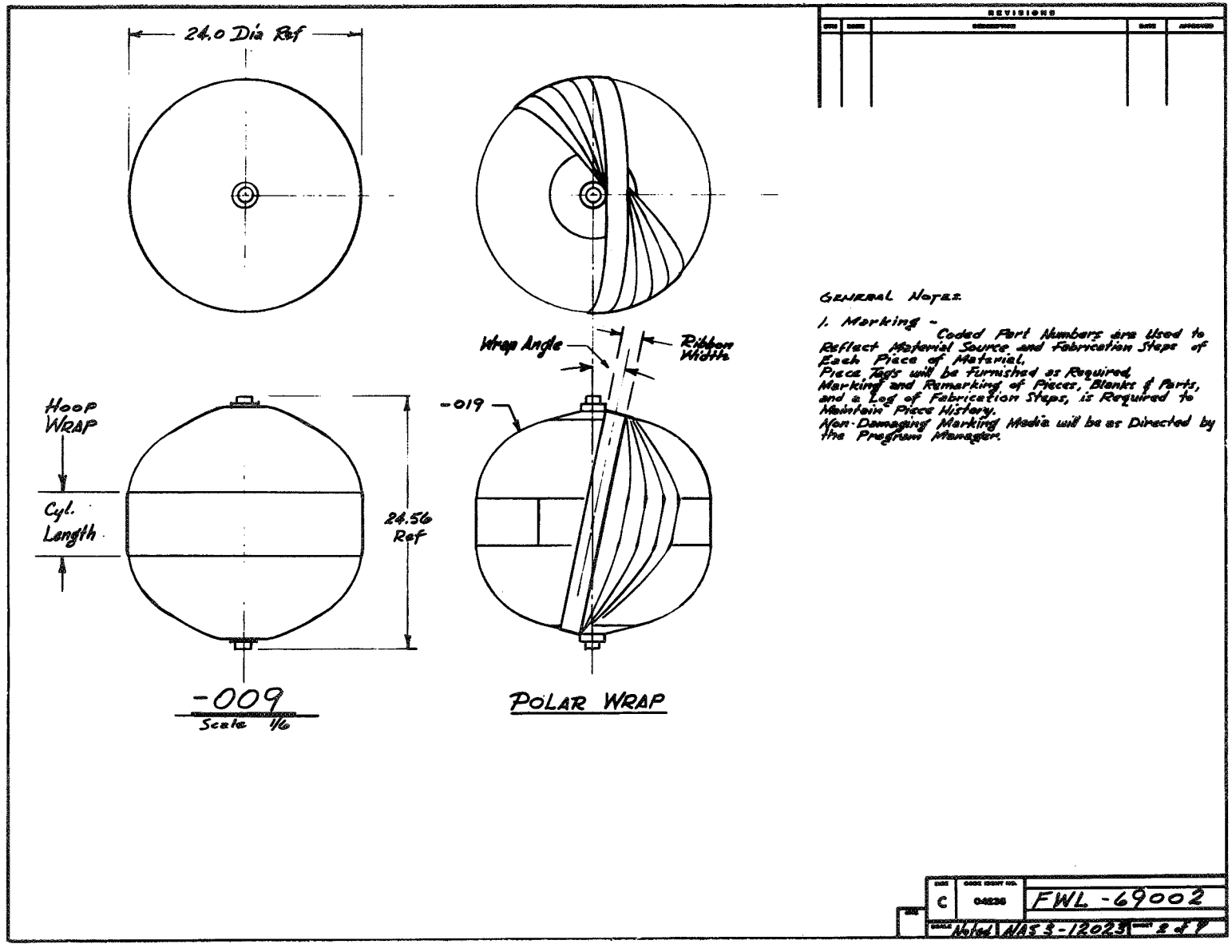

Figure 66.-Final Vessel Design - Page 2

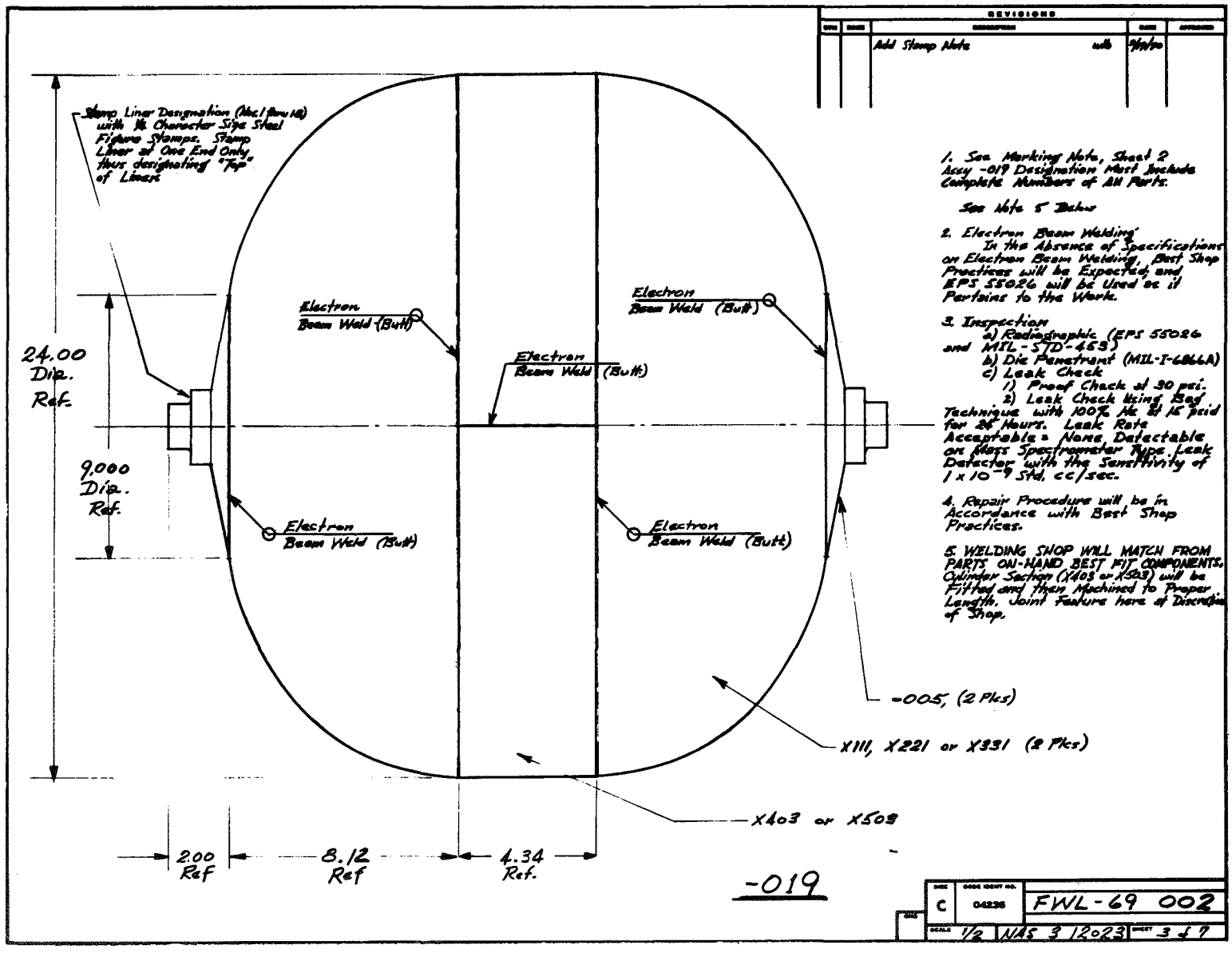

Figure 67.- Final Vessel Design - Page 3

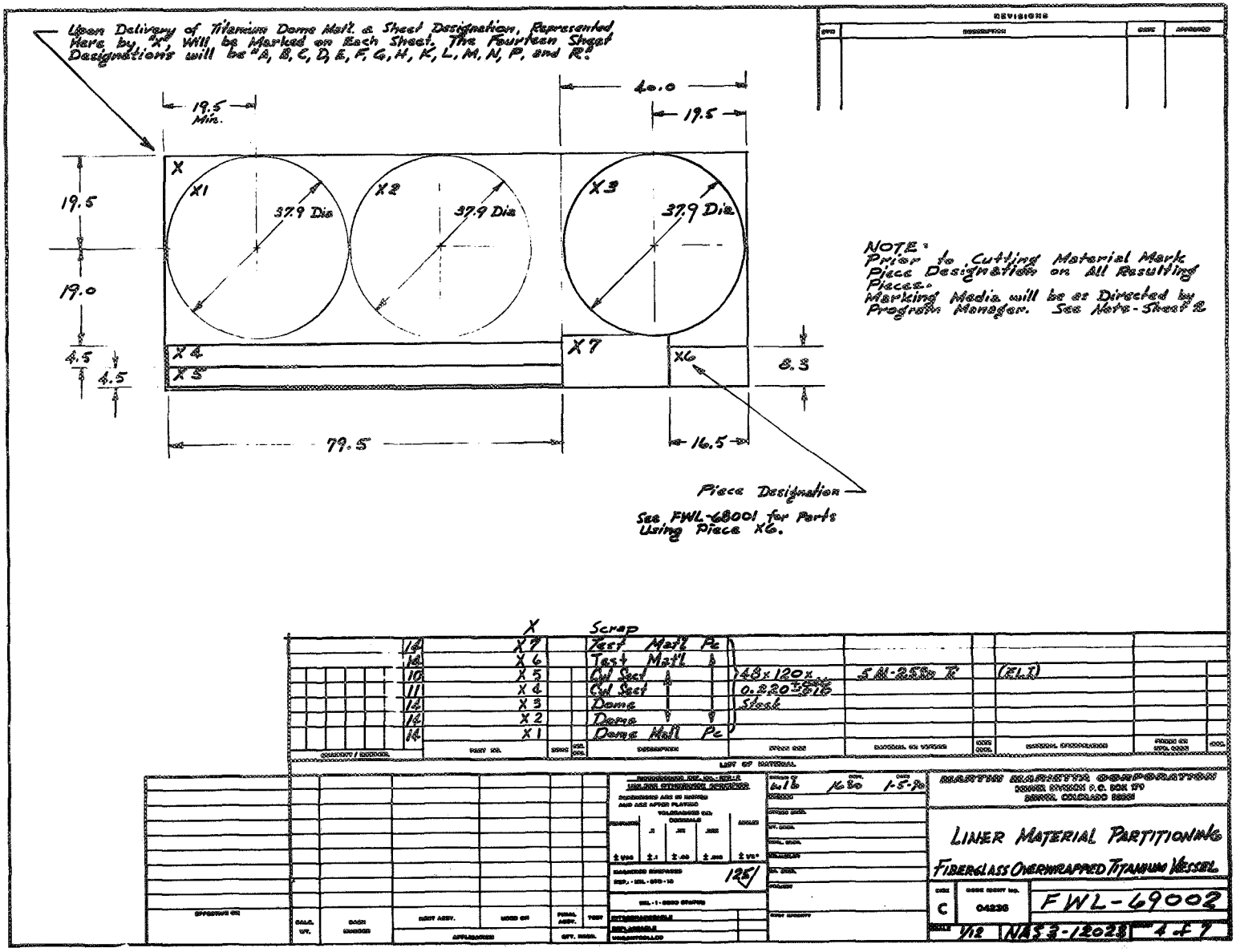

Figure 68.-Final Vessel Design - Page 4

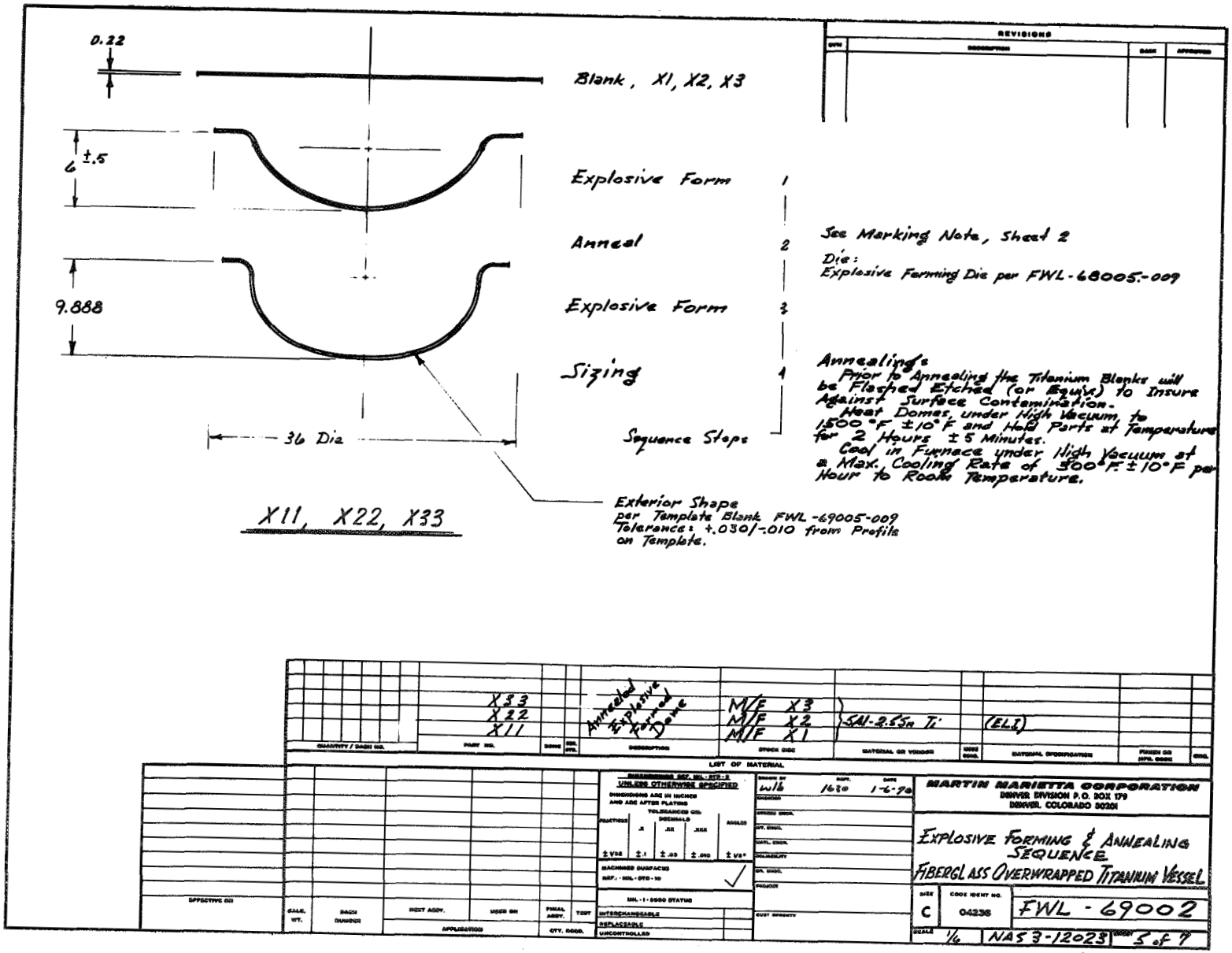

Figure 69.- Final Vessel Design - Page 5

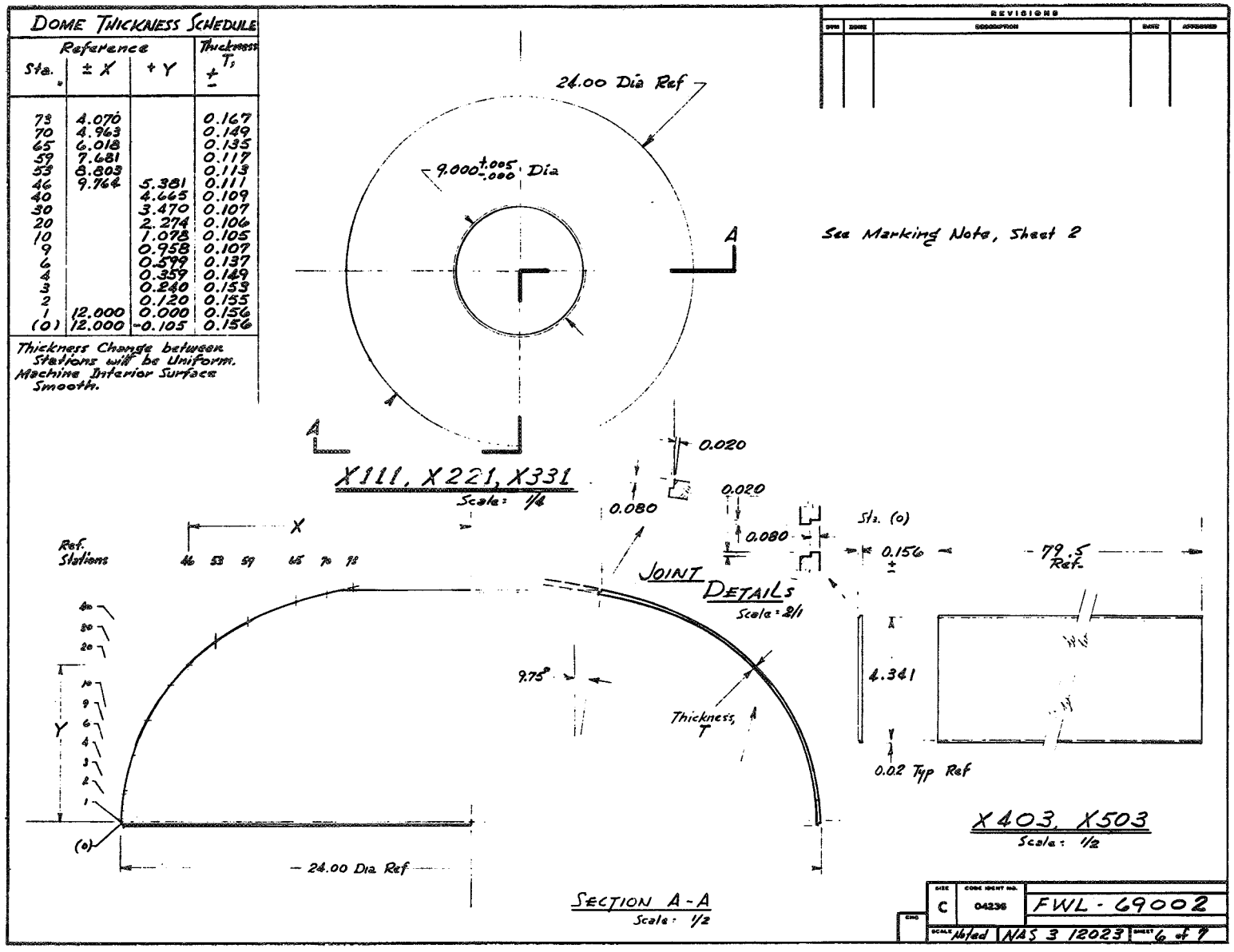

Figure 70.-Final Vessel Design - Page 6

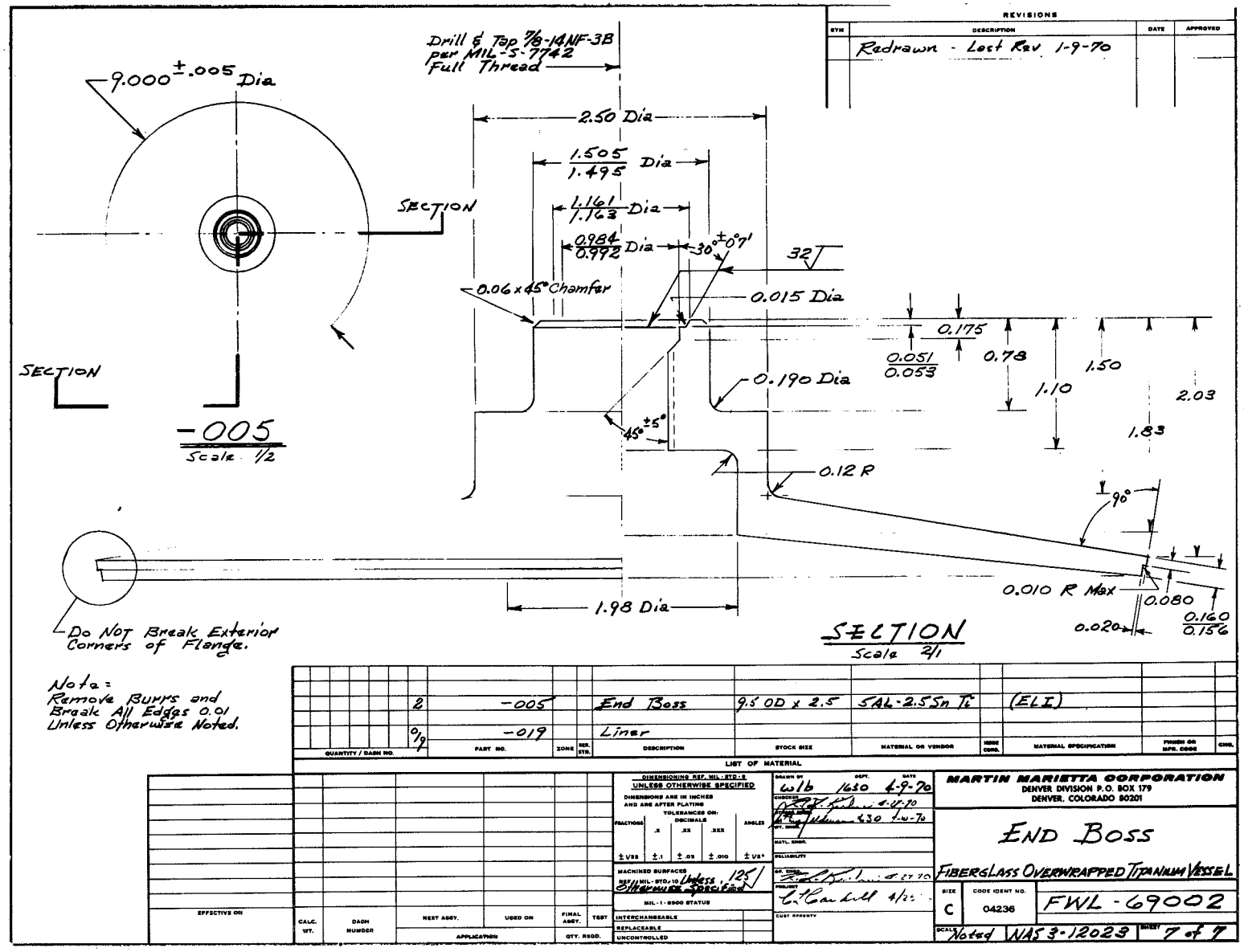

Figure 71.-Final Vessel Design - Page 7

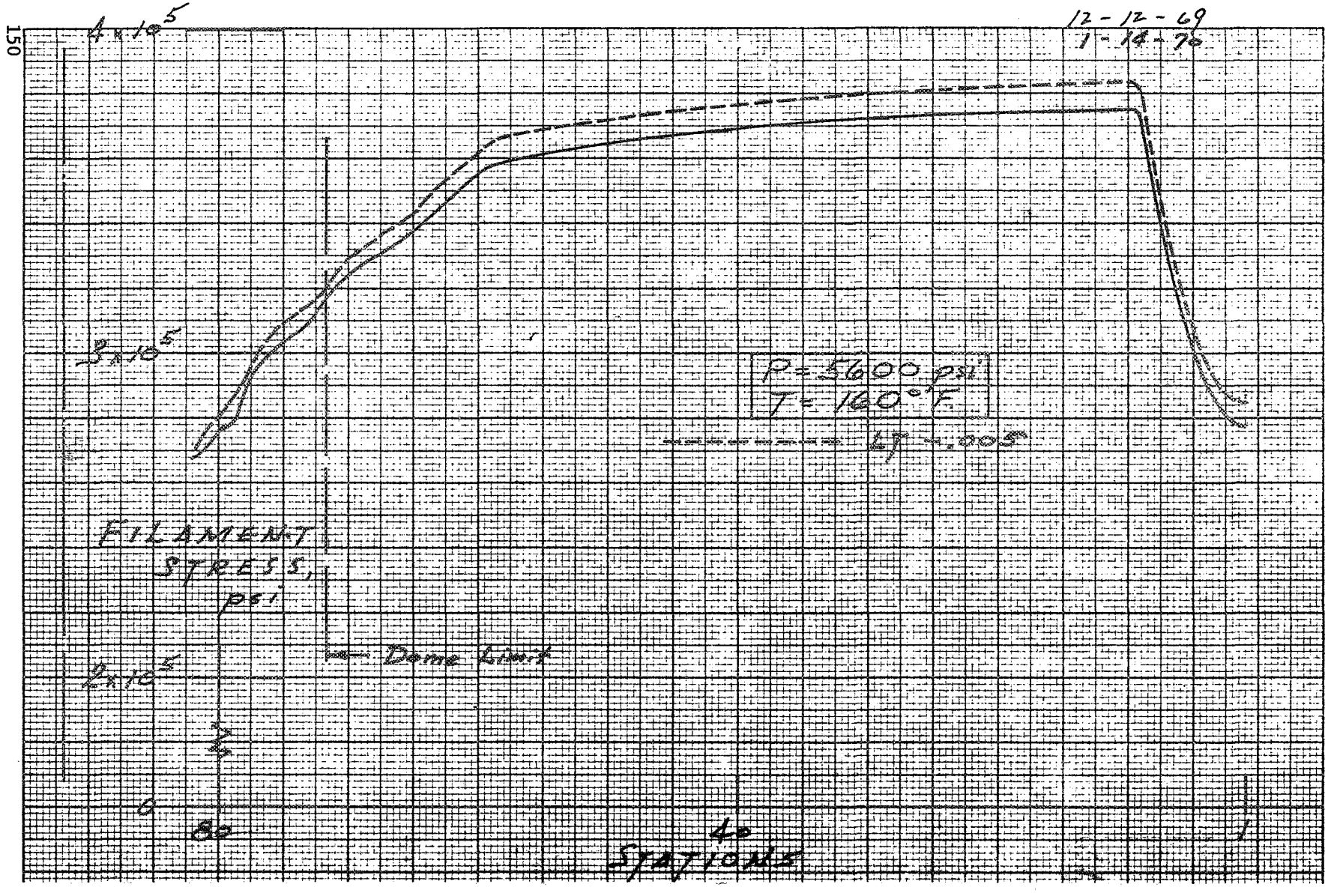

Figure 72. - Effect of Minus Tolerance on Filament Stress at Burst

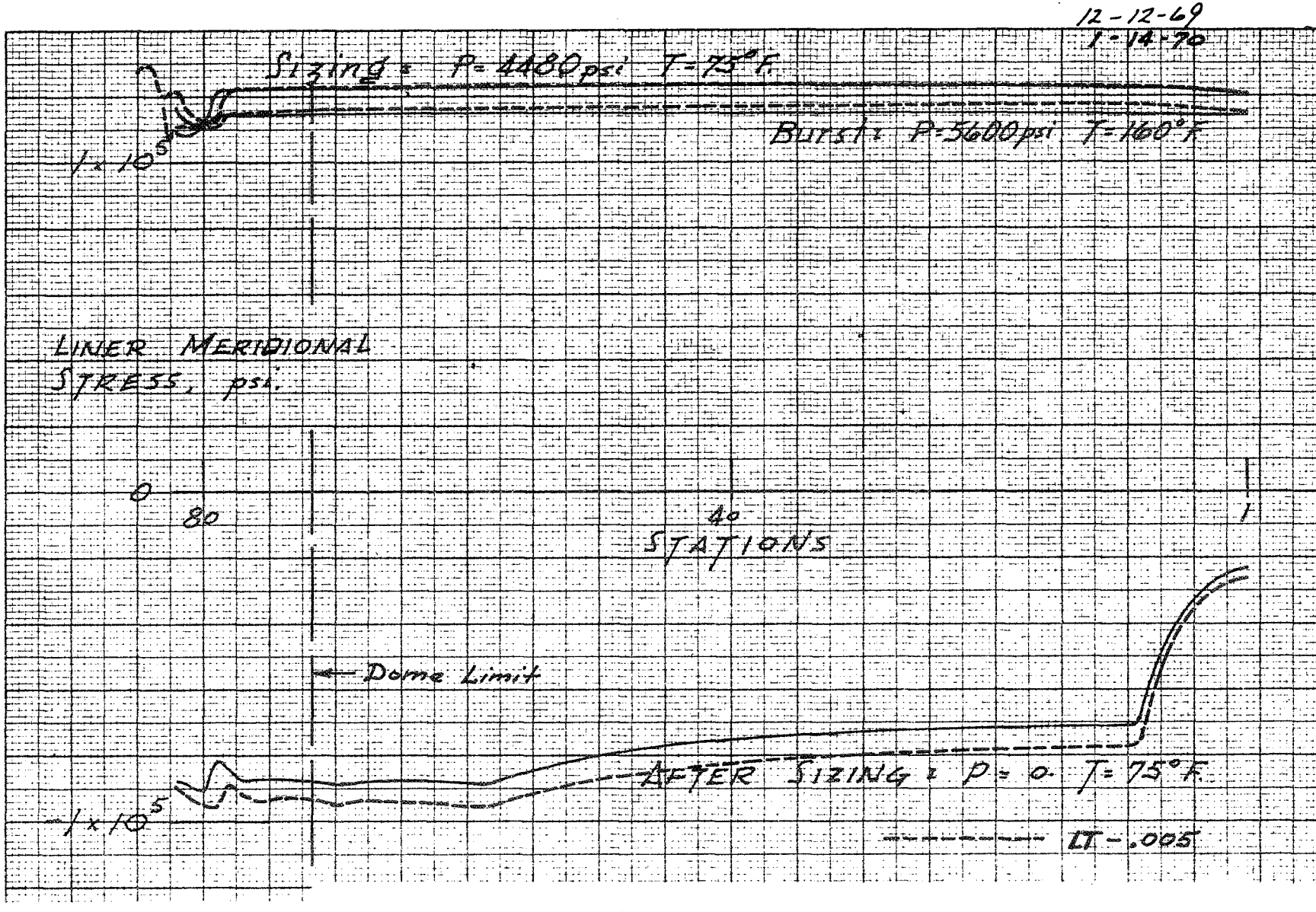

Figure 73. - Effect of Minus Tolerance on Liner Meridional Stress

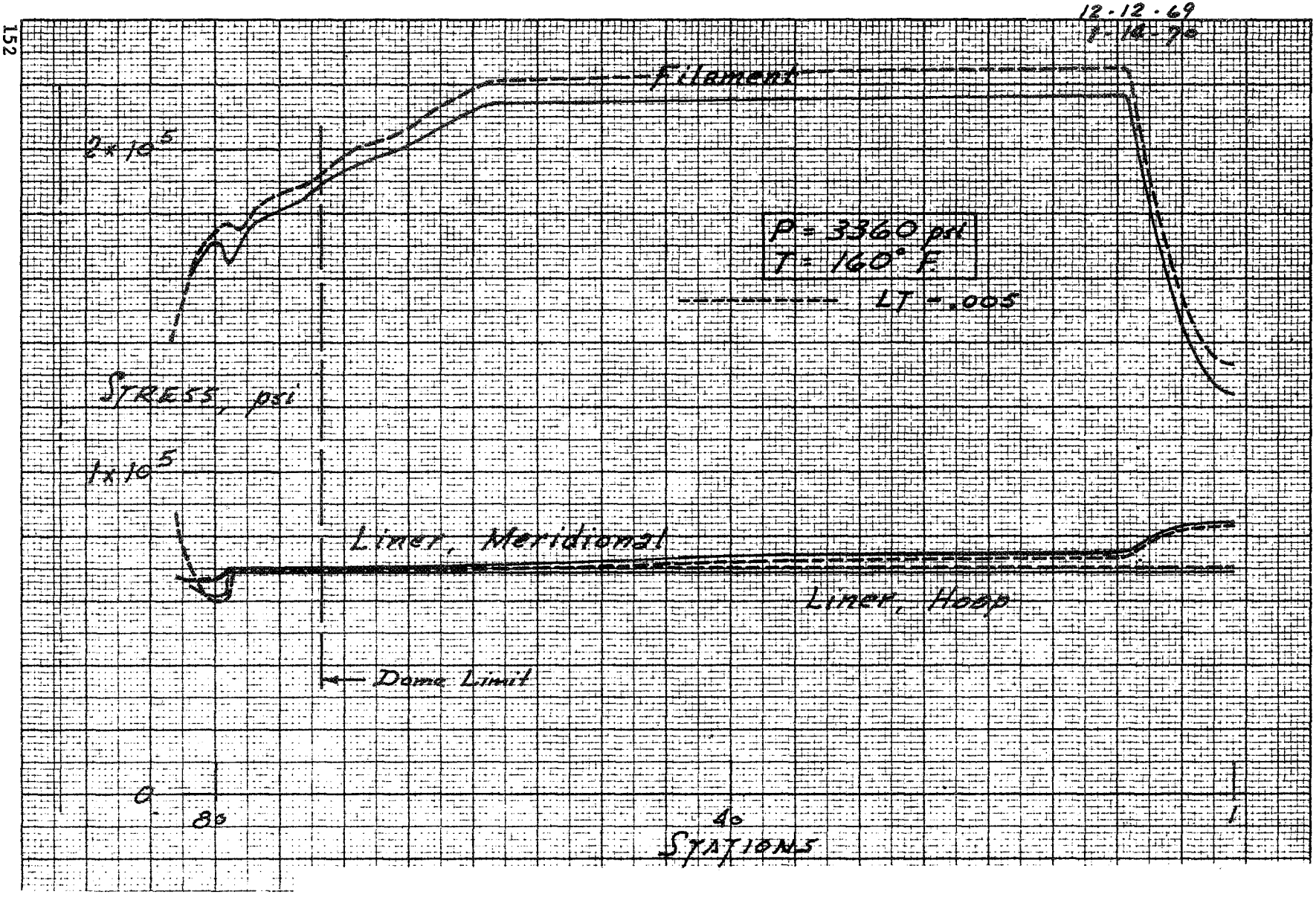

Figure 74. - Effect of Minus Tolerance on Stresses and Operating Pressure

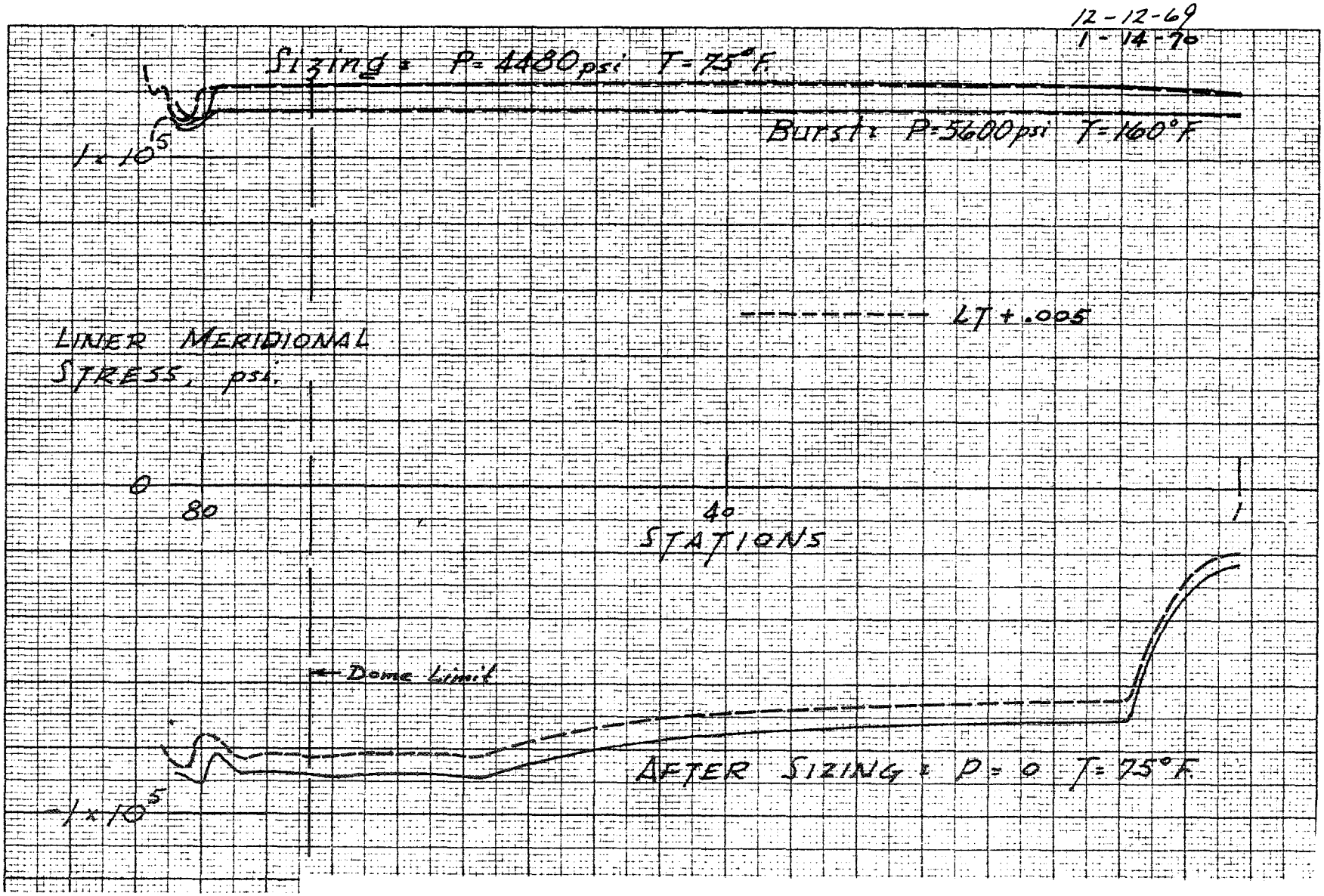

Figure 75. - Effect of Small Plus Tolerance on Liner Meridional Stress

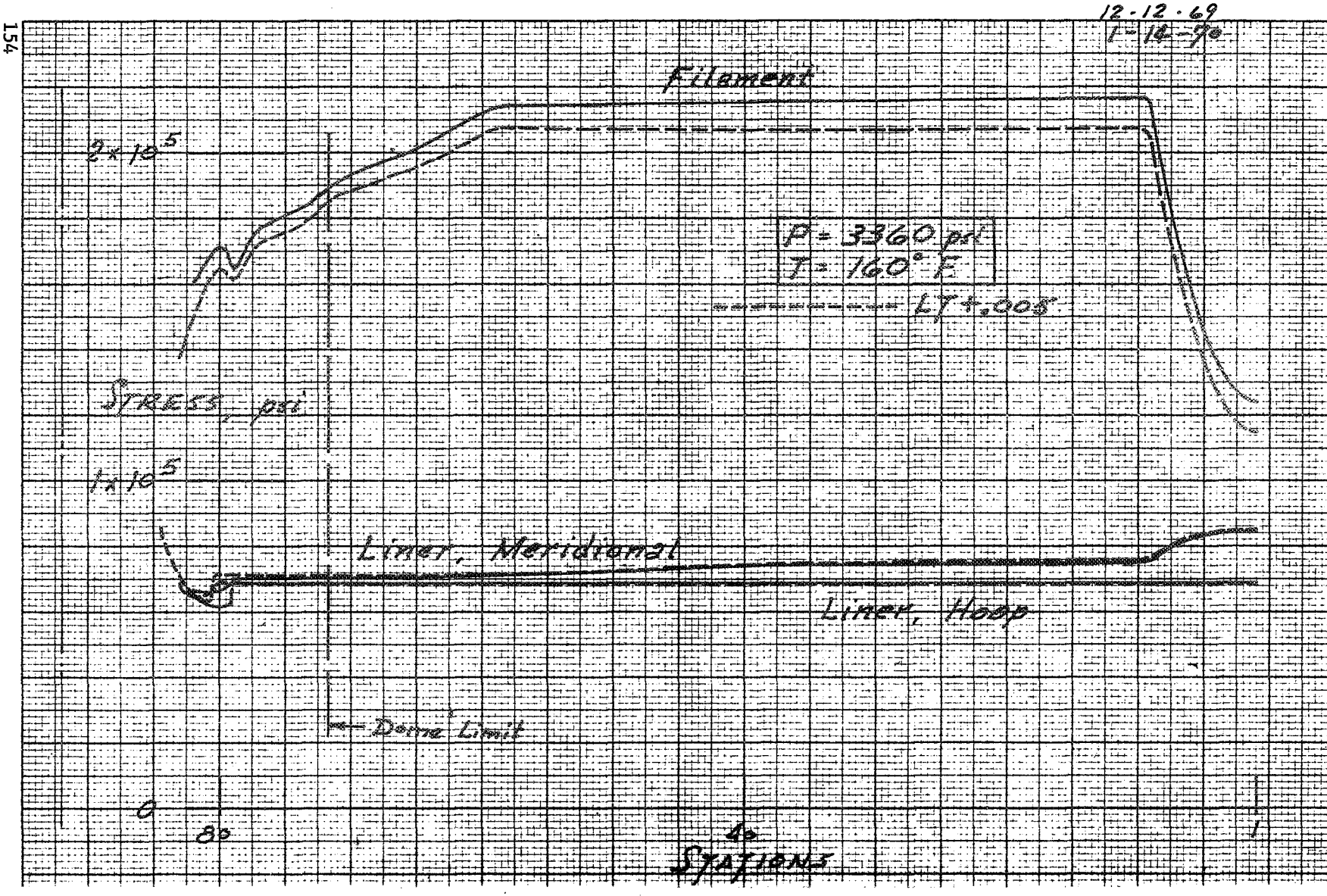

Figure 76. - Effect of Small Plus Tolerance on Stresses at Operating Pressure

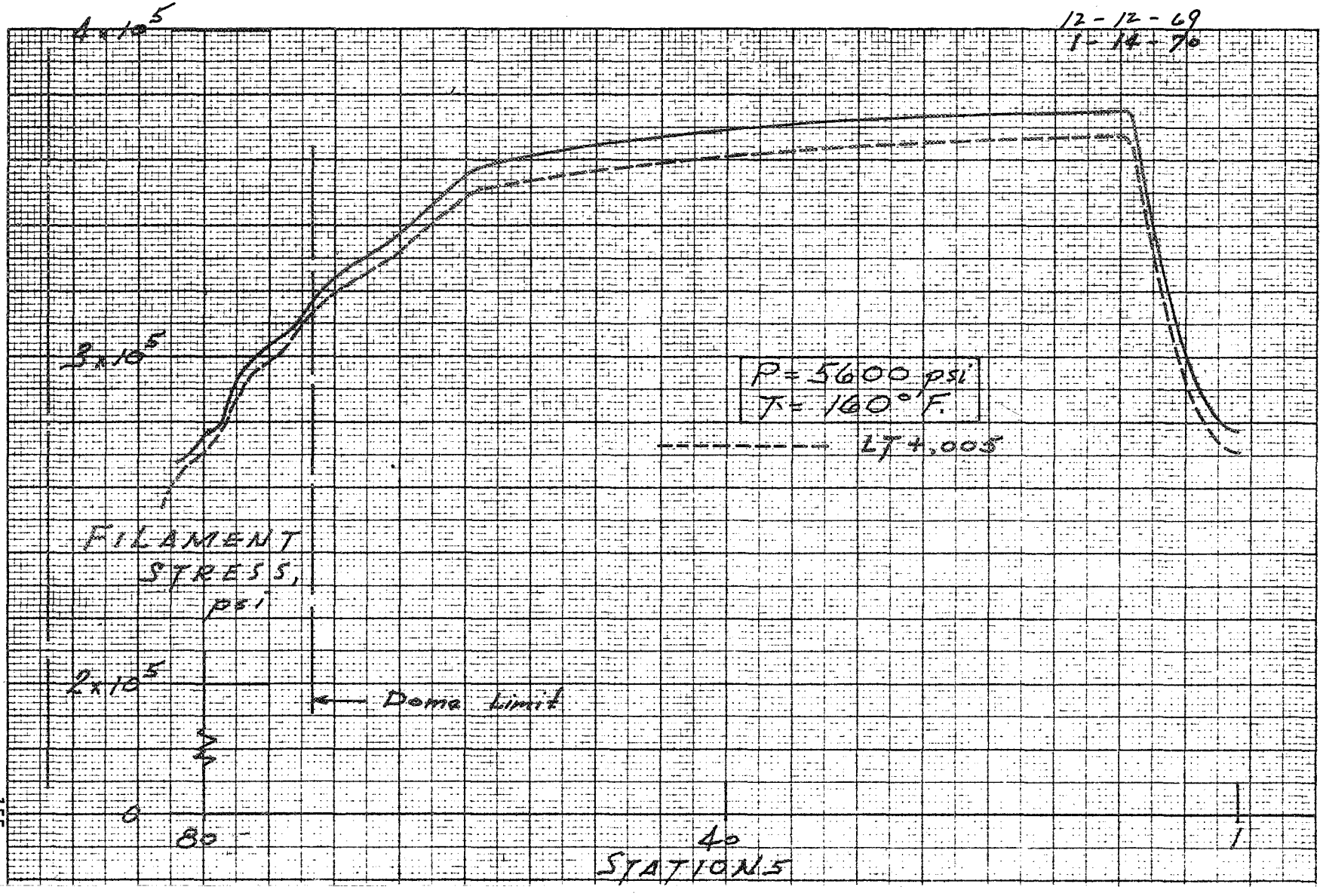

Figure 77. - Effect of Small Plus Tolerance on Filament Stress at Burst

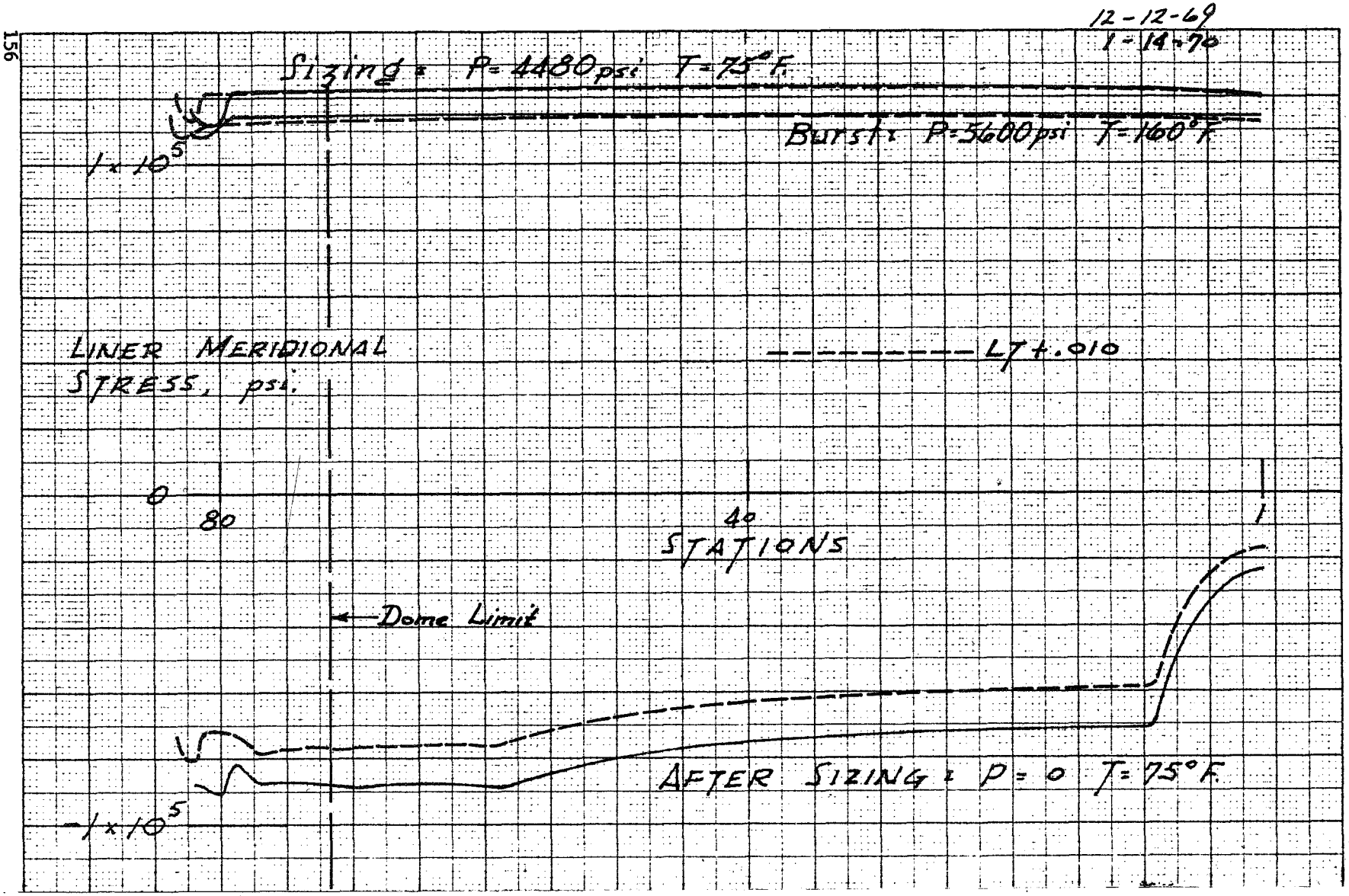

Figure 78. - Effect of Large Plus Tolerance on Liner Meridional Stress

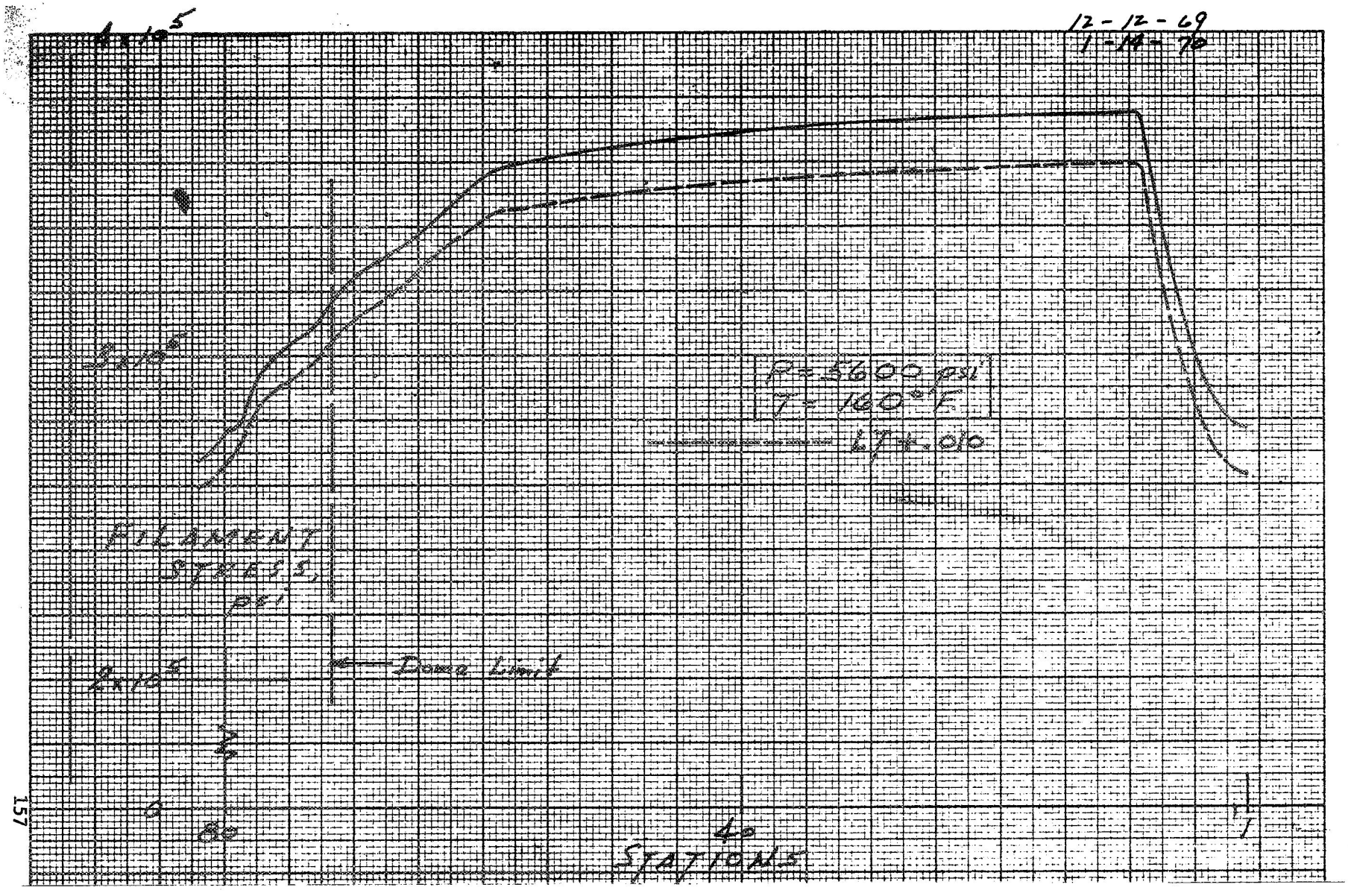

Figure 79. - Effect of Large Plus Tolerance on Stresses at Operating Pressure

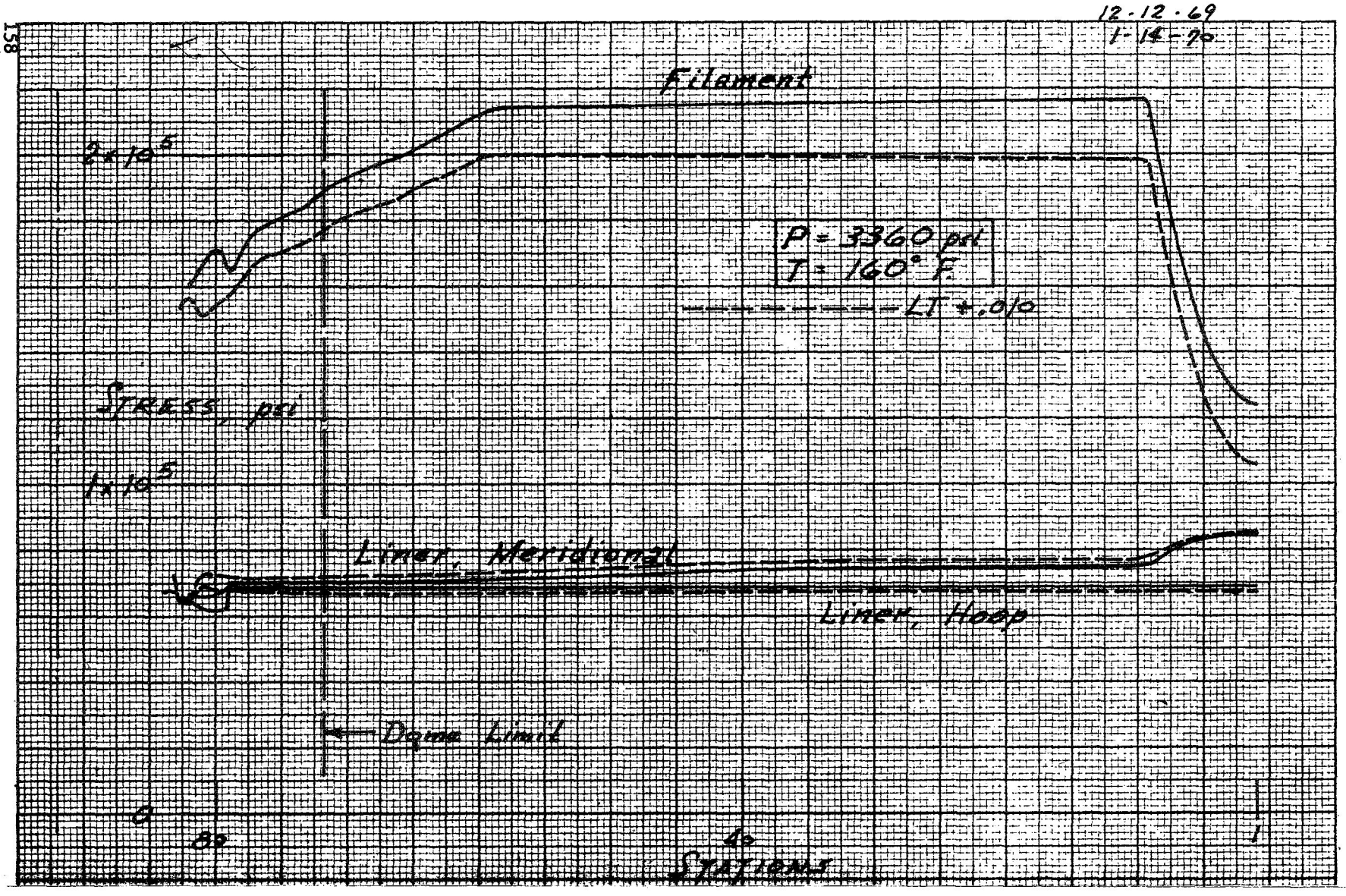

Figure 80. - Effect of Large Plus Tolerance on Filament Stress at Burst

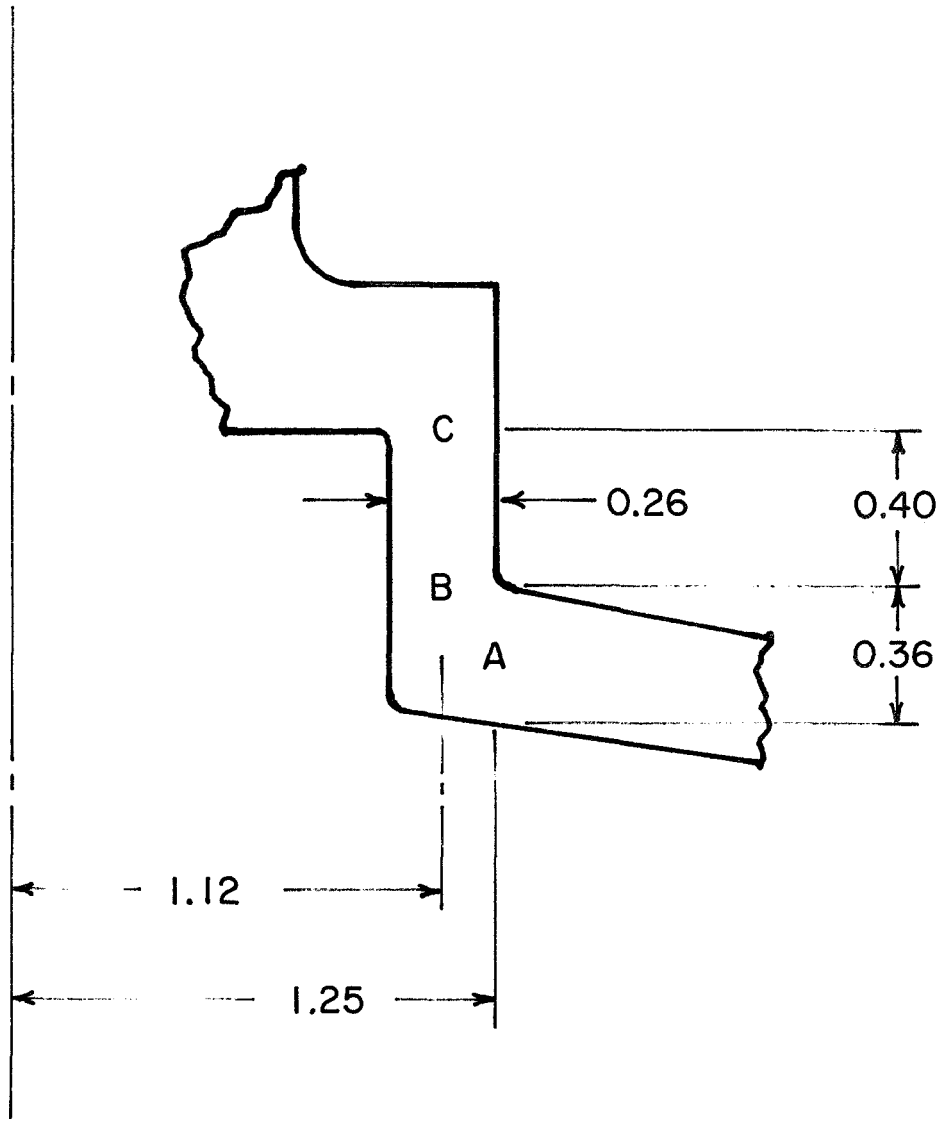

Figure 81.-Schematic of End Boss for Analysis

REPORT COPIES R	D	RECIPIENT	DESIGNEE
		National Aeronautics & Space Administration Lewis Research Center 21000 Brookpark Road Cleveland, Ohio 44135	
1		Attn: Contracting Officer, MS 500-313	
5		Liquid Rocket Technology Branch, MS 500-209	
1		Technical Report Control Office, MS 5-5	
1		Technology Utilization Office, MS 3-16	
2		AFSC Liaison Office, MS 4-1	
2		Library	
1		Office of Reliability & Quality Assurance, MS 500-111	
1		D. L. Nored, Chief, LRTB, MS 500-209	
3		J. R. Barber, Project Manager, MS 500-209	
1		E. W. Conrad, MS 500-204	
1		R. H. Kemp, MS 49-1	
2		Chief, Liquid Experimental Engineering, RPX Office of Advanced Research & Technology NASA Headquarters Washington, D.C. 20546	
2		Chief, Liquid Propulsion Technology, RPL Office of Advanced Research & Technology NASA Headquarters Washington, D.C. 20546	
1		Director, Launch Vehicles & Propulsion, SV Office of Space Science & Applications NASA Headquarters Washington, D.C. 20546	
1		Chief, Environmental Factors & Aerodynamics Code RV-1 Office of Advanced Research & Technology Washington, D.C. 20546	

REPORT COPIES R	D	RECIPIENT	DESIGNEE
1		Chief, Space Vehicles Structures Office of Advanced Research & Technology NASA Headquarters Washington, D.C. 20546	
1		Director, Advanced Manned Missions, MT Office of Manned Space Flight NASA Headquarters Washington, D.C. 20546	
6		NASA Scientific & Technical Information Facility P.O. Box 33 College Park, Maryland 20740	
1		Director, Technology Utilization Division Office of Technology Utilization NASA Headquarters Washington, D.C. 20546	
1	1	National Aeronautics & Space Administration Ames Research Center Moffett Field, California 94035 Attn: Library	C. A. Syvertson
1		National Aeronautics & Space Administration Flight Research Center P.O. Box 273 Edwards, California 93523 Attn: Library	
1		National Aeronautics & Space Administration Goddard Space Flight Center Greenbelt, Maryland 20771 Attn: Library	
1		National Aeronautics & Space Administration John F. Kennedy Space Center Cocoa Beach, Florida 32931 Attn: Library	

REPORT COPIES R	D	RECIPIENT	DESIGNEE
1		National Aeronautics & Space Administration Langley Research Center Langley Station Hampton, Virginia 23365 Attn: Library	
1		National Aeronautics & Space Administration Manned Spacecraft Center Houston, Texas 77001 Attn: Library	J. G. Thiobodaux, Jr. Chief, Propulsion & Power Division
1	1	National Aeronautics & Space Administration George C. Marshall Space Flight Center Huntsville, Alabama 35812 Attn: Library	J. Blumrich
1	1	Jet Propulsion Laboratory 4800 Oak Grove Drive Pasadena, California 91103 Attn: Library	W. Jensen
1		Defense Documentation Center Cameron Station Building 5 5010 Duke Street Alexandria, Virginia 22314 Attn: TISIA	
1		Office of the Director of Defense Research & Engineering Washington, D.C. 20301 Attn: Office of Asst. Dir. (Chem. Technology)	
1		RTD (RTNP) Bolling Air Force Base Washington, D.C. 20332	

REPORT COPIES R	D	RECIPIENT	DESIGNEE
1		Arnold Engineering Development Center Air Force Systems Command Tullahoma, Tennessee 37389 Attn: Library	Dr. H. K. Doetsch
1		Advanced Research Projects Agency Washington, D.C. 20525 Attn: Library	D. E. Mock
1		Aeronautical Systems Division Air Force Systems Command Wright-Patterson Air Force Base, Dayton, Ohio Attn: Library	D. L. Schmidt Code ARSCNC-2
1		Air Force Missile Test Center Patrick Air Force Base, Florida Attn: Library	L. J. Ullian
1		Air Force Systems Command Andrews Air Force Base Washington, D.C. 20332 Attn: Library	Capt. S. W. Bowen SCLT
1		Air Force Rocket Propulsion Laboratory (RPR) Edwards, California 93523 Attn: Library	
1		Air Force Rocket Propulsion Laboratory (RPM) Edwards, California 93523 Attn: Library	
1		Air Force FTC (FTAT-2) Edwards Air Force Base, California 93523 Attn: Library	Donald Ross
1		Air Force Office of Scientific Research Washington, D.C. 20333 Attn: Library	SREP, Dr. J. F. Masi

REPORT COPIES R	D	RECIPIENT	DESIGNEE
1		Space & Missile Systems Organization Air Force Unit Post Office Los Angeles, California 90045 Attn: Technical Data Center	
1		Office of Research Analyses (OAR) Holloman Air Force Base, New Mexico 88330 Attn: Library RRRD	
		U.S. Air Force Washington, D.C. Attn: Library	Col. C. K. Stambaugh, Code AFRST
1		Commanding Officer U.S. Army Research Office (Durham) Box CM, Duke Station Durham, North Carolina 27706 Attn: Library	
1		U.S. Army Missile Command Redstone Scientific Information Center Redstone Arsenal, Alabama 35808 Attn: Document Section	Dr. W. Wharton
1		Bureau of Naval Weapons Department of the Navy Washington, D.C. Attn: Library	J. Kay, Code RTMS-41
1		Commander U.S. Naval Missile Center Point Mugu, California 93041 Attn: Technical Library	
1		Commander U.S. Naval Weapons Center China Lake, California 93557 Attn: Library	W. F. Thorm Code 4562

REPORT COPIES R	D	RECIPIENT	DESIGNEE
1		Commanding Officer Naval Research Branch Office 1030 E. Green Street Pasadena, California 91101 Attn: Library	
1		Director (Code 6T80) U.S. Naval Research Laboratory Washington, D.C. 20390 Attn: Library	H. W. Carhart J. M. Krall i
1		Picatinny Arsenal Dover, New Jersey 07801 Attn: Library	I. Forsten
1		Air Force Aero Propulsion Laboratory Research & Technology Division Air Force Systems Command United States Air Force Wright-Patterson AFB, Ohio 45433 Attn: APRP (Library)	R. Quigley C. M. Donaldson
1		Space Division Aerojet-General Corporation 9200 East Flair Drive El Monte, California 91734 Attn: Library	S. Machlawski
1	1	Ordnance Division Aerojet-General Corporation 11711 South Woodruff Avenue Downey, California 90241 Attn: Library	W. L. Arter
1		Propulsion Division Aerojet-General Corporation P.O. Box 15847 Sacramento, California 95803 Attn: Technical Library 2484-2015A	R. Stiff

REPORT COPIES R	D	RECIPIENT	DESIGNEE
1		Air Products and Chemicals Company Allentown, Pennsylvania, 18105 Attn: P. J. DeRea	
1		Electronics Division Aerojet-General Corporation Azusa, California 91702	
1		ARO, Incorporated Arnold Engineering Development Center Arnold Air Force Station, Tennesee 37389 Attn: Dr. S. H. Goethert Chief Scientist	
1		Atlantic Research Corporation Shirley Highway & Edsall Road Alexandria, Virginia 22314 Attn: Security Office for Library	
1		Battelle Memorial Institute 505 King Avenue Columbus, Ohio 43201 Attn: Defense Metals Information Center	
1		Bell Aerosystems Box 1 Buffalo, New York 14205 Attn: T. Rainhardt	
1		The Boeing Company Aero Space Division P.O. Box 3707 Seattle, Washington 98124 Attn: Ruth E. Peerenboom (1190)	
1		Western Division McDonnell Douglas Aircraft Company, Inc. 3000 Ocean Park Blvd. Santa Monica, California 90406 Attn: J. M. Toth	J. L. Waisman

REPORT COPIES R	D	RECIPIENT	DESIGNEE
1		Hercules Powder Company Chemical Propulsion Division 910 Market Street Wilmington, Delaware 19804	
1		Narmco Research & Development Co. Whittaker Corporation 131 N. Ludlow Street Dayton, Ohio 45402	
1		Plastics Technical Evaluation Center Picatinny Arsenal Dover, New Jersey 07801	
1		Rocketdyne 6633 Canoga Avenue Canoga Park, California 91304 Attn: Library, Department 596-306	
1		Rohr Corporation Department 145 Chula Vista, California 91312	
1		TRW Systems 1 Space Park Redondo Beach, California 90200 Attn: Tech. Lib. Doc. Acquisitions	
1		Sandia Corporation Sandia Base Albuquerque, New Mexico 87115 Attn: H. E. Montgomery	
1		Swedlow, Incorporated 6986 Bandini Blvd., Los Angeles, California 90022	
1		Thiokol Chemical Corporation Wasatch Division P.O. Box 524 Brigham City, Utah 84302 Attn: Library Section	D. Hess

REPORT COPIES R	D	RECIPIENT	DESIGNEE
1		United Aircraft Corporation United Technology Center P.O. Box 358 Sunnyvale, California 94088 Attn: Librarian	
1		Chemical Propulsion Information Agency Applied Physics Laboratory 8621 Georgia Avenue Silver Spring, Maryland 20910	
1		The Garrett Corporation 20545 Center Ridge Road Cleveland, Ohio 44116	
1		Grumman Aircraft Engineering Corp. Bethpage Long Island, New York	
1		General Dynamics/Corvair P.O. Box 1128 San Diego, California 92712 Attn: Library and Information Services (128-00)	
1		B. F. Goodrich Company Aerospace & Defense Products 500 South Main Street Akron, Ohio 44311	
1		Goodyear Aerospace Corporation 1210 Massilon Rd. Akron, Ohio 44306	
1		Hamilton Standard Corporation Windsor Locks, Connecticut 06096 Attn: Library	
1		ABL, Division of Hercules Powder Company Cumberland, Maryland 21502 Attn: Thomas Bates	

REPORT COPIES R	D	RECIPIENT	DESIGNEE
1		IIT Research Institute Technology Center Chicago, Illinois 60616 Attn: C. K. Hersh, Chemistry Division	
1		Arde, Inc. 193 Route 17 Paramus, New Jersey 07652	
1		North American Aviation, Inc. Space & Information Systems Division 12214 Lakewood Blvd. Downey, California 90242 Attn: Technical Information Center D/096-722 (A107)	
1		U.S. Rubber Company Mishawaka, Indiana 46544	
1		General Electric Company Apollo Support Dept. P.O. Box 2500 Daytona Beach, Florida 32015 Attn: C. Day	
1		Aerojet-General Corporation Park West Building - Suite 227 20545 Center Ridge Road Cleveland, Ohio 44116 Attn: W. Snapp	
1		Marine Engineering Laboratory NSRDC ANNADIV Annapolis, Md. 21402 Attn: Karl H. Keller, Code 560	
1		Brunswick Corporation Defense Products Division P.O. Box 4594 43000 Industrial Ave. Lincoln, Nebraska 68504 Attn: J. Carter	

REPORT COPIES R	D	RECIPIENT	DESIGNEE
1		Celanese Corp. Box 1000 Summit, New Jersey 07901 Attn: J. D. Lassiter	
1		Aeronutronic Division of Philco Ford Corp. Ford Road Newport Beach, California 92663 Attn: Technical Information Department	Dr. L. H. Linder
1	1	Aerojet Nuclear Systems Company P.O. Box 13070 Sacramento, California 95813	G. L. Ryland
1		Structural Composites Industries 6344 North Irwindale Avenue P.O. Box 904 Azusa, California 91702 Attn: E. E. Morris	
1		Aerospace Corporation P.O. Box 95085 Los Angeles, California 90045 Attn: Library-Documents	